

Title: The Development of Two-dimensional Digital Operators
for the Filtering of Potential Field Data

Author: H. P. Parsneau

Department: Mining Engineering and Applied Geophysics

A thesis submitted to the Faculty of Graduate Studies
and Research in partial fulfilment of the requirements
for the Degree of Master of Engineering (Geophysics).

ABSTRACT

The collection and subsequent manipulation of gravity and magnetic data in applied geophysics can be conveniently described in terms of the sampling and filtering of continuous, two-dimensional waveforms. Viewed in this manner, most of the potential field operators in common use fall far short of their expectations.

The use of filter theory and modern processing techniques allows a more general approach to the problems of operator design, and a more accurate approximation of potential field operations. The inverse Hankel transform and a proposed wavelength filter have been used in this thesis for the derivation of zero-phase, two-dimensional potential field operators.

The concepts of frequency analysis and information theory adopted in this filtering approach lend new insight and understanding to the problems and methods of gravity and magnetic interpretation.

The title to appear on spine of bound copies:

THE DESIGN OF TWO-DIMENSIONAL POTENTIAL FIELD FILTERS

by

H. P. Parsneau

**THE DEVELOPMENT OF TWO-DIMENSIONAL DIGITAL OPERATORS
FOR THE FILTERING OF POTENTIAL FIELD DATA**

by

H. P. Parsneau, B. Eng.

**A thesis submitted to the Faculty of
Graduate Studies and Research in partial
fulfilment of the requirements for the
Degree of Master of Engineering (Geophysics).**

**Department of Mining Engineering
and Applied Geophysics,
McGill University,
Montreal.**

June 15, 1970.

TABLE OF CONTENTS

List of Illustrations	Page 1
List of Tables	4
Acknowledgement	5
Introduction	6
Chapter 1: Potential Fields and Filter Theory	9
1-1 Potential Field Surveys and Related Theory	9
Gravity and Magnetic Surveys	9
Potential Field Equations	11
The Equivalent Stratum	16
Continuation of Potential Fields ...	19
1-2 Fundamentals of Frequency Analysis	21
The Fourier Transform	21
The Convolution Integral and Filtering	25
Discrete Sampling of Continuous Waveforms	30
1-3 Frequency Analysis of Potential Field Data	35
Spectral Form of the Inverse Potential Problem	36
Potential Field Filtering	37
Chapter 2: Description and Design of Two-dimensional Potential Field Filters	41

TABLE OF CONTENTS (cont'd)

2-1	Characteristics of Some Potential Field Operators	Page 41
	Wavelength or Boxcar Filter	41
	The Second Vertical Derivative	44
	Continuation Operators	46
2-2	Filter Representation and Design	50
	Operators for Discrete Data	50
	Analytical Design Methods	54
	Transform Design Methods	66
	Practical Refinements in Operator Design	73
2-3	Description and Assessment of Some Proposed Operators	76
	Wavelength Filters	78
	The Second Vertical Derivative	86
	Continuation Operators	90
Chapter 3:	Application of Filters to Potential Field Data	101
3-1	Investigation of the Roger's Farm Sulphide Zone - St. Stephen, New Brunswick	101
	Local Geology	102
	Geophysical Surveys	103

TABLE OF CONTENTS (cont'd)

3-2 Filtering the Roger's Farm Potential Field Data and Discussion of Results	Page 105
Gravity Maps	105
Magnetic Maps	108
Chapter 4: Discussion and Conclusions	120
Appendix	123
Bibliography	128

LIST OF ILLUSTRATIONS

Figure		Page
1-1	Specifying an Element of Mass Distribution	13
1-2	The Equivalent Stratum	17
1-3	The Convolution Process	27
1-4	The Discrete Sampling of a Band-limited Function	31
1-5	Truncation and Sampling of a Semi-infinite Waveform	34
2-1	Ideal Wavelength Filters	42
2-2	Theoretical Frequency Response of the Second Vertical Derivative	42
2-3	Theoretical Frequency Response of Upward Continuation	48
2-4	Theoretical Frequency Response of Downward Continuation	49
2-5	Inversion of Wavelength Filter	56
2-6	Second Vertical Derivative Operator by the Hankel Transform Method	68
2-7	Center Point, Single Ring Residual Operator	77
2-8	Wavelength Filter - 0.4 Cycle / D.I. Low-pass	79
2-9	Wavelength Filter - 0.2 Cycle / D.I. Low-pass	80
2-10	Wavelength Filter - 0.075 Cycle / D.I. Low-pass	81
2-11	Radial Response of Wavelength Filters	82
2-12	Radial Response of Inverse Wavelength Filters and Center Point, Single Ring Operator	82
2-13	Inverse Wavelength Filter - 0.20 Cycle / D.I. High-pass	84

LIST OF ILLUSTRATIONS (cont'd)

Figure		Page
2-14	Inverse Wavelength Filter - 0.075 Cycle / D.I. High-pass	85
2-15	Derived Second Vertical Derivative Operator	87
2-16	Radial Response of the Derived Second Vertical Derivative Operator	88
2-17	Amplitude Response of Henderson and Zietz' (1949) Second Vertical Derivative Operator	89
2-18	Amplitude Response of Rosenbach's (1953) Second Vertical Derivative Operator	91
2-19	Derived Upward Continuation Operator for a Height of One Grid Unit	92
2-20	Derived Upward Continuation Operator for a Height of Two Grid Units	93
2-21	Amplitude Response of Peters' (1949) Upward Continuation Operator for a Height of One Grid Unit	95
2-22	Derived Downward Continuation Operator for a Depth of One Grid Unit	97
2-23	Amplitude Response of Henderson's (1960) Downward Continuation Operator for a Depth of One Grid Unit	98
2-24	Amplitude Response of Grant and West's (1967) Downward Continuation Operator for a Depth of One Grid Unit	99
3-1	The Roger's Farm Sulphide Zone	109
3-2	Bouguer Gravity Contours - Roger's Farm Zone	110
3-3	Second Vertical Derivative Map - Roger's Farm Gravity Data	111
3-4	Residual Map (0.075 Cycle / D.I. Cut-off) - Roger's Farm Gravity Data	112

LIST OF ILLUSTRATIONS (cont'd)

Figure		Page
3-5	Downward Continuation Map for a Depth of 100 Feet - Roger's Farm Gravity Data	113
3-6	Magnetic Contours - Roger's Farm Zone	114
3-7	Noise Filtered Magnetic Data (0.4 Cycle / D.I. Cut-off) - Roger's Farm Zone	115
3-8	Upward Continuation Map for a Height of 100 Feet - Roger's Farm Magnetic Data	116
3-9	Upward Continuation Map for a Height of 200 Feet - Roger's Farm Magnetic Data	117

LIST OF TABLES

Table		Page
1	Space and Spectral Properties of Some Potential Field Operators	51
Appendix		
A-1	Peters' (1949) Upward Continuation Coefficients for a Height of One Grid Unit	125
A-2	Peters' (1949) Downward Continuation Coefficients for a Distance of One Grid Unit	125
A-3	Trejo's (1953) Downward Continuation Coefficients for a Distance of One Grid Unit	126
A-4	Henderson's (1960) Downward Continuation Coefficients for a Distance of One Grid Unit ...	126
A-5	Grant and West's (1967) Downward Continuation Coefficients for a Distance of One Grid Unit	127
A-6	Henderson and Zietz' (1949) Second Vertical Derivative Coefficients	127
A-7	Rosenbach's (1953) Second Vertical Derivative Coefficients	127

ACKNOWLEDGEMENT

I would like to express my appreciation to Professor W.M. Telford of the Department of Mining Engineering and Applied Geophysics, McGill University, for his encouragement and guidance throughout the progress of this work. As thesis supervisor, Dr. Telford made many helpful suggestions regarding the form and content of the thesis, and provided geological and geophysical data over the Atlantic Nickel Property near St. Stephen, New Brunswick.

The author has spent the past two summers in Calgary, Alberta, where he was employed as a summer student by Chevron Standard Limited. During this association the author was accorded every opportunity to learn from the experience of company geophysicists. I would like to extend my thanks to these geophysicists, particularly to Mr. R.R. Clawson who originally suggested the topic of potential field filtering.

I am very grateful, also, to Professor C.C. Ku whose informative discussions on topics of frequency analysis and sampling theory helped to clarify several important concepts.

INTRODUCTION

The gravity and magnetic methods of applied geophysics involve the mapping and subsequent interpretation of potential field variations over the earth's surface. These variations or anomalies of the earth's main potential fields are due to local changes in density and magnetic properties within the earth's upper crust, and may reflect a wide variety of geological features. The sampling and analysis of potential field anomalies are of particular interest in exploration geophysics, since mineral deposits and related geological trends are often associated with density or magnetic susceptibility contrasts.

Although a particular gravity or magnetic anomaly cannot be traced back to a unique source, its amplitude, shape and areal extent help to limit the range of possibilities. Large-scale structural or lithological changes occurring in the deep geological section are usually accompanied by rather significant density and magnetic susceptibility contrasts. The resulting anomalous expressions are characterized by relatively large amplitude, low frequency variations of the surface field intensities. Because the effects of these deep features may extend over a considerable surface area they are referred to as regional components of the anomalous field. The anomalies of shallower sources, on the other hand, tend to be of low to moderate amplitude, and more localized in extent. They are referred to as the higher frequency or residual components of the field distortion. The anomalous gravity and magnetic fields

observed at the surface of the earth can therefore be described as a superposition of field effects originating from a subsurface distribution of sources. In interpreting potential field data, the geophysicist attempts to separate and explain the various components of the observed field and reconstruct geologically significant features. Separating the components of the anomalous field is an important part of the interpretation and will be a factor in the ultimate success of the survey.

The problem of anomaly discrimination can be conveniently approached from the point of view of frequency analysis. The variation of a potential field over the surface of the earth shows phase and amplitude properties analogous to those of electrical waveforms. The anomalous surface variation of the gravity and magnetic fields may therefore be interpreted as a two-dimensional waveform arising from the superposition of various wavelength components. Each subsurface source contributes its own spectrum of frequencies to the overall frequency spectrum. Consistent with this outlook, interpretational aids such as regional-residual separation, vertical derivative and continuation methods can be viewed as filtering operations. The adaptation of frequency analysis and information theory to the design of potential field operators provides several processing advantages as well as valuable insight into the problems of interpretation.

The primary purpose of this thesis is to present methods for the derivation and evaluation of two-dimensional potential field filters. Emphasis will be placed on the waveform char-

acteristics of potential field data, and ample background will be provided in the concepts of frequency analysis and sampling theory. Several operators have been derived to supplement the discussion, and some of these will be applied to actual gravity and magnetic data.

The thesis has been divided into four chapters. In the first chapter, relevant topics in potential field theory, frequency analysis, and discrete sampling will be covered, with particular reference to gravity and magnetic surveys. Chapter two will be concerned with the derivation and assessment of digital operators used as two-dimensional potential field filters. New operators will be derived and compared with those of previous authors. The third chapter will show how operators are applied to gravity and magnetic data in an attempt to enhance or subdue certain anomalous features of a potential field waveform. A number of operators derived in this thesis will be applied to gravity and magnetic data obtained over the Roger's Farm sulphide zone near St. Stephen, New Brunswick. In the final chapter, the role of operators in gravity and magnetic interpretation will be discussed and a number of conclusions drawn.

Chapter 1:

POTENTIAL FIELDS AND FILTER THEORY

1-1 Potential Field Surveys and Related Theory

Gravity and Magnetic Surveys

The earth, like all concentrations of mass, has a gravitational field which attracts other bodies. The force of attraction per unit mass particle is proportional to the earth's own mass, and inversely proportional to the square of the distance between the mass centers of the earth and unit particle. The gravitational acceleration at the earth's surface varies from about 978.0 cm/sec^2 at the equator to 983.3 cm/sec^2 at the poles. This latitudinal variation is caused by two partially offsetting effects directly related to the earth's rotation: the decrease in the vertical component of centrifugal force toward the poles, and the concentration of terrestrial mass about the equator. The gravity field is also disturbed locally by density changes within the earth's crust. Geological information contained in these localized, high frequency fluctuations can be extracted from the observed gravity field variation over the earth's surface.

A gravity measurement taken at a particular surface point samples the change in total gravitational field with respect to a survey base station. The standard unit of measurement is the milligal, equivalent to a gravitational acceleration of $1 \times 10^{-3} \text{ cm/sec}^2$. Gravity anomalies of interest in

geophysical exploration can be as small as 0.1 milligal and seldom attain magnitudes in excess of 5.0 milligals. Gravimeters employed in geophysical surveys can detect differences in gravitational acceleration of the order of one part in 10^8 (i.e. ± 0.01 milligal).

Before the data can yield intelligible geological information, a number of corrections must be applied in order to eliminate latitude, elevation, terrain, tidal, and instrument drift effects; since these also cause variations in the apparent gravity field.

The earth's natural magnetic field is the other predominant potential field of interest in geophysics. It can be approximated by a magnetic dipole inclined about 11 degrees to the earth's rotational axis and slightly offset from the earth's center. The orientation and magnitude of the total field vector varies from horizontal at 0.35 oersteds in the equatorial regions, to vertical at 0.65 oersteds near the geomagnetic poles.

Most rock types in the crust show some degree of magnetic susceptibility due to the presence of magnetic minerals, and will reinforce the earth's main field by induction. Various forms of remanent magnetization may accompany the normally induced component. These intrinsic or locked-in fields result from environmental conditions at the time of mineral crystallization, or else have been induced by lightning discharges. The widespread and often erratic distribution of magnetic minerals in crustal rocks contributes large amplitude, high fre-

quency fluctuations to the earth's main magnetic field. Geological information concerning composition, structure, and origin of crustal rocks is contained in such anomalous expressions. However, the presence of unknown remanent components, and the varying inclination of the earth's main field vector make geological interpretation somewhat difficult.

Measurement of the magnetic field variation over the earth's surface is accomplished with the aid of a magnetometer. Surface surveys usually select the vertical direction as reference, and measure the variation in vertical intensity over the ground. Aeromagnetic surveys, on the other hand, generally measure the total magnetic field. The unit of measurement in magnetic surveys is the gamma (10^{-5} oersteds). Instrument sensitivity is in the neighborhood of ± 5 gammas. The majority of magnetic anomalies lie in the range of 0.1 to 10.0 percent of the earth's field, but values over 100 percent have been observed.

Potential Field Equations

The interaction of gravitational mass, expressed by Newton's Law of Gravitation, is one example of a force field obeying the inverse square law. Similar relationships hold for electric and magnetic force fields, and the terms "electrical mass" and "magnetic mass" can be used to describe the appropriate source type. The general inverse square law takes the form:

$$F = k^2 \frac{m_1 m_2}{r^2} \quad (1-1)$$

where F is the force of interaction between two mass particles, m_1 and m_2 , separated by a distance r , and k^2 is a constant determined by the type of source and the units employed. The force F acts along the line joining the two particles.

Given a particular density distribution of source material, the resulting gravitational force of attraction per unit mass, at a point of observation $P(x,y,z)$, may be expressed as a volume integral:

$$F(r) = G \int_V \frac{\rho(\xi, \eta, \zeta)}{|r - r_0|^2} dv \quad (1-2)$$

where G is the gravitational constant, $\rho(\xi, \eta, \zeta)$ is the density function of the mass distribution, and V its volume; and where the position vectors r and r_0 locate the mass element dm and the point of observation, respectively (see Figure 1-1a, pg 13).

The potential field associated with all such distributions of mass bears the following relationship to the force field:

$$F(r) = -\nabla U(r) \quad (1-3)$$

$$\text{where } U(r) = -G \int_V \frac{\rho(r_0)}{|r - r_0|} dv \quad \text{is, in this case,}$$

the gravitational potential. A potential field is a single-valued, scalar function of position, continuous everywhere outside the volume of source distribution.

The forces associated with the interaction of gravitational mass are attractive and are taken in the positive sense.

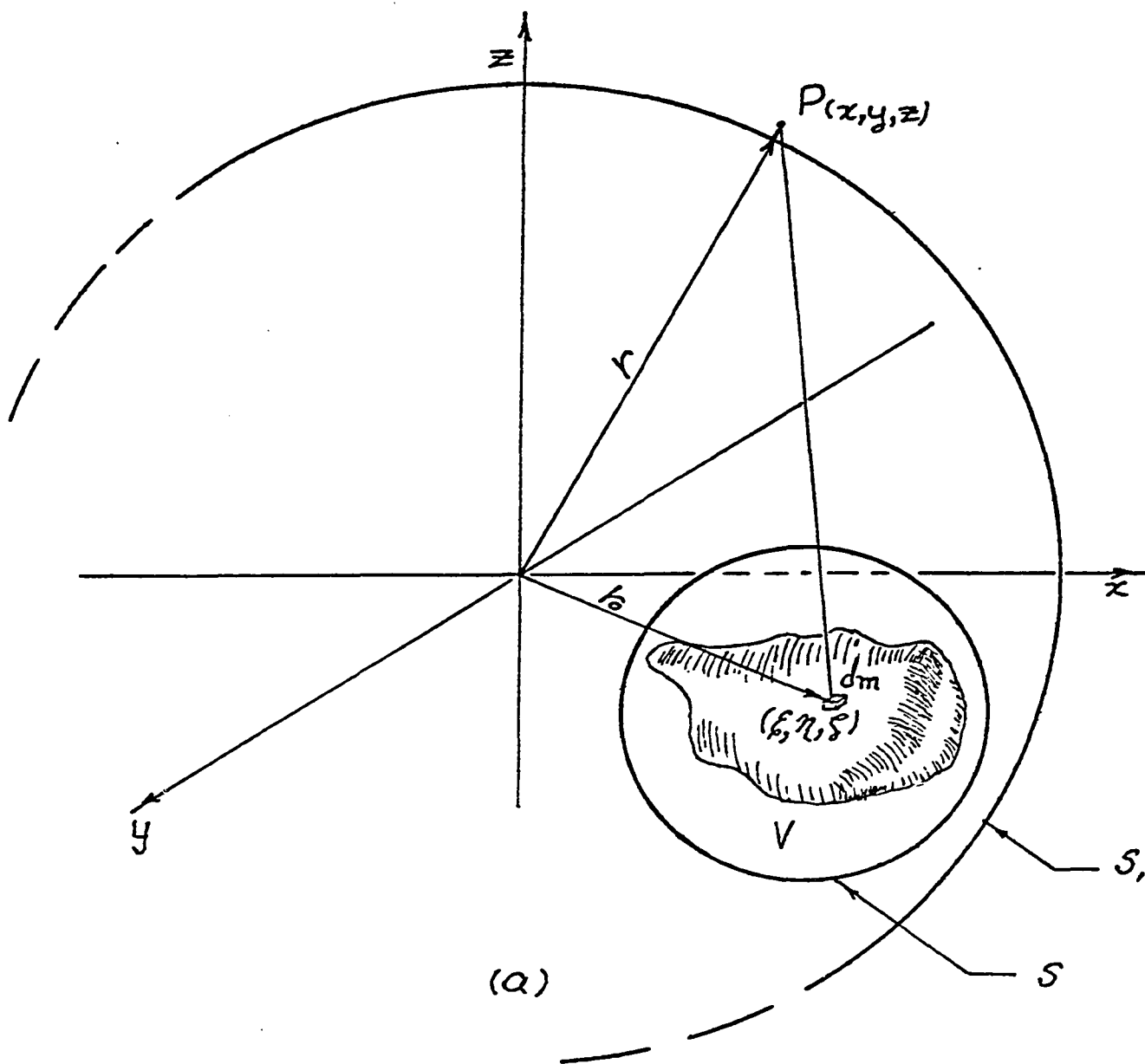
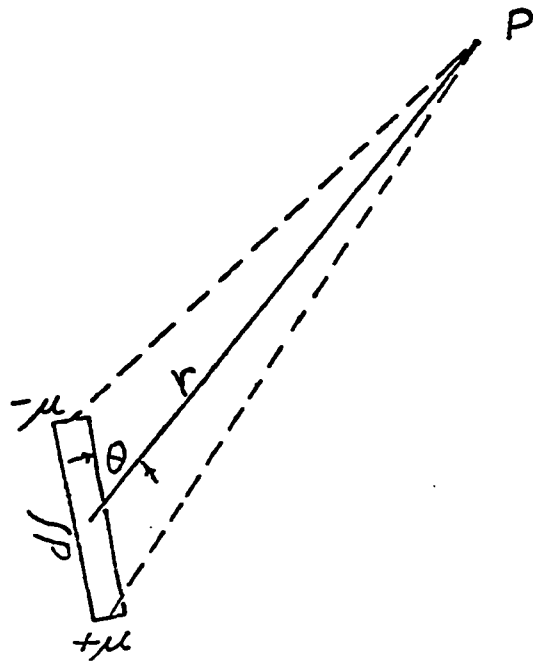
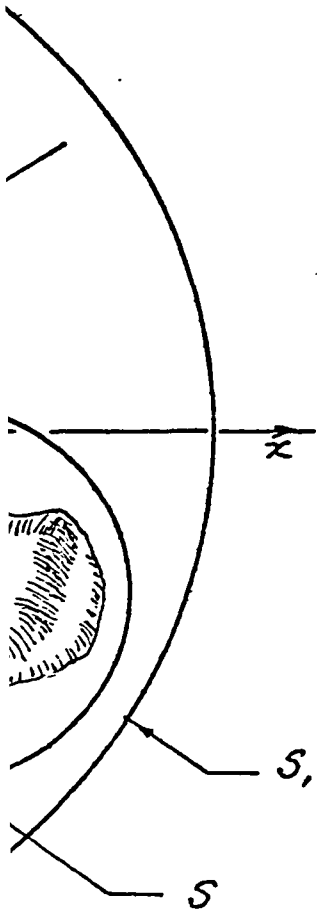


FIG. 1-1: SPECIFYING AN ELEMENT OF

(x, z)



A DIPOLE ELEMENT

(b)

ELEMENT OF MASS DISTRIBUTION.

Electric and magnetic mass distributions, on the other hand, contain both attracting and repelling elements so that negative and positive particles must be defined. The term "particles" used here is generally replaced by "charges" when dealing with electric fields and "poles" when concerned with magnetic fields. In the discussion to follow, only magnetic and gravity fields will be dealt with since they are of primary concern in this thesis.

In presenting the magnetic field equivalents of equations 1-2 and 1-3, the doublet or dipolar characteristic of magnetic mass must be introduced. The single magnetic pole is a mathematical abstraction and does not exist in nature. An element of magnetic mass can be visualized as a dipole of pole separation d and strength μ (as represented in Figure 1-1b). The magnetic field intensity at a point P, due to a dipole a distance r away, can be approximated by:

$$H(r) = \frac{2m \cos \theta \vec{r}}{r^4} + \frac{m \sin \theta \vec{\theta}}{r^3} \quad (1-4)$$

where the dipole length d is very much smaller than the distance r , $m = \mu d$ is the dipole moment, \vec{r} is the vector from the center of the dipole to the point P, θ is the angle between the dipole axis and the vector \vec{r} , and $\vec{\theta}$ is the unit vector measured in the direction of increasing θ . The magnetic force field about the dipole may also be written in terms of a potential field:

$$H(r) = -\nabla A(r) \quad (1-5)$$

where the magnetostatic potential is given by:

$$A(r) = -m \cdot \nabla \left(\frac{1}{r} \right)$$

Returning again to Figure 1-1a, page 13, we can imagine each element of mass dm to be in the form of a magnetic dipole. If it is assumed that the magnetic mass contained within the volume V has a continuously distributed magnetic moment per unit volume, $M(r_0)$, the total potential at P can be expressed as a volume integral:

$$A(r) = - \int_V M(r_0) \cdot \nabla \frac{1}{|r-r_0|} dv \quad (1-6)$$

Substituting this expression into equation 1-5, and assuming a constant direction of magnetization α , the resultant magnetic field strength at point P becomes:

$$H(r) = \nabla \frac{\partial}{\partial \alpha} \int_V M(r_0) \frac{1}{|r-r_0|} dv \quad (1-7)$$

which is the magnetic equivalent of equation 1-2.

The partial differential equations summarizing the properties of potential fields can be derived by applying the Divergence theorem to the system in Figure 1-1a. If ϕ is the potential function resulting from the distribution of mass in the volume V , we may write, according to the Divergence theorem:

$$\int_{V_i} \nabla \cdot (\nabla \phi) dv = \int_S (\nabla \phi) \cdot ds + \int_{S_i} (\nabla \phi) \cdot ds, \quad (1-8)$$

where V_i is the volume bounded by the surfaces S and S_i in Figure 1-1a. Since the volume V_i is devoid of source material,

the surface integrals on the right side of equation 1-8 are, by Gauss' theorem, equal in magnitude but of opposite sign. Equation 1-8 therefore reduces to Laplace's equation:

$$\nabla^2 \phi = 0 \quad (1-9)$$

At points external to the source distribution, gravity and magnetic potential fields obey Laplace's equation and are termed harmonic. Within the volume of mass distribution the potential functions satisfy Poisson's equations:

$$\nabla^2 U(r_0) = 4\pi G \rho(r_0) \quad (1-10a)$$

for the gravity field, and

$$\nabla^2 A(r_0) = 4\pi \nabla \cdot M(r_0) \quad (1-10b)$$

for the magnetostatic potential, where $\rho(r_0)$ and $M(r_0)$ are the density function and magnetic moment, respectively, at the particular point of observation. Equations 1-9 and 1-10 are referred to as the field equations of potential theory and are fundamental to the development of related topics.

The Equivalent Stratum

The equivalent stratum concept involves the replacement of a three-dimensional source distribution by a density coating over a level surface. The derivation given by Grant and West (1965, article 8-3) is summarized here for convenience. In Figure 1-2, page 17, a horizontal surface, $z=0$, of density distribution $\sigma(x,y)$, subtends a point of observation $P(0,0,-z)$. The gravitational potential at point P, due to the density layer may be written as:

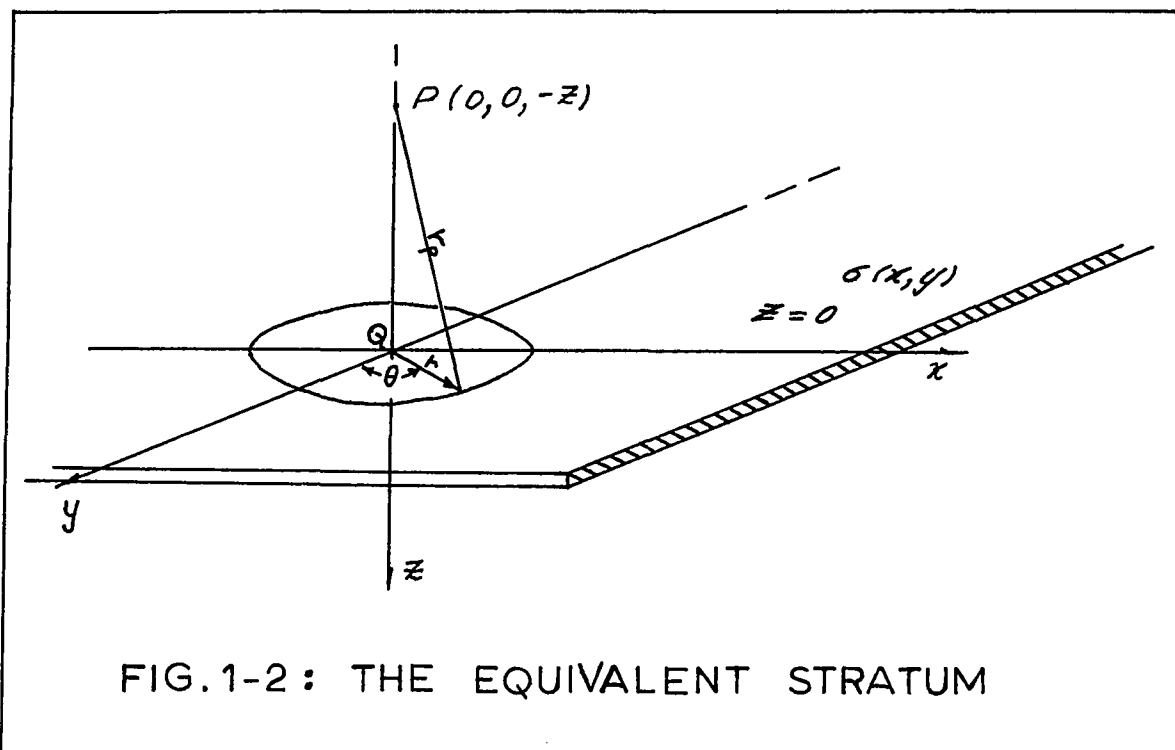


FIG.1-2: THE EQUIVALENT STRATUM

$$U_p = -G \int_0^{\infty} \int_0^{2\pi} \frac{\sigma(r, \theta) r d\theta dr}{(r_p^2 + z^2)^{1/2}}$$

and using equation 1-3, page 12, the corresponding gravitational force at point P is:

$$\Delta g_p = \frac{\partial U_p}{\partial z} = Gz \int_0^{\infty} \int_0^{2\pi} \frac{\sigma(r, \theta) r d\theta dr}{(r_p^2 + z^2)^{3/2}} \quad (1-11)$$

The above equation is valid at all points above the plane $z=0$. As z approaches zero, however, the gravity effect near Q becomes singular. The singularity can be isolated by surrounding Q with a small circle of radius ϵ , and rewriting equation 1-11 in the form:

$$\lim_{z \rightarrow 0} \Delta g_p = \lim_{z \rightarrow 0} \left[Gz \sigma(Q) \int_0^{\epsilon} \int_0^{2\pi} \frac{r d\theta dr}{(r^2 + z^2)^{3/2}} + Gz \int_{\epsilon}^{\infty} \int_0^{2\pi} \frac{\sigma(r, \theta) r d\theta dr}{(r^2 + z^2)^{3/2}} \right] \quad (1-12)$$

The second integral on the right is entirely free from singularities and vanishes in the limit. The remaining integral can be evaluated, assuming that ϵ is small enough to justify using a constant density function within the singularity circle. Then equation 1-12 becomes:

$$\Delta g_Q = 2\pi G \sigma(Q)$$

If the position of Q in the plane, $z=0$, has not been restricted, a more general form may be written:

$$\Delta g(x, y) = 2\pi G \sigma(x, y) \quad (1-13)$$

To an observer making a gravity measurement on or above the plane $z=0$, the unknown distribution of mass giving rise to the gravity effect, $\Delta g(x, y)$, has been replaced by an equivalent stratum of density function $\sigma(x, y)$.

The equivalent stratum of magnetic mass is associated, not with the force field, but with the magnetic potential:

$$A(x, y) = 2\pi k H_z h(x, y)$$

where k is the magnetic susceptibility of a homogeneous, magnetic surface, $h(x, y)$ is the topographical variation of this surface over the plane $z=0$, and H_z is the vertical component of the main field vector.

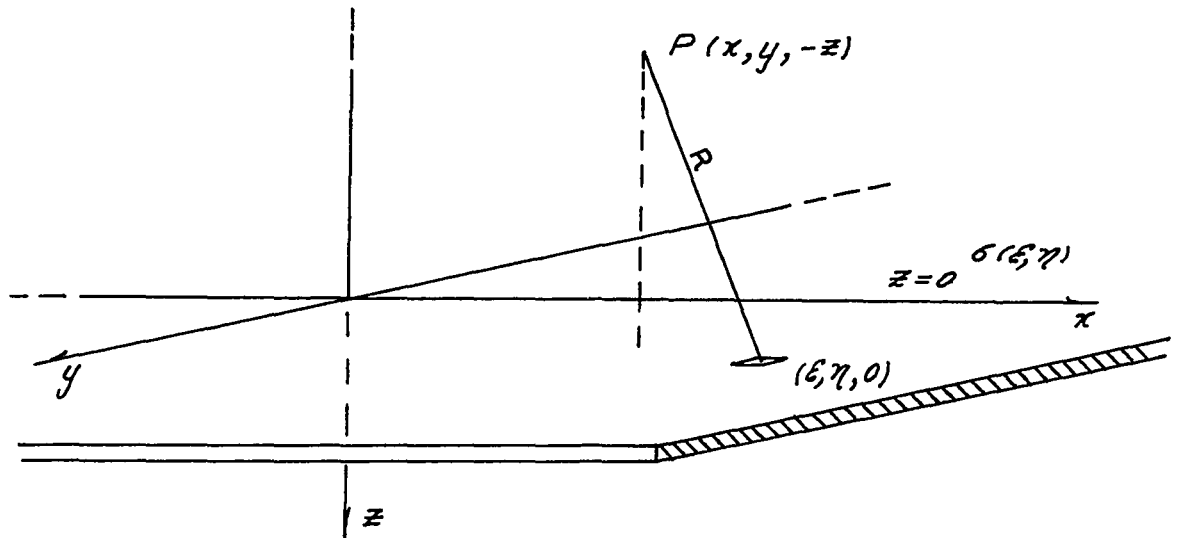
The equivalent stratum concept is a useful means of visualizing density distributions below the surface plane of a two-dimensional potential field survey. This is especially true

when interpretation methods involve the surface integration of the observed data.

Continuation of Potential Fields

Potential field data obtained on a plane $z=0$, above a three-dimensional mass distribution, can be extrapolated or continued upward to any desired height, provided that the region of continuation is harmonic. The vertical direction implied in the process is in keeping with the reference direction usually chosen in such surveys, and in this respect, it is the variation of the vertical component of the field which is involved in continuation.

In the diagram below, the underlying distribution has



been replaced by an equivalent stratum on the plane $z=0$. The gravity effect at the point $P(x, y, -z)$ due to the surface density variation $\sigma(\xi, \eta)$ is:

$$\Delta g_p = Gz \iint_{-\infty}^{\infty} \frac{\sigma(\xi, \eta) d\xi d\eta}{R^3}$$

where $R = \sqrt{(x-\xi)^2 + (y-\eta)^2 + z^2}$

According to equation 1-13, the density variation of the equivalent stratum is:

$$\delta(\xi, \eta) = \frac{\Delta g(\xi, \eta)}{2\pi G}$$

therefore, the total gravity effect at P becomes:

$$\Delta g_P = \frac{z}{2\pi} \iint_{-\infty}^{\infty} \frac{\Delta g(\xi, \eta)}{R^3} d\xi d\eta \quad (1-14)$$

where $\Delta g(\xi, \eta)$ is the sampled gravitational field on the plane $z=0$. Equation 1-14 represents the upward continuation of the gravitational field from the plane $z=0$ to the point P. The equivalent expression for the upward continuation of magnetic fields is:

$$Z_P = -\frac{\partial A_P}{\partial z} = \frac{z}{2\pi} \iint_{-\infty}^{\infty} \frac{Z(\xi, \eta)}{R^3} d\xi d\eta \quad (1-15)$$

where the symbol Z_P refers to the vertical component of the magnetic field intensity. Alternate and more rigorous derivations of the continuation integral are given by Grant and West (1965, chap. 8) and Kellogg (1929, chap. 5).

Downward continuation of the field below the plane $z=0$ is also possible, provided the region of continuation is harmonic. Where this process involves projection of the observed field below the surface of the ground, the harmonic restriction becomes difficult to ensure. In practice, the effect of intervening mass distributions must be eliminated, or at least attenuated, before realistic results can be obtained.

The value of continuation methods in the interpretation

of potential field data lies in the discrimination afforded between shallow and deep anomalous sources. Shallow anomalies, responsible for higher frequency variations in the observed field, are attenuated with respect to deeper sources during the process of upward continuation. In downward continuation the reverse is true, as higher frequency components become more apparent against the lower frequency, deeper effects. The connection between the continuation integral, equation 1-14, and frequency analysis of potential field data will be discussed in section 1-3 of this chapter.

1-2 Fundamentals of Frequency Analysis

The Fourier Transform

A periodic function $f(t)$, which is sectionally continuous with only a finite number of discontinuities, can be represented by an infinite series of sines and cosines. This Fourier series takes the form:

$$f(t) = \sum_{n=-\infty}^{\infty} \alpha_n e^{in\omega_0 t} \quad (1-16)$$

where the constants α_n are given by:

$$\alpha_n = \frac{1}{T} \int_{-T/2}^{T/2} f(t) e^{-in\omega_0 t} dt$$

in which T is the period of $f(t)$ and $\omega_0 = 2\pi/T$ is the fundamental frequency.

Very often the functions to be analysed are non-periodic and require a more generalized form of the above expression.

Substituting for α_n in equation 1-16 and letting the period T approach infinity:

$$f(t) = \int_{-\infty}^{\infty} \left[\int_{-\infty}^{\infty} f(t) e^{-j2\pi\omega t} dt \right] e^{j2\pi\omega t} d\omega \quad (1-17)$$

where $\lim_{T \rightarrow \infty} \omega_0 = 2\pi d\omega$ and $\lim_{T \rightarrow \infty} n\omega_0 = 2\pi\omega$, with ω , the frequency variable, expressed in cycles / unit of t . Equation 1-17 is a statement of Fourier's Integral Theorem, and relates either the time domain or the space domain to its frequency spectrum. The quantity in brackets is called the Fourier transform of the function $f(t)$, and describes the frequency domain of the waveform. The Fourier integral is referred to as the inverse Fourier transform, being a reciprocal operation of the former. The transform pair may be written as:

$$\text{Fourier transform:} \quad F(\omega) = \int_{-\infty}^{\infty} f(t) e^{-j2\pi\omega t} dt \quad (1-18)$$

$$\text{inverse Fourier transform:} \quad f(t) = \int_{-\infty}^{\infty} F(\omega) e^{j2\pi\omega t} d\omega \quad (1-19)$$

where $F(\omega)$ is the Fourier transform of the waveform $f(t)$. Unless $f(t)$ is an even function, the Fourier transform will consist of both real and imaginary components:

$$F(\omega) = R(\omega) + jX(\omega) = A(\omega) e^{j\phi(\omega)}$$

where $A(\omega)$ is the amplitude spectrum of $f(t)$, and $\phi(\omega)$ is the phase spectrum. These transforms are a well-known and convenient means of analyzing aperiodic waveforms in electrical

engineering. The only serious restrictions on $f(t)$ are that its integral from $t = -\infty$ to ∞ exists, and that any discontinuities in the function are finite.

Fourier transform techniques are also used in geophysical interpretation, particularly in the analysis of seismic data, and to a lesser extent, in the treatment of potential field data. When an acoustic energy pulse is directed into the earth during a seismic survey, a portion of the energy is reflected back to the surface as a result of density and velocity changes in the geological section. A surface array of geophones will detect the arrival of reflected energy and respond by producing a set of electrical waveforms. When amplified and directed through an appropriate set of filters, each signal or seismic trace will yield geological information associated with the density and velocity variations. Frequency analysis of seismic records, using the Fourier transform, is normally the first step in setting design criteria for seismic filters.

The filtering and frequency analysis of two-dimensional potential field data, the primary concern of this thesis, will require a two-dimensional version of the Fourier and inverse Fourier transforms:

$$F(u, v) = \int_{-\infty}^{\infty} \int_{-\infty}^{\infty} f(x, y) e^{-j2\pi(ux + vy)} dx dy \quad (1-20)$$

$$f(x, y) = \int_{-\infty}^{\infty} \int_{-\infty}^{\infty} F(u, v) e^{j2\pi(ux + vy)} du dv \quad (1-21)$$

where u and v are the frequencies along the x and y cartesian axes. In the event that $f(x, y)$ is circularly symmetric about the origin, the above equations become:

$$F(u, v) = 4 \int_0^{\infty} \int_0^{\infty} f(x, y) \cos(2\pi ux) \cos(2\pi vy) dx dy \quad (1-22)$$

$$f(x, y) = 4 \int_0^{\infty} \int_0^{\infty} F(u, v) \cos(2\pi ux) \cos(2\pi vy) du dv \quad (1-23)$$

Alternatively, we may introduce polar co-ordinates in equation 1-20:

$$u = \rho \cos \phi, \quad v = \rho \sin \phi$$

$$x = r \cos \theta, \quad y = r \sin \theta$$

and obtain:

$$F(\rho) = \int_0^{\infty} \int_0^{2\pi} f(r) e^{-i2\pi\rho r(\cos(\theta-\phi))} r d\theta dr$$

Using the zero-order Bessel function of first kind in the form:

$$J_0(z) = \frac{1}{2\pi} \int_0^{2\pi} e^{-iz \cos \beta} d\beta$$

we may write, finally:

$$F(\rho) = 2\pi \int_0^{\infty} f(r) J_0(2\pi\rho r) r dr \quad (1-24)$$

Similar treatment of equation 1-21 yields:

$$f(r) = 2\pi \int_0^{\infty} F(\rho) J_0(2\pi\rho r) \rho d\rho \quad (1-25)$$

where r is the radial distance measured from the origin and ρ is the frequency in that direction. Equations 1-24 and 1-25 are known as the Hankel and inverse Hankel transforms of zero order and exist only if $f(x, y) = f(r)$ is a circularly symmetric function.

The Convolution Integral and Filtering

The well established concepts of filter theory, employed in the analysis of electrical waveforms, are directly applicable to the filtering of seismic and potential field data. The fundamental relation inherent in all filtering operations is the convolution integral:

$$f_o(t) = \int_{-\infty}^{\infty} f_i(\tau) W(t-\tau) d\tau \quad (1-26)$$

where $f_i(\tau)$ is the input waveform and could represent an electrical signal such as a seismic trace, $W(t)$ is the weighting function or transfer function which operates on the data input, and $f_o(t)$ is the filter output.

The significance of the convolution integral will be more clearly understood if a transformation is made to the frequency domain. Taking the Fourier transform of each side of equation 1-26:

$$\begin{aligned} \int_{-\infty}^{\infty} f_o(t) e^{-j2\pi\omega t} dt &= \int_{-\infty}^{\infty} \left[\int_{-\infty}^{\infty} f_i(\tau) W(t-\tau) d\tau \right] e^{-j2\pi\omega(t-\tau)} e^{-j2\pi\omega\tau} dt \\ &= \int_{-\infty}^{\infty} W(t-\tau) e^{-j2\pi\omega(t-\tau)} d(t-\tau) \int_{-\infty}^{\infty} f_i(\tau) e^{-j2\pi\omega\tau} d\tau \end{aligned}$$

that is:

$$F_o(\omega) = Y(\omega) \cdot F_j(\omega) \quad (1-27)$$

where $F_o(\omega)$, $Y(\omega)$, and $F_j(\omega)$ are the Fourier transforms of the filter output, the weighting function, and the input waveform, respectively. Equation 1-27 shows that convolution in the time or space domain corresponds to multiplication in the frequency domain. In the same way it may be shown that frequency domain convolution represents time or space domain multiplication.

The convolution of an input waveform with a filter function is shown both graphically and schematically in Figure 1-3, page 27. The top diagrams (Figures 1-3a to 1-3c) show the actual manipulation involved during convolution. The weighting function $W(t)$ is reversed and superimposed on the input waveform so that its ordinate, or zero point, coincides with a particular position $\tau = t'$. In this way a correspondence is set up between the " τ axis" of the input waveform and the " t axis" of the output. The product of the two functions is then integrated over all values of τ and the resulting value plotted along the output axis at $t = t'$. This procedure is followed for all values of t , giving the convolved output of Figure 1-3c. The frequency domain diagrams, located below the corresponding time domain plots, show how the amplitude spectrum of the input waveform is modified. The phase spectrum, not shown here, has also been altered. The transfer function $W(t)$ is referred to as the impulse response of the filter,

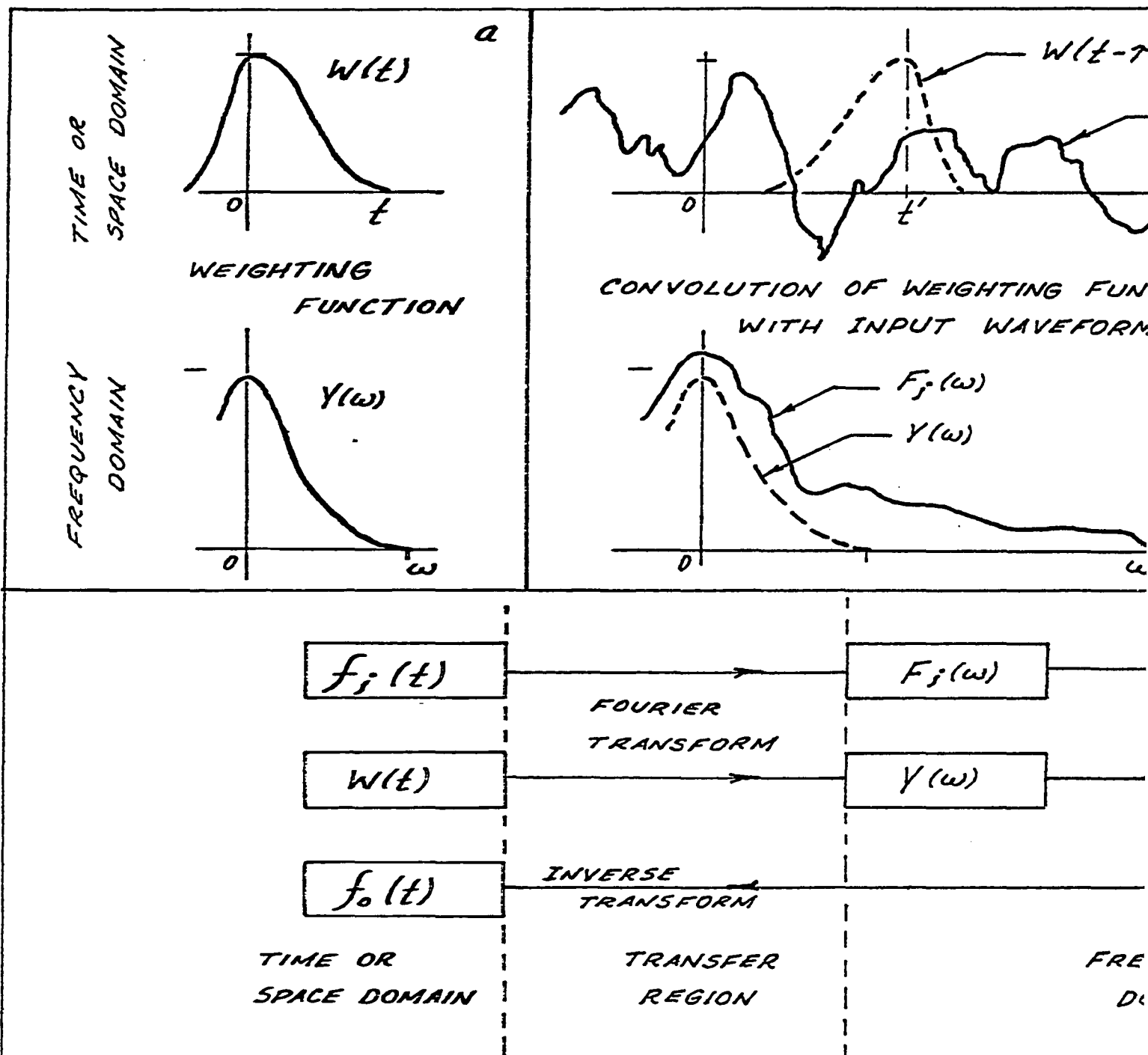
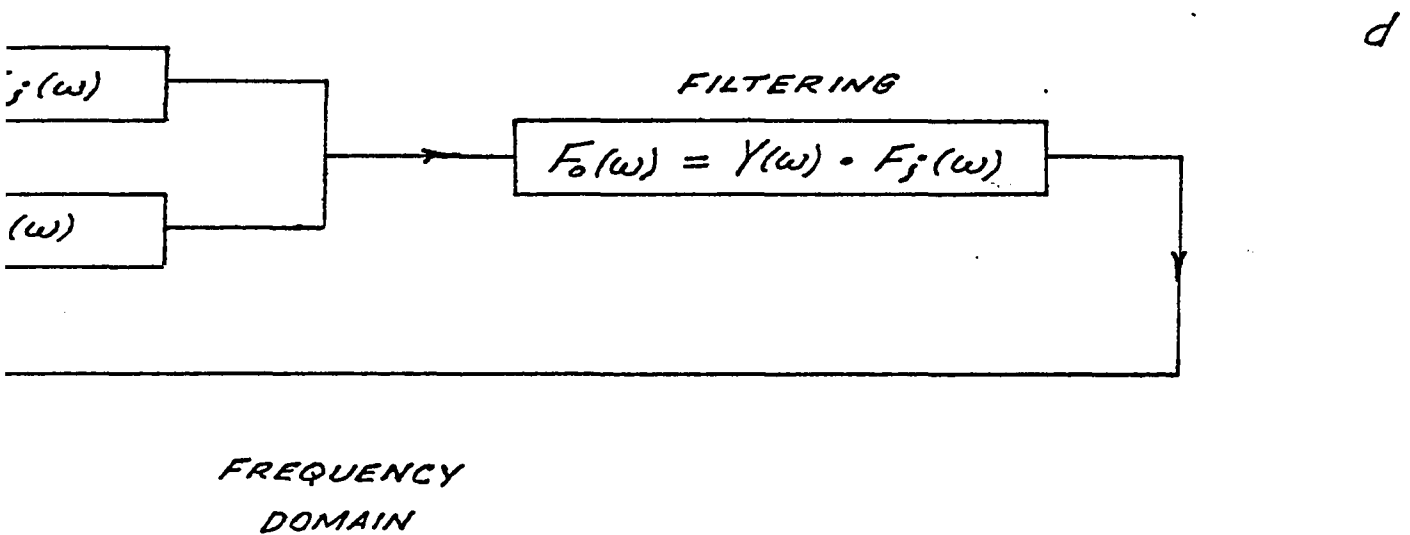
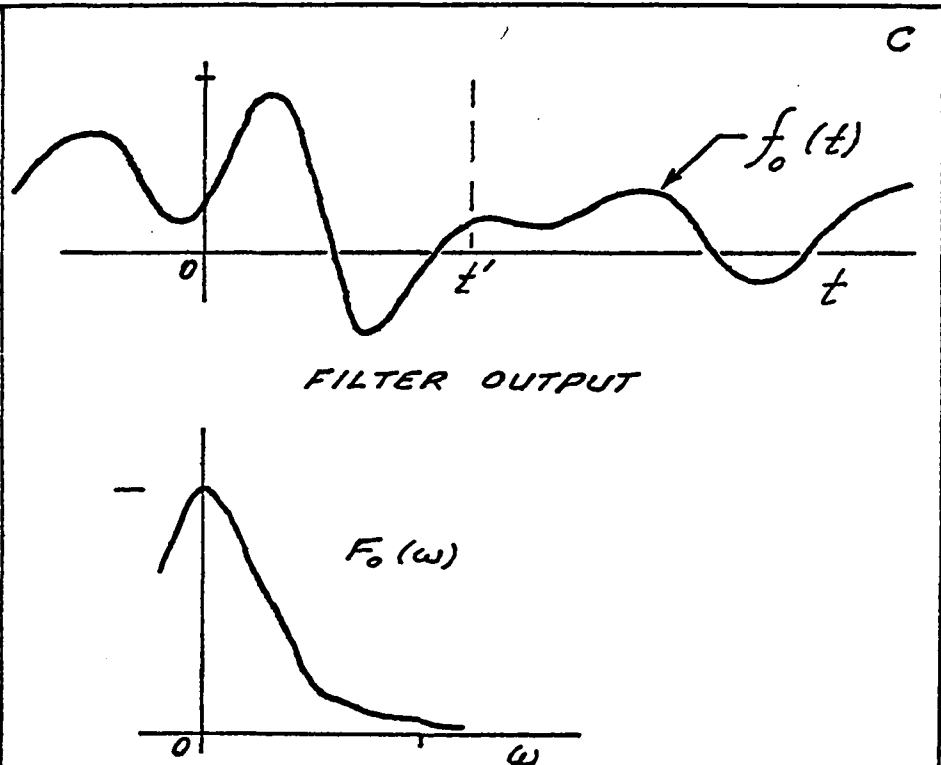
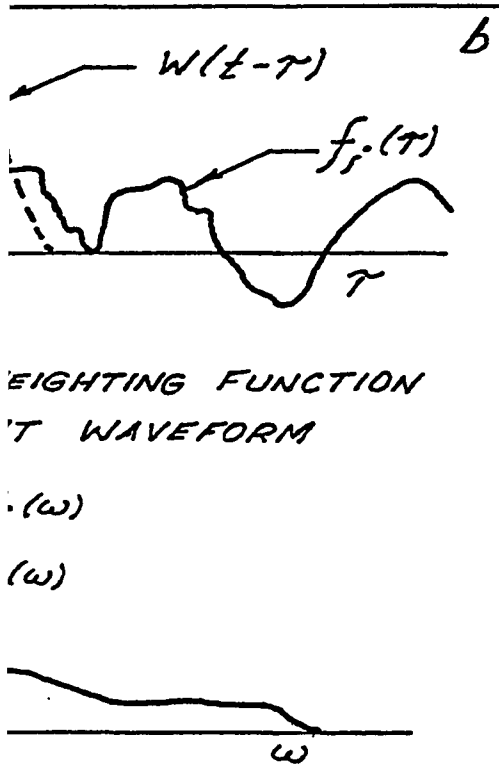


FIG.1-3: THE CONVOLUTION



EVOLUTION PROCESS

since convolution with a unit impulse as the input waveform gives:

$$f_o(t) = \int_{-\infty}^{\infty} \delta(\tau) W(t-\tau) d\tau = W(t)$$

where $\delta(t) = \begin{cases} 0 & t < 0 \\ 1 & t = 0 \\ 0 & t > 0 \end{cases}$ is the unit impulse. In the example of Figure 1-3, $W(t)$ may be considered the transfer function of a "smoothing filter", as high frequency components of $f_j(\tau)$ have been attenuated. Figure 1-3d is a schematic representation of a set of transform operations exactly equivalent to the convolution process.

In the filtering of electrical waveforms it is useful to think of the signal being directed through a stationary filter, since the output depends only on past and present values of the input. Filtering of space domain data, on the other hand, generally makes use of all surrounding information, and a "running filter" concept, as adopted in the foregoing description, would seem to be more appropriate. These two outlooks are exactly equivalent mathematically, since convolution is commutative; that is:

$$\int_{-\infty}^{\infty} f_j(\tau) W(t-\tau) d\tau = \int_{-\infty}^{\infty} W(\tau) f_j(t-\tau) d\tau$$

or $f * W = W * f$ where the asterisk denotes convolution.

The filtering of gridded potential field data, to be dealt with at some length in this thesis, will require the use of a

two-dimensional form of the convolution integral:

$$f_o(x, y) = \iint_{-\infty}^{\infty} f_i(\xi, \eta) W(x-\xi, y-\eta) d\xi d\eta \quad (1-28)$$

Autocorrelation and cross-correlation are two concepts closely related to the convolution integral and of considerable importance in spectral analysis. The autocorrelation function:

$$f_{AC}(t) = \int_{-\infty}^{\infty} f(\tau) f(\tau-t) d\tau \quad (1-29)$$

is similar to the convolution of a function with itself, except that there is no reversal before multiplication. In the time and space domains the autocorrelation of a real waveform is an even function, with the peak value occurring at the point $t = 0$. The frequency response of autocorrelation is the power spectrum of the input waveform. The cross-correlation function, given by:

$$f_{cc}(t) = \int_{-\infty}^{\infty} f(\tau) g(\tau-t) d\tau \quad (1-30)$$

is used to measure the degree of correlation between two waveforms $f(t)$ and $g(t)$. If the cross-correlation is characterized by a well-defined central peak at $t = t'$, the two functions are said to exhibit a high correlation at the point $\tau = t'$. Autocorrelation and cross-correlation are used extensively in the processing of seismic data, for such purposes as design of digital filters, power spectrum analyses, and trace correlation. Treatment of these subjects is given by Wadsworth, Robinson et Al. (1953) and Robinson and Treitel (1967). Cross-correlation

techniques have been applied to gravity and magnetic data to help bring out linear trends in geological structure.

Discrete Sampling of Continuous Waveforms

Up to this point the discussion has centered around spectrum analysis, as related to continuous or partially continuous functions. In many instances, observed functions are sampled at discrete points so that numerical methods of analysis might be employed. The use of digital recording in a wide variety of monitoring systems is a common example of high density, discrete sampling. Potential field surveys in geophysics are conducted by sampling the continuous field at discrete station points. Because of the importance of discrete sampling in many forms of analysis, its effects on the original function are of interest.

If a band-limited function $f(t)$ is sampled at n discrete, equally spaced points f_n , the Sampling Theorem states that a unique and exact reconstruction of $f(t)$ can be obtained from f_n , provided the sample interval is less than or equal to $1/2\omega_c$. The symbol ω_c denotes the frequency above which the amplitude spectrum of the band-limited function is zero. Figure 1-4a, page 31, shows a band-limited function and its amplitude spectrum. Discrete sampling of a function $f(t)$ is equivalent to multiplying the waveform by an infinite sequence of equally spaced unit impulses. The unit impulse sequence, shown in Figure 1-4b is denoted by:

$$III\left(\frac{t}{\tau}\right) = \sum_{n=-\infty}^{\infty} \delta\left(\frac{t-n}{\tau}\right)$$

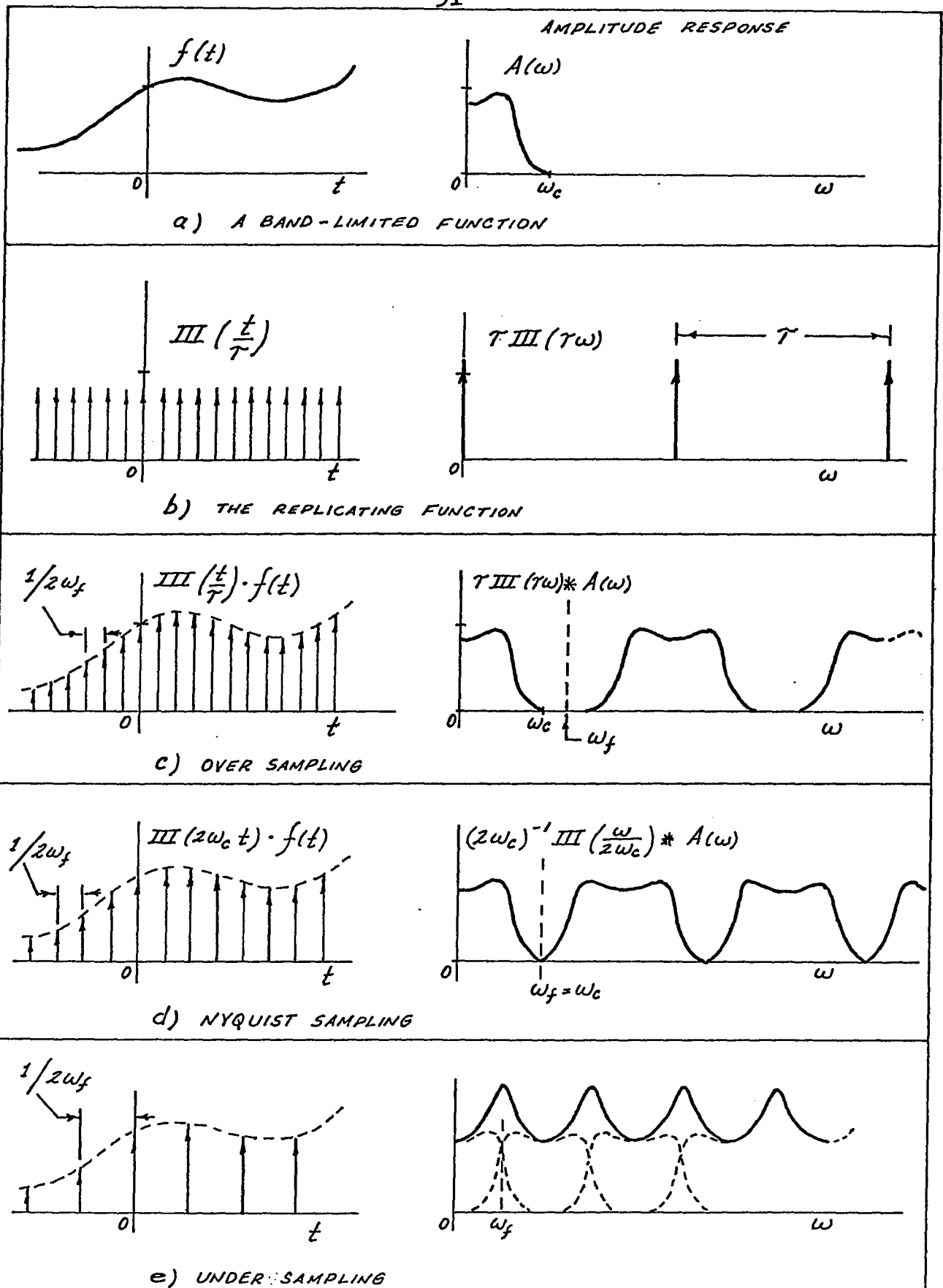


FIG. 1-4 : DISCRETE SAMPLING OF A
BAND-LIMITED FUNCTION.

and is referred to as the Replicating function. Its Fourier transform is a multiple of itself and may be written (Bracewell, 1965):

$$F\left\{\text{III}\left(\frac{t}{\tau}\right)\right\} = \tau \text{III}(\tau\omega)$$

Consequently, when $f(t)$ is sampled, its frequency spectrum $F(\omega)$ is convolved with an infinite sequence of impulses of spacing τ , causing replication of $F(\omega)$ at a period of $1/\omega_f$. The "folding frequency", ω_f , is the highest frequency which can be detected with a particular sample spacing Δs , and satisfies the following condition:

$$\omega_f = \frac{1}{2\Delta s}$$

The folding point ω_f is also known as the Nyquist frequency. It can be seen in Figures 1-4c and 1-4d that if ω_c , the band limit of the function, is less than or equal to ω_f the frequency response of $f(t)$ can be extracted from the periodic spectrum. If the sampling density is reduced past this limit, as in Figure 1-4e, the periodic reproductions of $F(\omega)$ overlap, causing distortion in the vicinity of the folding frequency. This is simply a restatement of the Sampling Theorem, in that the original spectrum of a sampled, band-limited function can be recovered if the sample density is adequate. The recovery process is called interpolation and consists of convolving the sample sequence f_n with the "sinc" function:

$$f(t) = f_n * \text{sinc}(2\omega_f t)$$

$$\text{where } \text{sinc}(x) = \frac{\sin(\pi x)}{\pi x}$$

Discrete sampling of continuous, semi-infinite functions, such as in digital waveform analysis or potential field surveys, must be restricted to a practical sample size. The abrupt termination or chopping-off of the function at the sample boundaries contributes high frequency, low amplitude components to the data. The presence of noise also contributes to the upper portion of the spectrum. For these reasons, such functions cannot generally be considered "band limited" when sampled. Even with relatively dense sampling, a substantial portion of high frequency noise may exist above the folding frequency, and thus, fold back on the lower spectrum. This distortion of the lower spectrum by frequency components above the folding point is called aliasing, and can be a serious problem in the sampling of noisy waveforms.

Selection of the sampling interval or station spacing in gravity and magnetic surveys is based largely on the size of target anomalies expected. If the frequency content of an anomaly is in the vicinity of the Nyquist or folding point, aliased noise could partially obscure the target. In such cases it might be advisable to increase the sample density. Figure 1-5, page 34, shows the effects of discrete sampling and truncation of a semi-infinite, continuous waveform.

The discrete sampling of two-dimensional waveforms is a direct extension of the one-dimensional case. The Replicating function over the x-y plane may be viewed as a "bed of nails", sampling over two-dimensional space.

Additional treatment of discrete sampling may be found in

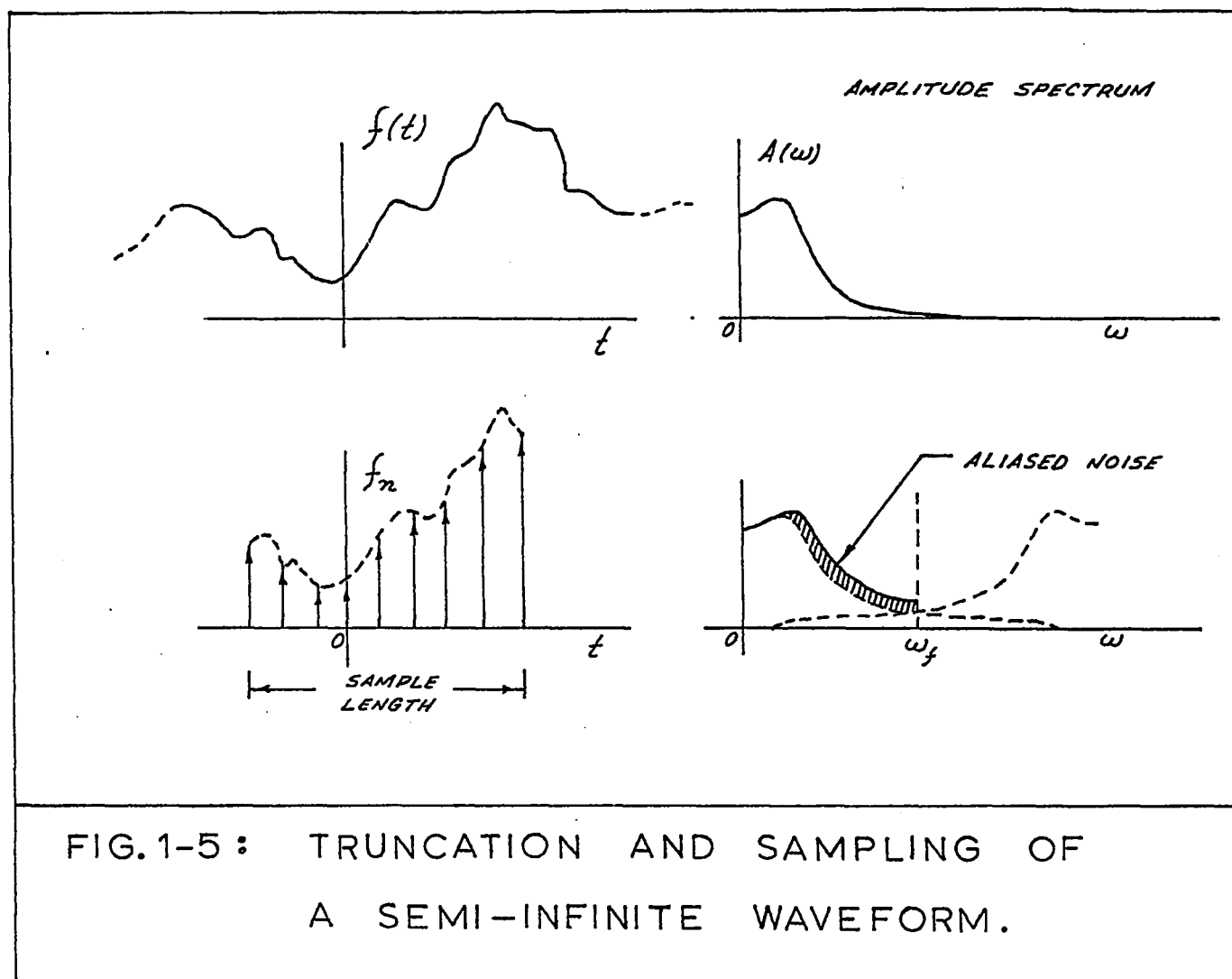


FIG.1-5: TRUNCATION AND SAMPLING OF
A SEMI-INFINITE WAVEFORM.

texts by Bracewell (1965, chap. 10) and Papoulis (1962, chap. 3).

1-3 Frequency Analysis of Potential Field Data

Variation of the earth's gravity or magnetic field over a horizontal survey plane has all the features of a continuous two-dimensional waveform. The total field can be visualized as a superposition of potential effects from individual mass elements. Sources just below the plane cause high frequency, local distortion, while deeper mass concentrations contribute most of the low frequency variation. Since the purpose of gravity and magnetic surveys in applied geophysics is to extract geological information from these potential field variations, frequency analysis of the data should prove useful.

Actually, the adoption of a frequency analysis approach to gravity and magnetic interpretation has a number of distinct advantages:

- 1) The size, shape, and location of potential field anomalies are waveform properties which can be conveniently represented in terms of spectral amplitude and phase response. The variation in anomaly frequency content provides a basis for source discrimination.

- 2) The well established body of Information theory, perfected and applied in electrical engineering and seismic processing, can be adapted to two-dimensional potential field data.

- 3) Frequency response is an exceedingly useful

criterion for the design and analysis of two-dimensional gridded operators.

4) Spectral analysis and filtering of discretely sampled data are well suited to digital processing techniques. Large quantities of data can therefore be handled in a relatively short time.

5) Finally, the added insight provided by another point of view is of great value in understanding the purpose and effects of various methods of data processing and interpretation.

Spectral Form of the Inverse Potential Problem

Separation of density or magnetic susceptibility variations on the basis of their potential field frequency expression is not a straightforward proposition. The most obvious reason, common to many forms of spectral investigation, is the spectral overlap of source disturbances. In dealing with potential fields, there is a more fundamental reason associated with the inverse potential problem. About any known distribution of mass there exists only one possible potential field. The inverse statement, however, is not true, in that any number of source configurations can be found to explain a certain potential expression. This inability to determine a unique source on the basis of observed potential field information is amply demonstrated in all phases of gravity and magnetic interpretation. The inverse potential problem, when reduced to simplest terms, means that effects of density (or magnetic susceptibility), depth and

shape of massive bodies cannot be separated simply by observing their gravity (or magnetic) anomalies. A simple illustration is sufficient to show how the frequency spectrum is affected. Consider two anomalous masses of approximately the same volume and density contrast, one a shallow, flat-lying, blanket-like body; the other a spherical body of greater depth. The potential field spectrum of the shallow anomaly would be characterized by a considerable portion of low frequency component by virtue of its blanket-like shape. The spherical body would also contribute significant low frequency response because of its greater depth. Thus, even though the two bodies are vastly different structurally, their low frequency components may be virtually impossible to separate.

Despite the ambiguity induced by the inverse potential problem and normal spectral overlap, a substantial degree of source discrimination is possible. High frequency distortion of a continuous potential field can result only from the presence of nearby sources, and it may be assumed, although with far less certainty, that low frequency distortion is more likely a result of distant masses. In applying these observations to discretely sampled potential field data, we must realize that sampling or station noise, coupled with the aliasing effect, contributes both high and low frequency distortion.

Potential Field Filtering

One of the first comments suggesting that certain processing techniques for gravity and magnetic data were similar to

waveform filtering was made by Nettleton (1954). The paper discussed separation of shallow residual anomalies from deep regional features. Dean (1958) discussed the advantages of exploiting frequency analysis in gravity and magnetic interpretation and provided theoretical background. A table of possible potential field filters is given on page 113 of his paper. Mesko (1965) considered frequency analysis as applied to gravity interpretation, while Darby and Davies (1967) presented methods for the analysis and design of two-dimensional filters. Examination of the frequency characteristics of previously published grid operators, as well as the design of new two-dimensional operators was undertaken by Fuller (1967).

Manipulation of gravity and magnetic data can take several forms, depending on the complexity of the potential field waveform, the purpose of the investigation, and the quality of the data. Discrimination between relatively high frequency, shallow effects (residual), and the more gradational, deeper trends (regional) is generally termed regional-residual separation. This may be accomplished graphically on contoured data or by the application of coefficient sets (refer to Nettleton, 1954). In areas of poor residual definition superimposed over a complex or predominant regional, second vertical derivative or continuation methods might be used to amplify the higher frequency features. Techniques are also available for delineation of trends in the data which may reflect important geological controls. These and other interpretational aids can be

considered filtering operations. To demonstrate this fact, consider the previously derived continuation integral, equation 1-14, page 20:

$$\Delta g_p = \frac{z}{2\pi} \iint_{-\infty}^{\infty} \frac{\Delta g(\xi, \eta) d\xi d\eta}{[(x-\xi)^2 + (y-\eta)^2 + z^2]^{3/2}} \quad (1-14)$$

This relation can be expressed in the form of the convolution integral, equation 1-28, page 29:

$$\Delta g_p = \iint_{-\infty}^{\infty} \Delta g(\xi, \eta) \cdot W(x-\xi, y-\eta) d\xi d\eta$$

where Δg_p , the upward continued gravity effect, is the filter output, $\Delta g(\xi, \eta)$ is the observed gravity data or input waveform, and

$$W(x-\xi, y-\eta) = \frac{z/2\pi}{[(x-\xi)^2 + (y-\eta)^2 + z^2]^{3/2}}$$

is the filter weighting function. If the Fourier transform is taken for each side of equation 1-14, we obtain (refer to Grant and West, 1965, page 218):

$$\iint_{-\infty}^{\infty} \Delta g_p e^{-j2\pi(ux+vy)} dx dy = e^{-2\pi z \sqrt{u^2+v^2}} \iint_{-\infty}^{\infty} \Delta g(\xi, \eta) e^{-j2\pi(u\xi+v\eta)} d\xi d\eta$$

$$\text{or} \quad F_{up}(u, v) = e^{-2\pi z \sqrt{u^2+v^2}} \cdot F_D(u, v) \quad (1-31)$$

where $F_{up}(u, v)$ and $F_D(u, v)$ are the Fourier transforms of the upward continuation output and the input data, respectively, and z is the height of continuation. If we invert the process and seek to obtain the downward continued field $\Delta g(\xi, \eta)$, the

corresponding transform relation obviously becomes:

$$F_D(u, v) = e^{2\pi z \sqrt{u^2 + v^2}} \cdot F_{UP}(u, v) \quad (1-32)$$

Equations 1-31 and 1-32 show that upward and downward continuation of potential fields are actually filtering operations, each exhibiting a definite frequency response:

$$\text{upward continuation : } Y_{UP}(u, v) = e^{-2\pi z \sqrt{u^2 + v^2}} \quad (1-33)$$

$$\text{downward continuation: } Y_D(u, v) = e^{2\pi z \sqrt{u^2 + v^2}}$$

The design of two-dimensional discrete filters will be the subject of Chapter 2.

DESCRIPTION AND DESIGN OF TWO-DIMENSIONAL POTENTIAL FIELD FILTERS

2-1 Characteristics of Some Potential Field Operators

The use of potential field operators is not new to gravity and magnetic interpretation. In the past, their derivation and application were confined to the space domain and computations were done by hand. Consequently, the filtering aspects of potential field modifications were either poorly understood or ignored altogether. In recent years, greater access to digital computers and increased awareness of the importance of spectral analysis in operator design have substantially altered the approach.

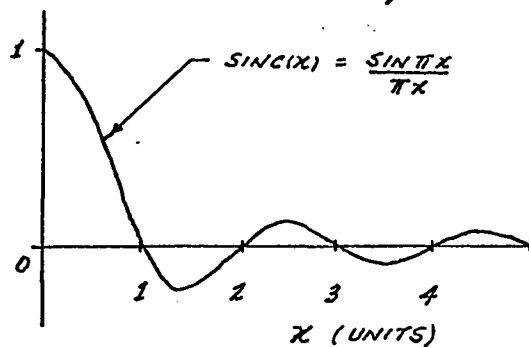
In this section, space and spectral properties of several important potential field operators will be described, and their significance to potential field data discussed.

Wavelength or Boxcar Filter

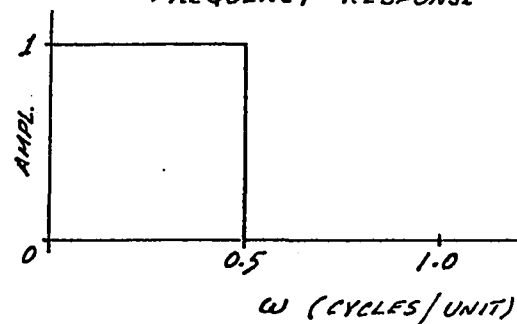
The wavelength filter, in its various forms, may be considered analogous to standard electrical filters of the high-pass, low-pass, and band-pass types. The one-dimensional form of the continuous wavelength filter is the "sinc" or interpolating function shown in Figure 2-1a, page 42. Its amplitude spectrum shows a cut-off at 0.5 cycles/unit, where the "unit" is measured along the space domain axis. The two-dimensional extension of the sinc function:

$$\text{sinc}(x) \cdot \text{sinc}(y) = \frac{\sin(\pi x) \cdot \sin(\pi y)}{\pi^2 xy}$$

Q) ONE - DIMENSIONAL



FREQUENCY RESPONSE



b) TWO - DIMENSIONAL

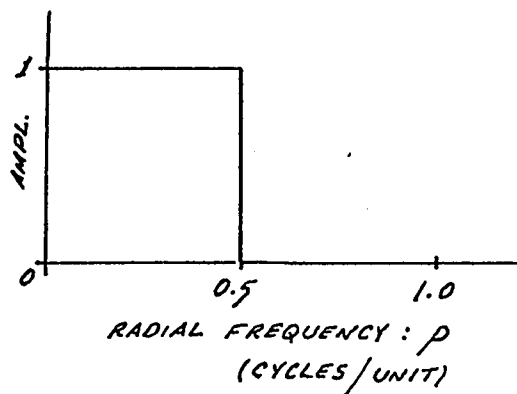
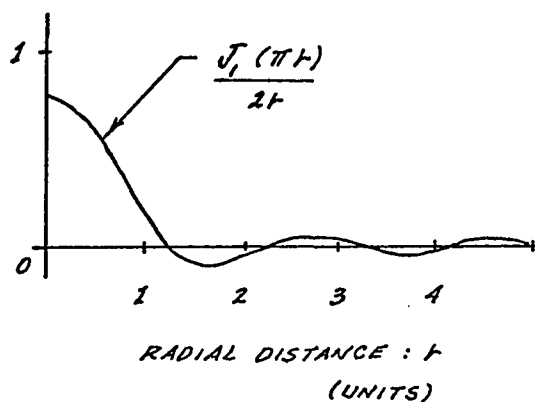


FIG. 2-1: IDEAL WAVELENGTH FILTERS

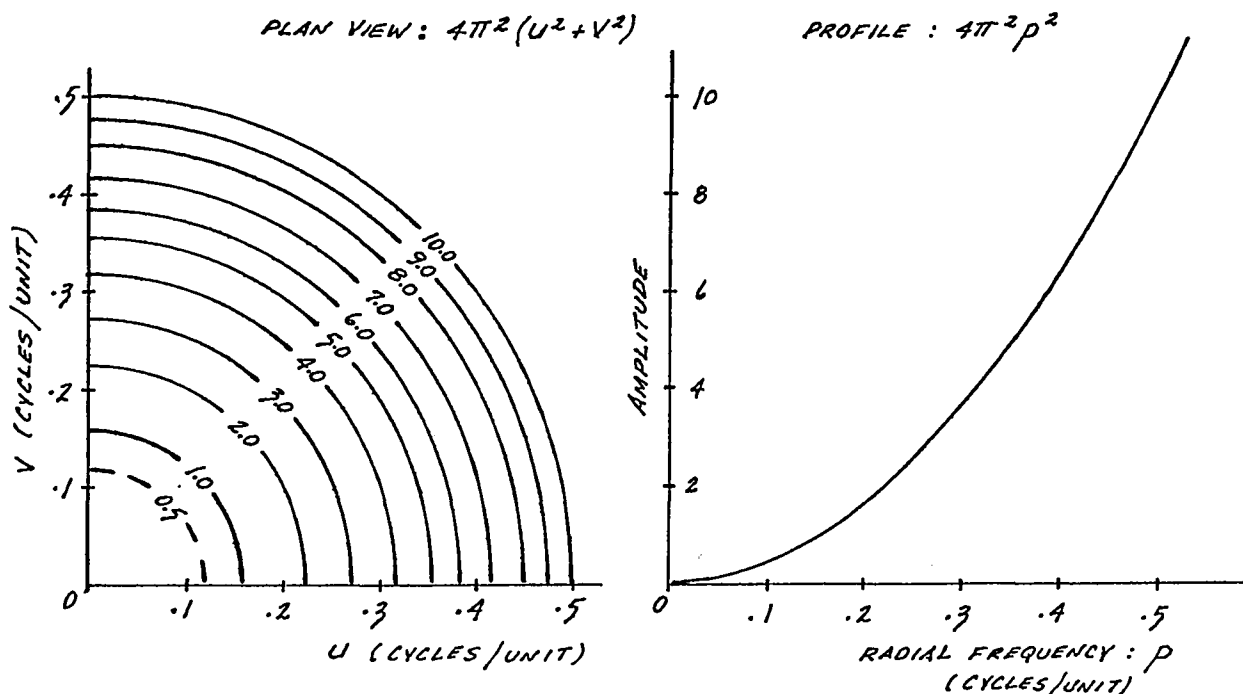


FIG. 2-2: THEORETICAL FREQUENCY RESPONSE OF THE SECOND VERTICAL DERIVATIVE

does not exhibit circular symmetry in the frequency domain and therefore proves inconvenient as a two-dimensional wavelength filter. Zerflueh (1967) made use of this cartesian form and found it necessary to apply trial and error smoothing to approach circular symmetry. The author has found that the use of an attenuated Bessel function of first order and kind is a more useful approach, since its Hankel transform, and therefore frequency response, is:

$$2\pi \int_{r=0}^{\infty} \left[\frac{J_1(\pi r)}{2r} \right] \cdot J_0(2\pi \rho r) r dr = \begin{cases} 1 & \text{FOR } \rho < 0.5 \text{ CYCLES/UNIT} \\ 1/2 & \text{FOR } \rho = 0.5 \quad " \\ 0 & \text{FOR } \rho > 0.5 \quad " \end{cases} \quad (2-1)$$

where r is radial distance over two-dimensional space, ρ is radial frequency, and J_0 and J_1 represent the zero-order and first-order Bessel functions of first kind. The proof of relation 2-1 is given in Appendix A1, page 123. Figure 2-1b, page 42, shows a radial profile of the two-dimensional wavelength operator and its frequency response.

Because addition in the space domain is equivalent to addition in the frequency domain, i.e.

$$F \left\{ f_1 + f_2 \right\} = F_1(\omega) + F_2(\omega)$$

where F denotes the Fourier transform, the conversion of the fundamental wavelength or boxcar filter to band-pass and high-pass versions is a simple process. The subtraction of two low-pass filters of different cut-off frequencies, ρ_1 and ρ_2 , results in a band-pass operator of bandwidth $\rho_2 - \rho_1$. A high-pass filter can be obtained by subtracting the standard wave-

length or low-pass filter from a unit impulse δ , since the frequency response of the unit impulse is unity for all wavelengths. The versatility and design possibilities demonstrated by the standard wavelength filter will be of considerable value in two-dimensional potential field filtering.

An obvious application of the wavelength filter is in regional-residual separation of gravity and magnetic data. Its success in this role would depend on the degree of discrimination between regional and residual spectrums. Where local conditions or sampling errors contribute a high noise level to the potential field, the flexibility of the wavelength filter allows derivation of a convenient smoothing function. Griffin (1949), Nettleton (1954), and others have discussed the use of operators for regional removal from gravity and magnetic data. Except for the operators suggested by Zerflueh (1967) most are only poor approximations to the wavelength filter. With the present availability of digital computers, discrete versions of the continuous wavelength filter can be convolved with potential field data to give a more realistic output.

The Second Vertical Derivative

A strong gravity or magnetic regional trend may partially conceal or camouflage the high frequency residual information of shallower sources. Even though these shallow effects may not be obvious on a contoured map, vertical derivatives of the observed field will detect and amplify them with respect to the deeper features. Vertical derivative methods can therefore be

likened to high-gain, high-pass filters.

The second vertical derivative is generally favored over the first and higher vertical derivatives for several reasons. It is a more convenient filter both in terms of derivation and the interpretation of its output. Although quantitative evaluation of derivative results is not practical in itself, the second vertical derivative output bears a strong resemblance to a residual map. A well-designed second derivative operator should be capable of amplifying most of the useful high frequency information without requiring the excessively large gains of higher orders. In addition, the amount of noise induced by the calculation process increases with derivative order, so that higher derivatives are just as likely to obscure as enhance geological information. Odd order derivatives, like the first vertical derivative, have been used to bring out gradient features of the gravity or magnetic field, but their results are difficult to interpret.

If we assume that the gravity or magnetic force field $f(\xi, \eta)$, over a horizontal survey plane, is harmonic and therefore obeys Laplace's equation:

$$\frac{\partial^2 f(\xi, \eta)}{\partial \xi^2} + \frac{\partial^2 f(\xi, \eta)}{\partial \eta^2} = 0$$

then, the second vertical derivative of the waveform can be obtained directly as:

$$\frac{\partial^2 f(\xi, \eta)}{\partial \xi^2} = - \left(\frac{\partial^2}{\partial \eta^2} + \frac{\partial^2}{\partial \xi^2} \right) f(\xi, \eta) \quad (2-2)$$

Taking the Fourier transform of both sides of equation 2-2, we find:

$$F \left\{ \frac{\partial^2 f(\xi, \eta)}{\partial z^2} \right\} = 4\pi^2 (u^2 + v^2) \cdot F(u, v) \quad (2-3)$$

where $F(u, v)$ is the Fourier transform of the potential field waveform $f(\xi, \eta)$. Obtaining the second vertical derivative is therefore equivalent to applying a filter of frequency response:

$$Y(u, v) = 4\pi^2 (u^2 + v^2)$$

Figure 2-2, page 42, shows the theoretical second derivative frequency response both in plan and profile. Only the first quadrant of the amplitude response is shown since it is circularly symmetric.

Peters (1949), Henderson and Zietz (1949), Elkins (1951), and Rosenbach (1953) have dealt with the second vertical derivative as a space domain operator, while Darby and Davies (1967) have considered both its space and spectral properties.

Continuation Operators

The filtering properties of upward and downward continuation were derived in section 1-3 and are summarized in equations 1-31 to 1-33. The frequency response of upward continuation:

$$Y_{up} = e^{-2\pi z \sqrt{u^2 + v^2}}$$

may be termed high frequency rejection. The downward continuation operator is basically a high frequency amplifier, with response:

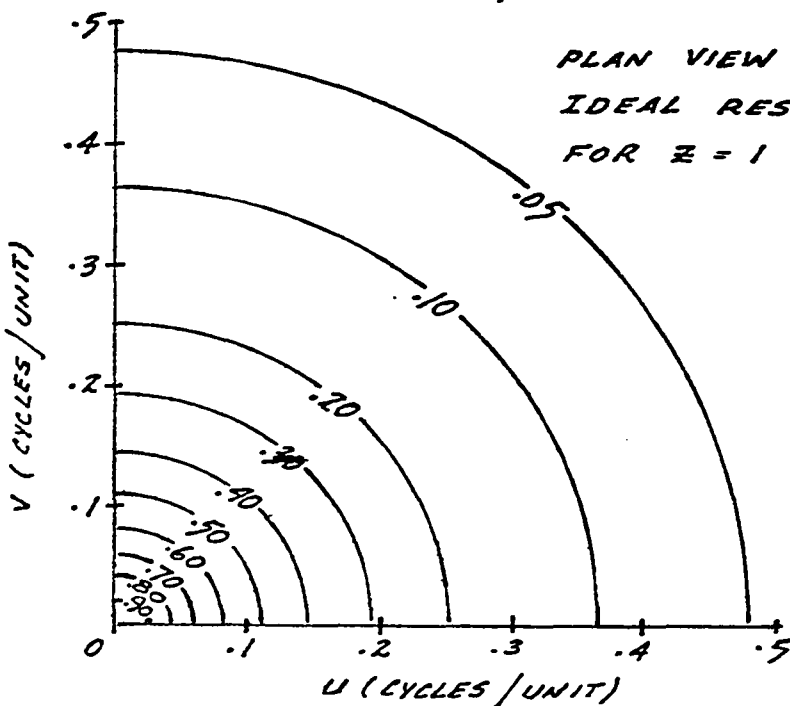
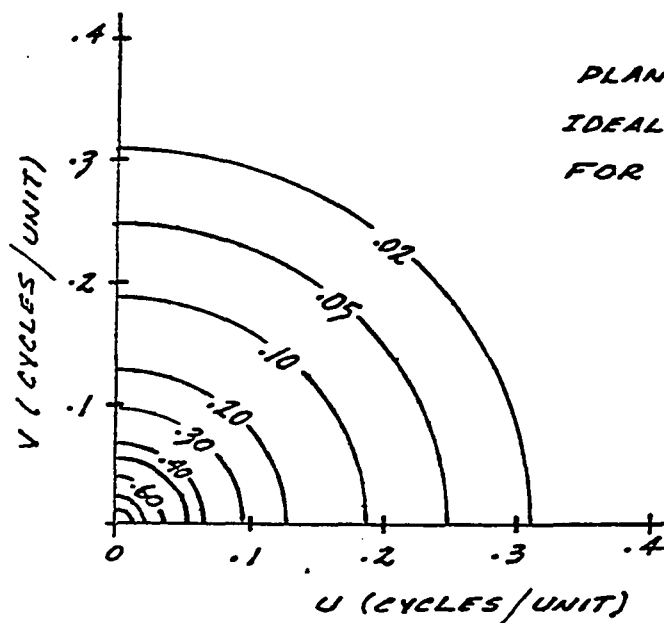
$$Y_d = e^{2\pi z \sqrt{u^2 + v^2}}$$

In both cases, z is the distance of continuation and u and v are the frequencies in the x and y cartesian directions.

Figures 2-3 and 2-4, pages 48 and 49, give plan and profile views of these theoretical frequency functions.

The continuation of potential fields has received a substantial amount of attention in geophysical literature. Classical papers by Bullard and Cooper (1948), Peters (1949), and Henderson (1960) provide ample background as well as several space domain methods of operator design. Dean (1958) and Fuller (1967) approach the design problem by an alternate route, making use of the theoretical frequency responses given above.

Upward and downward continuation, unlike most other potential field operations, have an inherent physical significance, since they map the field changes involved in movement away from or toward source distributions. The main constraint on this process is that the region of continuation be harmonic. The ability to project the observed gravity or magnetic field above or below a survey plane would be a valuable asset to the interpreting geophysicist, and this fact probably accounts for the popularity of the continuation concept. Although a good approximation to the upward continuation process can be obtained with very little difficulty, the inverse operation, that of downward continuation, is greatly affected by the noise content in data and the presence of unknown density or magnetic susceptibility changes in the region. These factors, coupled with several operator design problems, must be taken into account when deriving or applying a practical downward continuation operator. The assumptions and procedures involved in the derivation of the

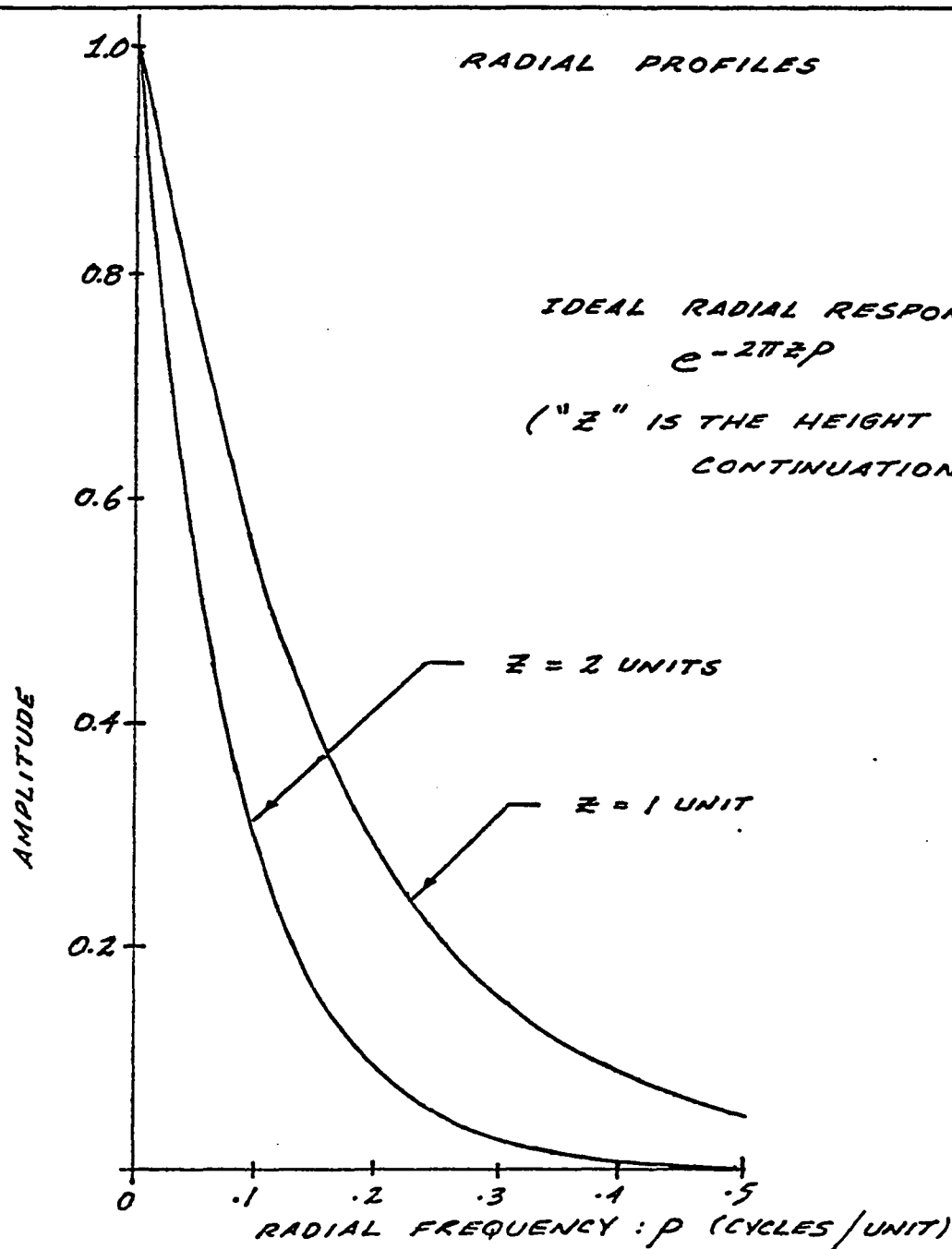


AMPLITUDE

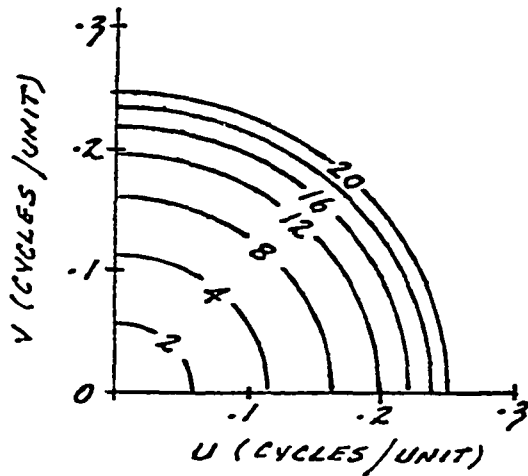
FIG. 2-3: THEORETICAL FREQUENCY RESPONSE OF UPWARD CONTINUATION

$$e^{-2\pi z \sqrt{U^2 + V^2}}$$

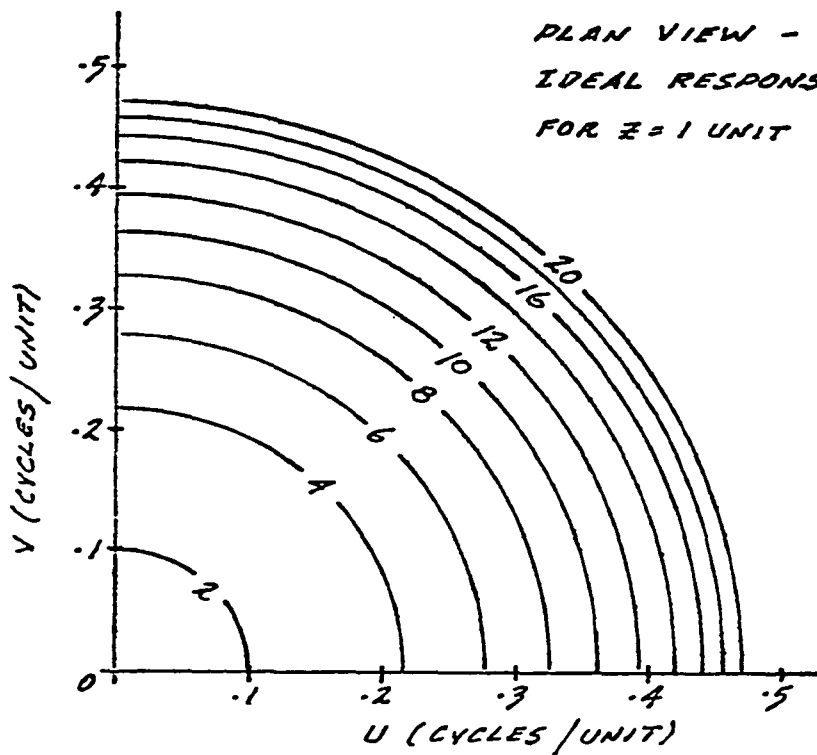
$$e^{-2\pi z \sqrt{U^2 + V^2}}$$



FREQUENCY RESPONSE
 CONTINUATION



PLAN VIEW -
 IDEAL RESPONSE: $e^{2\pi z \sqrt{U^2 + V^2}}$
 FOR $z = 2$ UNITS



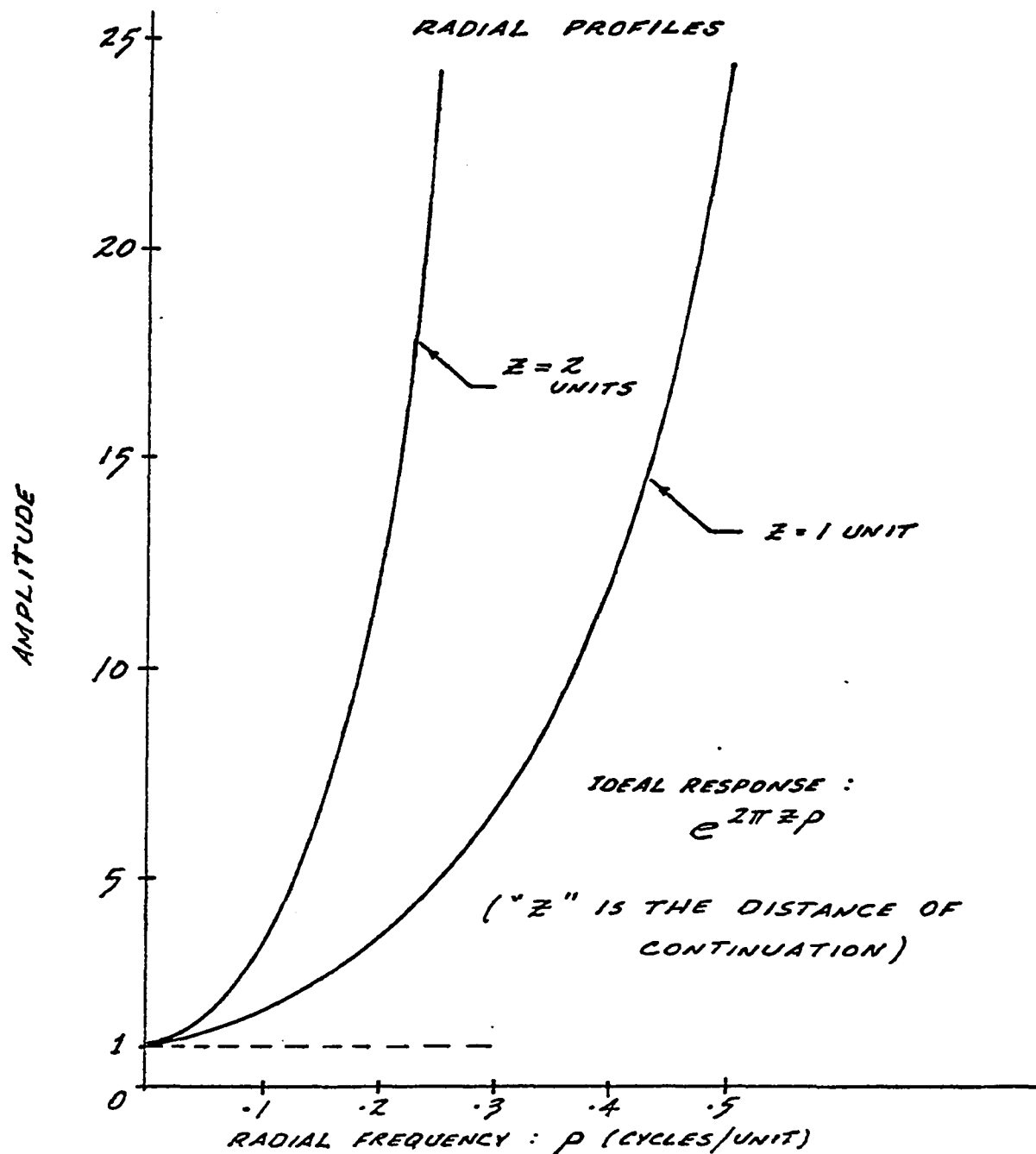
PLAN VIEW -
 IDEAL RESPONSE: $e^{2\pi z \sqrt{U^2 + V^2}}$
 FOR $z = 1$ UNIT

AMPLITUDE

FIG. 2-4: THEORETICAL FREQUENCY R
 OF DOWNWARD CONTINUATIC

$$\sqrt{u^2 + v^2}$$

$$\sqrt{1^2 + v^2}$$



EQUENCY RESPONSE
CONTINUATION

continuation integral have already been considered in section 1-1 (pages 19 to 21).

Before proceeding to design considerations, it might be instructive to comment on the circular symmetry exhibited by the above operators, both in the space and frequency domains. The phase and directional properties of the potential field spectrum define the location and orientation of source anomalies. The purpose of the filters described above is to modify only the amplitude spectrum of the gravity and magnetic data, leaving location and trend information undisturbed. The operators must therefore have a phase response of zero and a circularly symmetric amplitude spectrum. The space domain expression, or impulse response, of the filter will also exhibit circular symmetry under these conditions, as required by the inverse Hankel transform. Operators capable of phase and trend modifications, although not discussed in this thesis, can be developed for more specialized interpretational schemes.

Space and spectral properties of some potential field operators are summarized in Table 1, page 51. The list is intended to serve as a guide in the discussions to follow and in no way represents an exhaustive documentation of the filter possibilities.

2-2 Filter Representation and Design

Operators for Discrete Data

The mathematical concepts of Information theory must be

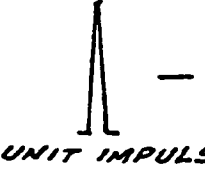
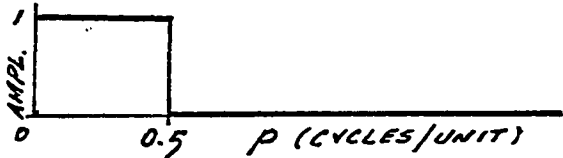

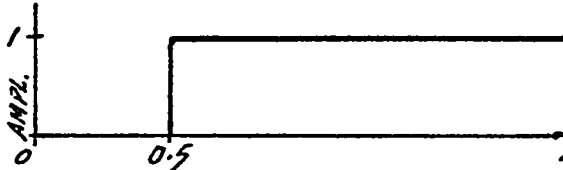
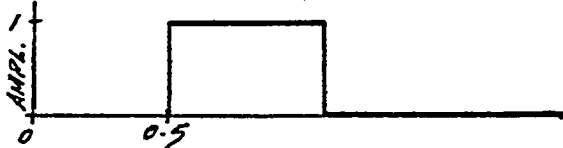
<i>FILTER</i>	<i>PURPOSE</i>	<i>TWO-DIMENSIONAL WEIGHTING</i>
<i>WAVELENGTH</i> <i>LOW-PASS</i> <i>HIGH-PASS</i> <i>BAND-PASS</i>	<i>NOISE FILTERING AND RESIDUAL REMOVAL</i>	J_1
	<i>REGIONAL REMOVAL</i>	
	<i>ATTENUATION OF HIGH AND LOW FREQUENCY EFFECTS</i>	$\frac{J_1(\pi f')}{2f'}$
<i>SECOND VERTICAL DERIVATIVE</i>	<i>HIGH FREQUENCY (RESIDUAL) AMPLIFICATION AND LOW FREQUENCY REJECTION.</i>	$\frac{\partial^2}{\partial z^2} =$
<i>UPWARD CONTINUATION</i>	<i>HIGH FREQUENCY ATTENUATION AS A RESULT OF POTENTIAL FIELD EXPANSION AWAY FROM THE SOURCE DISTRIBUTION</i>	$(\chi^2 +$
<i>DOWNWARD CONTINUATION</i>	<i>HIGH FREQUENCY AMPLIFICATION OF THE POTENTIAL FIELD INVOLVED IN MOVEMENT TOWARDS A SOURCE DISTRIBUTION.</i>	$2\pi \int_{p=0}^{\infty} e^{2\pi i p z}$

TABLE 1 : SPACE AND SPECTRAL PROPERTIES OF POTENTIAL FIELD OPERATORS

	TWO-DIMENSIONAL WEIGHTING FUNCTION	RADIAL FREQUENCY RESPONSE
	$\frac{J_1(\pi r)}{2r}$	
	 $- \frac{J_1(\pi r)}{2r}$ UNIT IMPULSE	
	$\frac{J_1(\pi r')}{2r'} - \frac{J_1(\pi r)}{2r}$	
FREQUENCY	$\frac{\partial^2}{\partial z^2} = - \left(\frac{\partial^2}{\partial x^2} + \frac{\partial^2}{\partial y^2} \right)$	$Y(u,v) = 4\pi^2(u^2 + v^2) = 4\pi^2 p^2$
CONTINUATION FROM V	$\frac{z/2\pi}{(x^2 + y^2 + z^2)^{3/2}}$	$Y_{UP}(u,v) = e^{-2\pi z \sqrt{u^2 + v^2}} = e^{-2\pi z p}$ "z" IS THE HEIGHT OF CONTINUATION, AND "p" IS THE RADIAL FREQUENCY.
CONTINUATION FROM U	$2\pi \int_0^\infty e^{2\pi z p} J_0(2\pi p r) p dp$	$Y_D(u,v) = e^{2\pi z \sqrt{u^2 + v^2}} = e^{2\pi z p}$ "z" IS THE DISTANCE OF CONTINUATION, AND "p" IS THE RADIAL FREQUENCY.

GENERAL PROPERTIES OF SOME OPERATORS

reduced to numerical forms capable of handling digitized data. The data itself is assumed to be defined at each grid point of a two-dimensional cartesian system. If the potential field has not been uniformly sampled, the required grid values can be interpolated from a contour map of the original survey. The two-dimensional convolution integral, equation 1-28, page 29, may be approximated numerically by:

$$f_o(x, y) = \sum_{m=-M}^M \sum_{n=-N}^N C_{mn} f_j(m \Delta x, n \Delta y) \Delta x \Delta y \quad (2-4)$$

where $C_{mn} = W(x-m\Delta x, y-n\Delta y)$ is a set of coefficients representing the filter weighting function at $2M \times 2N$ discrete points, $\pm M$ and $\pm N$ representing the survey limits. The two-dimensional Fourier and inverse Fourier transforms may be represented by the numerical forms:

$$F(u, v) = \sum_{m=-M}^M \sum_{n=-N}^N f(m \Delta x, n \Delta y) e^{-j2\pi(um \Delta x + vn \Delta y) \Delta x \Delta y} \quad (2-5)$$

$$f(x, y) = \sum_{k=-K}^K \sum_{l=-L}^L F(k \Delta u, l \Delta v) e^{j2\pi(xk \Delta u + yl \Delta v) \Delta u \Delta v} \quad (2-6)$$

The numerical equivalents of the zero-order Hankel and inverse Hankel transforms (equations 1-24 and 1-25, page 24) are:

$$F(\rho) = 2\pi \sum_{m=0}^M f(m \Delta r) J_0(2\pi \rho m \Delta r) m (\Delta r)^2 \quad (2-7)$$

$$f(r) = 2\pi \sum_{k=0}^K F(k \Delta \rho) J_0(2\pi k \Delta \rho r) k (\Delta \rho)^2 \quad (2-8)$$

In the above equations Δx , Δy and Δf are increments of distance bounded by the limits $\pm M$ and $\pm N$. Similarly, Δu , Δv , and $\Delta \rho$ are increments of frequency within the limits $\pm K$ and $\pm L$.

The operators used in digital convolution are in the form of coefficient sets. Each coefficient C_{ij} defines the filter's weighting function or impulse response at the particular grid point (i, j) . The summation of coefficient-data products in equation 2-4, page 52, is a numerical approximation of the convolution process. Equation 2-5 can be used to examine the two-dimensional frequency response of a certain coefficient set, while equations 2-7 and 2-8 will be of value in operator design.

It is probably unnecessary to point out the great importance numerical analysis assumes in all phases of engineering and applied mathematics. Where large amounts of data must be processed on digital computers, or when mathematical operations cannot be conveniently handled analytically, numerical methods are generally applicable. Care must be taken, however, to understand all the implications involved in going from the exact problem to the numerical approximation. The folding frequency and aliasing effects, noted previously in the discrete sampling of continuous waveforms, are examples of numerically induced disturbances. Successful application of numerical methods depends on the recognition of certain advantages, and at the same time, a thorough understanding of the inherent limitations.

Analytical Design Methods

If the criteria for operator design are restricted to the space domain they will be termed analytic. Although this usage might be somewhat ambiguous, it is meant to distinguish between direct numerical derivation in the space domain and transform methods, which make use of spectral properties.

Regional-residual operators developed and used in the past were more empirical than analytical. The simplest consist of a single ring, of some preselected radius, around which the gravity or magnetic values are averaged. The average is taken as the regional, and when subtracted from the value at the center point gives the "residual effect" at that point. It is apparent that results will depend largely on the circle radius selected and the complexity of the potential field. Further information on the center point, single ring operator is given by Griffin (1949) and Nettleton (1954).

The wavelength operator introduced in section 2-1 is well suited to the analytical derivation of coefficient sets. Once the areal extent of the operator has been fixed by selecting the desired cut-off frequency, the required coefficient set can be obtained by simply evaluating the following function at each grid point:

$$C_{mn} = \frac{S \int_0^S \left(\frac{\pi}{S} \sqrt{m^2 + n^2} \right)}{2 \sqrt{m^2 + n^2}} \quad (2-9)$$

where C_{jj} is the coefficient at grid point (j, j) and

$S = D.I. / 2f_{co}$ is a scale factor, D.I. being the grid spacing

or data interval, and f_{co} the cut-off frequency in cycles/D.I. The symbol $J_1(\)$ represents the first-order Bessel function of first kind.

In designing high-pass operators the standard wavelength filter is merely inverted. Figure 2-5b, page 56, shows that the sinc function approaches the unit impulse as the distance Δx approaches zero. The discrete unit impulse, however, is exactly equivalent to the grid-sampled sinc function (see Figure 2-5c), and accordingly, like the continuous impulse, exhibits a response of unity in the frequency domain. In a similar manner it can be shown that the two-dimensional discrete unit impulse, defined by the function:

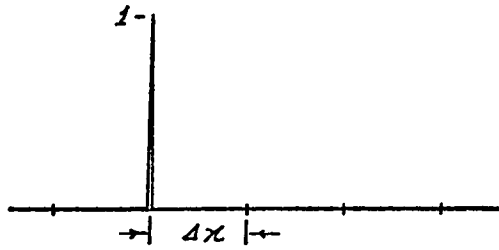
$$I(m,n) = \frac{\sin(\pi m \Delta x) \cdot \sin(\pi n \Delta y)}{\pi^2 m n \Delta x \Delta y}$$

where $\Delta x = \Delta y$ is usually set equal to 1 unit, has a frequency response of unity over the u-v frequency plane. The inverse or high-pass operator, as shown in Figure 2-5e, page 56, is the difference between the discrete unit impulse and the corresponding wavelength or low-pass operator.

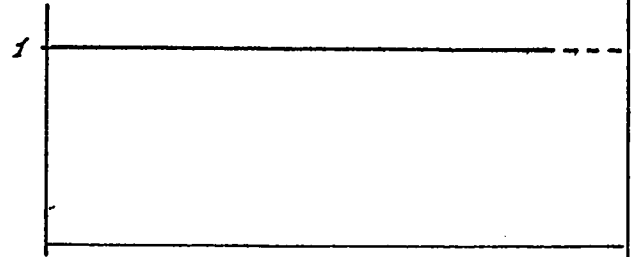
Band-pass filters may be obtained by subtracting two wavelength operators of different frequency cut-offs.

Numerical methods proposed for the approximation of derivative and continuation operations generally fall into one of two categories. Direct approximation of the convolution integral might be attempted whenever the two-dimensional expression can be conveniently reduced to a one-dimensional form. Another

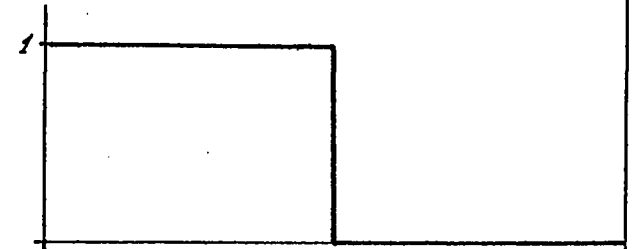
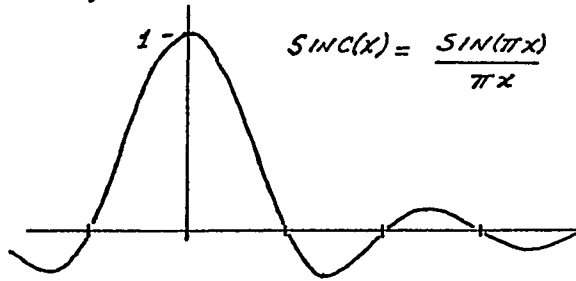
a) THE UNIT IMPULSE



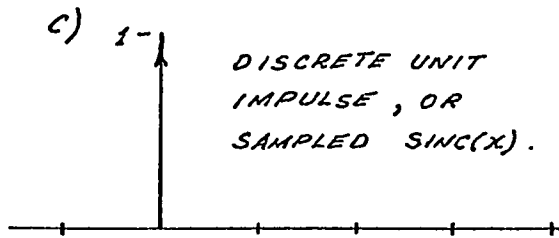
AMPLITUDE RESPONSE



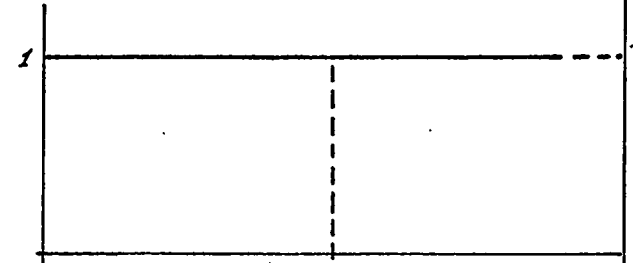
b)



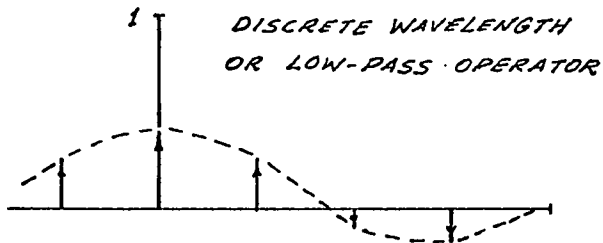
c)



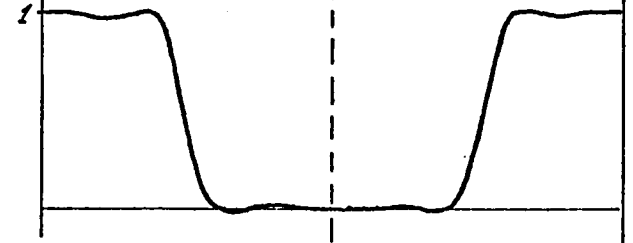
DISCRETE UNIT
IMPULSE, OR
SAMPLED $\text{sinc}(x)$.



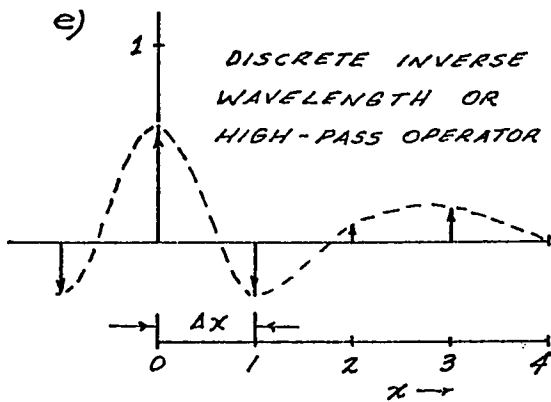
d)



DISCRETE WAVELENGTH
OR LOW-PASS OPERATOR



e)



DISCRETE INVERSE
WAVELENGTH OR
HIGH-PASS OPERATOR

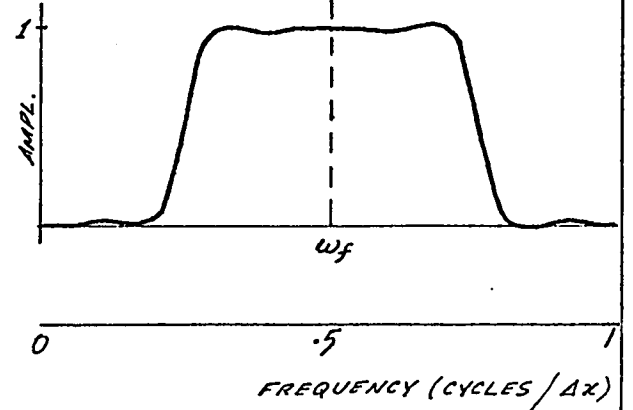


FIG. 2-5: INVERSION OF WAVELENGTH FILTER

approach which has been applied in the derivation of continuation and derivative operators, expands the potential field in vertical or horizontal directions according to Taylor's theorem. In view of the emphasis given analytical techniques of operator design in the literature, a brief description of several methods and resulting operators will follow. Although the hand calculation schemes proposed are, by modern standards, outdated, the numerical concepts involved in the development of these "template operators" are both interesting and instructive.

In a well-known paper, Peters (1949) described methods for executing continuation and derivative operations as related to magnetic interpretation. Introducing polar co-ordinates and averaging the data on circles about the operator origin, the continuation integral assumes a one-dimensional form:

$$f(x, y, -h) = \int_0^{\infty} \frac{\bar{f}(r) h r dr}{(h^2 + r^2)^{3/2}} \quad (2-10)$$

where $\bar{f}(r) = \frac{1}{2\pi} \int_0^{2\pi} f(r, \theta) d\theta$, $f(r, \theta)$ is the observed potential field data expressed in polar co-ordinates, and $f(x, y, -h)$ represents the upward continued value of the field to a height h . With the point $(x, y, 0)$ as operator origin, Peters selected nine circles varying in radius from $r_1 = 1$ to $r_9 = \sqrt{125}$ grid units and approximated the integral of equation 2-10 by the sum:

$$f(x, y, -h) = \frac{\bar{f}(r_0) + \bar{f}(r_1)}{2} \int_0^{r_1} \frac{h r dr}{(h^2 + r^2)^{3/2}} + \frac{\bar{f}(r_1) + \bar{f}(r_2)}{2} \int_{r_1}^{r_2} \frac{h r dr}{(h^2 + r^2)^{3/2}} + \dots$$

Integrating and collecting terms, the expression reduces to the form:

$$f(x, y, -h) = C_0 \bar{f}(r_0) + C_1 \bar{f}(r_1) + \dots + C_9 \bar{f}(r_9) \quad (2-11)$$

where the constants C_r represent the operator coefficients. Since they were to be hand computed, the circle averages $\bar{f}(r)$ are determined on the basis of a limited number of grid points: the two inner circles use four points each, while the others use eight. Peters' upward continuation operator for $h=1$ grid unit appears in digital form in Table A-1 of the Appendix (page 125). Each entry in the table represents the weighted coefficient value at the indicated grid point. Since the operator is circularly symmetric only the first quadrant need be defined. Grid points which do not enter the calculation have been left blank and assigned a coefficient weight of zero. The format just described will be used to tabulate coefficient sets studied in this thesis, since it provides both a convenient basis for comparison as well as the digital form required for frequency analysis.

One weakness of the upward continuation operator of Table A-1 is the sparse coefficient coverage for larger radii. This effect contributes distortion to the frequency response and results in a poor approximation of the continuation integral. On the other hand, increasing the coefficient density would not have been an attractive proposition in view of the great deal of time required for hand calculations. Peters points out that interpolation formulae may be used to obtain better approx-

imations to the average data function $\bar{f}(r)$. Henderson and Zietz (1949 - b) made use of the trapezoidal rule in a slightly different treatment of equation 2-10.

A similar, but more accurate approach is possible with the aid of a digital computer. A coefficient may be determined at each grid point by evaluating the upward continuation impulse response directly (see Fuller, 1967):

$$C_{mn} = \frac{h / 2\pi}{(m^2 + n^2 + h^2)^{3/2}}$$

where C_{ji} is the weighted value of the operator at the grid point (j, j) . The numerical form of the convolution integral (equation 2-4, page 52) can then be used to obtain the upward continued field.

Potential field data may be expanded above or below the plane of observation according to Taylor's theorem, provided the field is harmonic in this region. The expansions above and below the plane $z=0$ for the continuation distance h may be written as follows:

upward:

$$\begin{aligned} f(x, y, -h) = & f(x, y, 0) - \frac{h}{1!} f'(x, y, 0) + \frac{h^2}{2!} f''(x, y, 0) - \frac{h^3}{3!} f'''(x, y, 0) \\ & + \frac{h^4}{4!} f^{IV}(x, y, 0) - \dots \quad (2-12) \end{aligned}$$

downward:

$$\begin{aligned} f(x, y, h) = & f(x, y, 0) + \frac{h}{1!} f'(x, y, 0) + \frac{h^2}{2!} f''(x, y, 0) + \frac{h^3}{3!} f'''(x, y, 0) \\ & + \frac{h^4}{4!} f^{IV}(x, y, 0) + \dots \quad (2-13) \end{aligned}$$

where $f(x, y, 0)$ is the observed field intensity at the point of continuation, and

$$f'(x, y, 0) = \left[\frac{\partial f(x, y, z)}{\partial z} \right]_{z=0} \quad \text{etc.}$$

Peters was able to solve for the downward continued field $f(x, y, h)$ by adding equations 2-12 and 2-13 and applying Laplace's equation to the remaining even derivatives. In order to make use of the circle averaging pattern developed for the upward continuation process, it was necessary to convert to polar co-ordinates and approximate the average data function by the expansion:

$$\overline{f(r)} \doteq b_0 + b_2 r^2 + b_4 r^4 \quad (2-14)$$

The resulting expression for downward continuation becomes:

$$f(x, y, h) \doteq 2 \left[b_0 - 2 b_2 h^2 + \frac{8}{3} b_4 h^4 \right] - f(x, y, -h) \quad (2-15)$$

The constants b_0 , b_2 and b_4 were obtained by a least squares treatment of equation 2-14 using the center point and nine circle averages. The last term on the right side of equation 2-15 is the upward continued field derived earlier on the basis of the same circle averages. The digitized downward continuation operator for $h=1$ grid unit is given in Table A-2 of the Appendix (page 125).

Trejo (1953) pointed out that the fourth degree parabola approximation to $\overline{f(r)}$ in equation 2-14 was locally valid near the operator origin, but could not be used for the larger radii. The constants b_0 , b_2 and b_4 , determined on the basis of all the circle averages, distort the parabola by including the

sparsely sampled outer averages and results in a corresponding distortion of the operator.

Trejo proposed a method of finite differences in combination with Peters' upward continuation coefficients. Adding the expansions expressed in equations 2-12 and 2-13, page 59, and ignoring derivatives higher than the second, the downward continued field is approximated by:

$$f(0,0,h) \doteq f(0,0,-h) + 2 \left[f(0,0,0) + \frac{h^2}{2!} f''(0,0,0) \right] \quad (2-16)$$

where no loss of generality is involved in choosing the origin at the point of continuation. Laplace's equation and the application of finite differences to the four grid points nearest the origin transform the second vertical derivative term to:

$$-\frac{h^2}{2!} \left(\frac{\partial^2}{\partial x^2} + \frac{\partial^2}{\partial y^2} \right) f(x,y,0) \Big|_{x=y=0} \doteq 4f(0,0,0) - f(h,0,0) - f(-h,0,0) - f(0,h,0) - f(0,-h,0)$$

thus equation 2-16 becomes:

$$f(0,0,h) \doteq 6f(0,0,0) - f(h,0,0) - f(-h,0,0) - f(0,h,0) - f(0,-h,0) - f(0,0,-h)$$

The first five field values on the right are those obtained at the origin and the four nearest grid points. The upward continued field $f(0,0,-h)$ may be represented by a previously determined coefficient set. Trejo used Peters' upward continuation coefficients for the operator shown in Table A-3, page 126.

Henderson's approach to the downward continuation problem (see Henderson, 1960) determines the upward continued values at five levels above the survey plane. The Lagrangian interpolation

formula is then used to extrapolate the continuation function below the datum. The downward continued field takes the form:

$$f(0,0,z) = \sum_{m=0}^5 (-1)^m \frac{z(z+a)(z+2a)(z+3a)(z+4a)(z+5a)}{a^5 (z+ma)(m+5)! m!} \cdot f(0,0,-ma) \quad (2-17)$$

where a is the grid spacing, z the depth of continuation, and $f(0,0,-ma)$ is the upward continued field at a distance $m \cdot a$ above the survey plane. The upward continuation coefficients at each level were developed in a manner similar to the method used by Peters. Henderson's downward continuation operator for $z = a$ is given in Table A-4, page 126. In its original form, ten circles, varying in radius from 1 to 25 grid units, were used in the averaging process. The large radial extent of the operator (25 grid units) causes a serious loss of data around the survey margins. Since the technique was designed for hand calculation, the digitized operator, like those of Peters, exhibits poor coefficient coverage. So far in discussing operator design, we have ignored the fact that the downward continuation process is very sensitive to high frequency effects from shallow sources. Although the initial assumption of a harmonic field is required for continuation downward, this is virtually never the case in practical application. To prevent excessive amplification of these high frequency noise effects, some form of smoothing must be applied to the data or be built into the operator itself. Although Peters does not discuss this problem, his operators are of such low gain that they do not overamplify high frequencies. Henderson favors adjustment of the interpolated data spacing so as to exclude frequencies above some noise level.

This approach is generally unsatisfactory because of the aliasing of higher frequencies to the lower end of the spectrum. Also, if the interpolation interval is too large, a significant loss of useful information may result, severely restricting the delineation of target anomalies.

Another method of downward continuation, first suggested by Bullard and Cooper (1949) and later by Grant and West (1965), incorporates mathematical smoothing in the design of the operator. The continuation integral (equation 1-14, page 20) is inverted by taking the Fourier transform of each side, isolating the spectrum of the downward continued field, and then applying the inverse transform. Upon conversion to polar co-ordinates the downward continuation convolution integral is obtained:

$$f(0,0,z) = 2\pi \int_0^\infty \int_0^{2\pi} \int_0^\infty e^{2\pi(z\rho - \gamma\rho^2)} \cdot J_0(2\pi\rho r) \rho d\rho \int_0^\infty f(r,\theta) r d\theta dr \quad (2-18)$$

where ρ is radial frequency, $f(r,\theta)$ is the observed data in polar co-ordinates, γ is the attenuation factor of the filter response, and the quantity in brackets is the filter weighting function. A numerical approximation of the weighting function around averaging circles was attempted by Grant and West (1965) and resulted in the coefficient set of Table A-5, page 127. The exponential attenuation of the amplitude spectrum built into this operator seems to be a rather severe method of smoothing, and is liable to attenuate low as well as high frequency components.

Analytically derived versions of the second vertical derivative operator have been introduced by Henderson and Zietz (1949 - a), Elkins (1951), and Rosenbach (1953). Henderson and Zietz made use of the fact that if a potential field is averaged about a vertical axis (the operator axis) the resulting even function may be written as a zero-order Bessel function solution of Laplace's equation:

$$\Delta T(x, r) = \sum_{k=1}^k A_k e^{-u_k x} \cdot J_0(u_k r) \quad (2-19)$$

where $\Delta T(x, r)$ is the averaged variation of the force field at a radial distance r , A_k is a set of constants, $J_0(u_k r)$ is the Bessel function of zero order and first kind (u_k being its positive roots). Taking the second vertical derivative of equation 2-19 and setting x and r to zero:

$$\frac{\partial^2 \Delta T}{\partial x^2} = \sum_{k=1}^k u_k^2 A_k \quad (2-20)$$

The constants A_k may be determined by circle-averaging the survey data about the operator origin and solving a set of simultaneous equations based on the relation:

$$\overline{\Delta T}(r) = \sum_{k=1}^k A_k J_0(u_k r)$$

where $\overline{\Delta T}(r)$ represents the data averaged over the survey plane.

One operator designed by Henderson and Zietz takes the form:

$$\left[\frac{\partial^2 f(r)}{\partial x^2} \right]_{r=0} = \frac{1}{3S^2} \left[21f(0) - 8 \sum_1 f(s) + 3 \sum_1 f(\sqrt{2}s) - \frac{1}{4} \sum_1 f(2s) \right]$$

where $f(r)$ represents the observed gravity or magnetic field a distance r from the origin, S is the grid interval, and $\sum_1 f(s)$ is the sum of observed grid values around a circle of

radius S . The digitized operator is given in Table A-6, page 127.

The work of Elkins (1951) extended from Peters' method of representing the data by an even function and differentiating twice according to Laplace's equation. A least squares solution in terms of circle averages was used to obtain second vertical derivative operators. The amplitude responses of Elkins' operators exhibit low gain and resemble the response of a simple residual pass filter.

One of the most successful attempts at approximating the theoretical second vertical derivative, both in terms of spectral circular symmetry and gain, was made by Rosenbach (1953). Using Laplace's equation and Taylor's expansion he was able to obtain simultaneous equations for various grid patterns and solve for the second vertical derivative. Rosenbach's equation 16, based on one of these patterns, takes the form:

$$\left[\frac{\partial^2 f(r)}{\partial z^2} \right]_{r=0} \doteq \frac{1}{24S^2} \left[96f(0) - 18 \sum f(S) - 8 \sum f(\sqrt{2}S) + \sum f(\sqrt{5}S) \right]$$

and is represented digitally in Table A-7, page 127.

The weaknesses associated with most of the analytically derived operators in the foregoing descriptions stem from forced simplification rather than from the basic design methods themselves. Coefficient coverage and, therefore, operator accuracy had to be sacrificed for practical hand calculation schemes. For the same reason, the most important criterion of operator design, that of frequency response, could not be applied. With

the aid of the Fourier transform and the digital techniques now available, the results of analytical design methods can be significantly improved.

Transform Design Methods

Two methods, referred to here as a) the transform and b) the inverse transform methods, make direct use of frequency response and allow closer control of operator filter characteristics. They also afford the opportunity to employ techniques of frequency analysis and digital processing to give a more general approach to the design problem. A major portion of the research undertaken in connection with this thesis has been concerned with the development of this approach and its adaptation to the Hankel and inverse Hankel transforms.

a) The Transform Method - If the operator response is specified at $M \times N$ discrete points, the coefficient set C_{mn} , representing the filter weighting function, can be determined by a simultaneous solution of the discrete Fourier transform (equation 2-5, page 52). Since the operators are assumed to exhibit circular symmetry, we will reduce the problem to a one-dimensional form by introducing the discrete Hankel transform (equation 2-7, page 52):

$$F(\rho) = 2\pi \sum_{r=0}^M C_r J_0(2\pi \rho r \Delta r) \cdot r (\Delta r)^2 \quad (2-21)$$

where $F(\rho)$ is the known amplitude response and C_r the unknown coefficient at the radial distance r . Δr is an increment of distance in the radial direction. If we adopt the least squares energy criterion for the simultaneous solution of equation 2-21,

the resulting normal equations may be expressed in matrix form:

$$\begin{bmatrix} B_{11} & B_{12} & \dots & \dots & B_{1M} \\ B_{21} & B_{22} & \dots & \dots & B_{2M} \\ \vdots & \vdots & & & \vdots \\ B_{j1} & B_{j2} & \dots & \dots & B_{jM} \\ \vdots & \vdots & & & \vdots \\ B_{M1} & B_{M2} & \dots & \dots & B_{MM} \end{bmatrix} \cdot \begin{bmatrix} C_1 \\ C_2 \\ \vdots \\ C_j \\ \vdots \\ C_M \end{bmatrix} = \begin{bmatrix} D_1 \\ D_2 \\ \vdots \\ D_j \\ \vdots \\ D_M \end{bmatrix} \quad (2-22)$$

where

$$B_{ij} = \int \sum_p J_0(2\pi\rho j) \cdot J_0(2\pi\rho j) ,$$

$$D_j = \frac{1}{2\pi(\Delta r)^2} \sum_p F(\rho) J_0(2\pi\rho j)$$

and C_j is the coefficient at a radial distance j . The derivation of these normal equations is summarized in article A2 of the Appendix, page 124. A computer program was written to solve equation 2-22 for the discrete coefficients C_j , with the desired operator frequency response as input. Because the general term of the summation on the right side of equation 2-21 is zero at the origin (i.e. at $r=0$), the coefficient C_0 must be found by some other means. The simultaneous solution or transform approach has several defects. Because the coefficients are derived from a set of equations based on oscillating functions, they alternate between positive and negative values. The resulting amplitude spectrum exhibits a periodic mismatch which can be quite serious, particularly at low frequencies. This effect can be reduced to some extent by smoothing the coefficient set and modifying the theoretical amplitude response. Figure 2-6, page 68, shows the result of an attempt to obtain a second

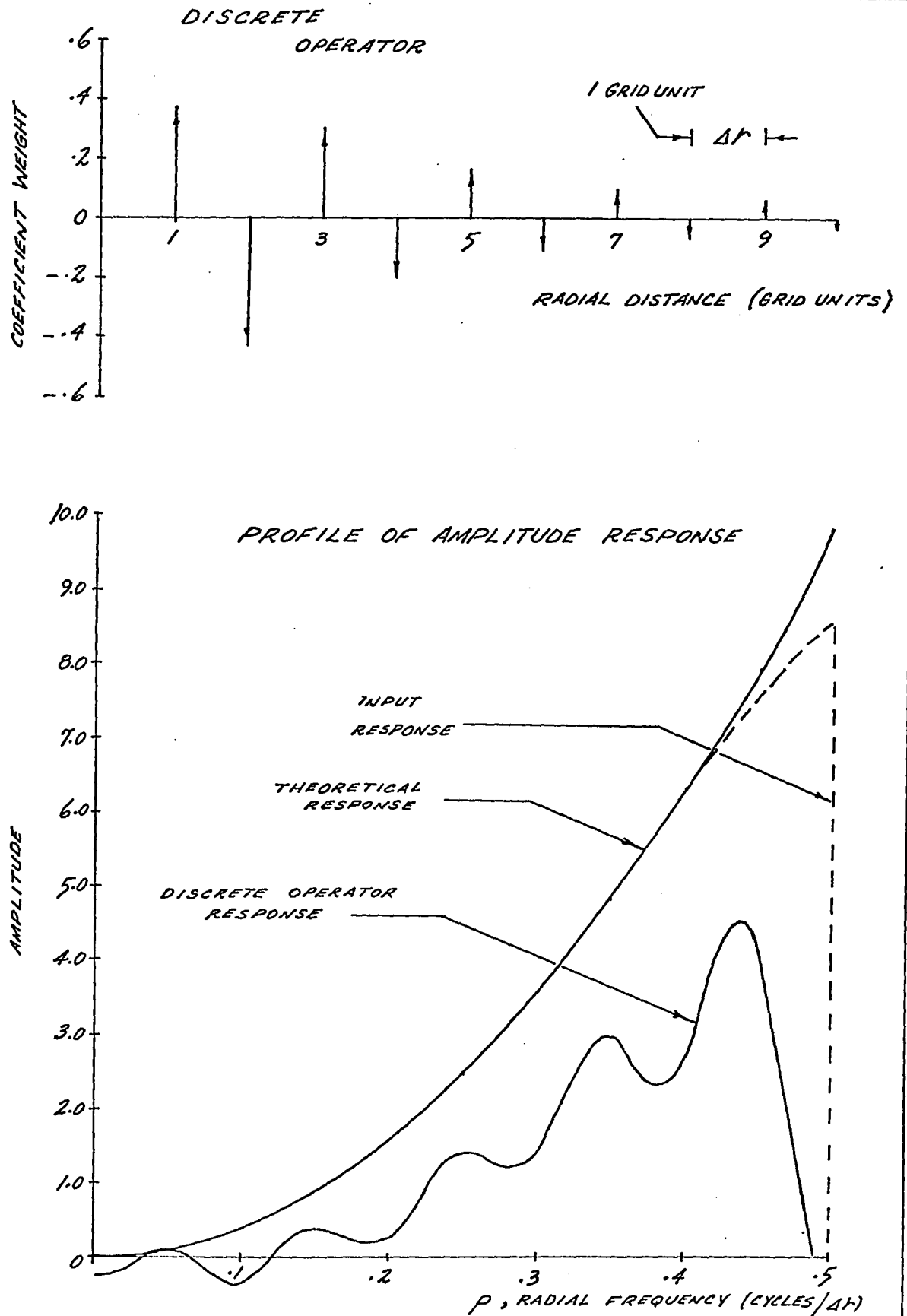


FIG. 2-6: SECOND VERTICAL DERIVATIVE OPERATOR BY THE HANKEL TRANSFORM METHOD.

vertical derivative operator using the Hankel transform procedure. The input amplitude response was attenuated exponentially and cut off at the Nyquist frequency (0.5 cycles/D.I.) prior to solution. The Nyquist cut-off forces the response of the least squares approximation to plunge steeply in the vicinity of the folding point. Although this abrupt falling-off at high frequencies may be desirable in terms of noise reduction, distortion of the low and central band regions will occur if the cut-off is too severe. The mismatch at low and intermediate frequencies is probably the most serious problem. The low frequency variations of the gravity field are generally the high amplitude, and thus, high energy components. This is not always true of the magnetic field which may have high amplitude components over the entire spectrum. Slight low frequency mismatch in the spectrum of an applied operator will therefore cause substantial low frequency distortion of the field. Dean (1953) used the Fourier transform to derive one-dimensional downward continuation operators. In addition to the problems mentioned above, he found that a large number of coefficients were required to obtain a reasonable amplitude response.

The Hankel transform method as described here produces a set of discrete radial weights which can not be conveniently applied to gridded data. In view of the least squares criterion and the simultaneous method of solution, radial interpolation of the coefficients to obtain grid values would probably prove unsuccessful. The treatment does serve to demonstrate, however,

the difficulties involved in the transform approach. The application of a two-dimensional, cartesian extension of this method would require the solution of a very large number of simultaneous equations and would still suffer from most of the inherent defects just discussed.

b) The Inverse Hankel Transform Method - The second approach, making use of the inverse transform, is the simplest and perhaps the most useful means of operator design. Darby and Davies (1967) and Fuller (1967) used the inverse Fourier transform in the design of two-dimensional discrete filters. The frequency responses of the resulting coefficient sets, although showing some deviation from circular symmetry, were generally much superior to the spectral characteristics of previous operators.

The inverse Hankel transform of zero order was found to provide a more exact, and yet more streamlined means of derivation. Applying the discrete version of the inverse Hankel transform (equation 2-8, page 52), the coefficient at a radial distance r may be approximated by:

$$C(r) \doteq 2\pi \sum_{k=0}^K F(k\Delta\rho) J_0(2\pi k\Delta\rho r) k(\Delta\rho)^2 \quad (2-23)$$

where $F(k\Delta\rho)$ is the stipulated amplitude response, presumably known for all frequencies, and k the frequency variable. The coefficient at any grid point (j,j) is evaluated simply by setting $r = \sqrt{j^2 + j^2}$ and performing the spectral summation indicated in equation 2-23. The limit of integration K should be set

somewhat higher than the grid folding frequency in order to prevent a spectral discontinuity at the grid folding point. Also, the frequency increment $\Delta\rho$ must be taken small enough to ensure an adequate approximation to the inverse Hankel transform. Any severe discontinuities present in the input amplitude response $F(k\rho)$ will cause a corresponding irregularity in the derived coefficient set. It is therefore necessary, in the case of high-gain, high-pass operators, to introduce some form of spectrum attenuation in the vicinity of the grid folding point. This topic will be discussed further in part 4 of this section when several design refinements are considered.

The size or areal extent of the operator will depend on the nature of the filtering operation and the degree of accuracy required. Greater operator size is necessary in the approximation of continuation operations, for example, than in derivative techniques, since continuation weighting functions are greater in surface coverage and fundamentally more difficult to represent by finite coefficient sets. In general, the larger the coefficient set, the closer its amplitude response will reflect the input response. For each problem, however, there is a point of diminishing returns at which the additional accuracy gained is not worth the extra coefficients. Another factor of considerable importance is the amount of data lost during the convolution process as a result of an operator's size. A coefficient set extending ten grid units from the origin will require an outer margin of data, ten grid units in width, surrounding the

designated region of interest. Finally, the practical size of the operator, as used in digital convolution, will be limited by the digital processing facilities available. The above factors should be weighed carefully in any comprehensive design scheme.

Several operators were derived by the inverse Hankel transform method in the preparation of this thesis. All resulting coefficient sets exhibit good radial response and excellent circular symmetry in the frequency domain. The largest of these operators extends a distance of eight grid units from the origin in the x and y axial directions. A significant advantage in using the inverse Hankel transform approach is that a discrete operator can be found for any specified amplitude response. Such versatility may prove important for specialized filtering applications.

Because of the inherent spectral characteristics of potential field data, frequency response, as obtained from the Fourier transform, is probably the single most important criterion of operator design. Whether the inverse transform method, some analytical approach or a combination of these is adopted in the design of a particular operator, facilities should be available for evaluating its two-dimensional Fourier transform. A computer program based on the discrete Fourier transform (equation 2-5, page 52) was written for this purpose. Since the operators considered in this thesis are circularly symmetric about the origin, the transform reduces to:

$$F(u,v) = \sum_{m=-M}^M \sum_{n=-N}^N C_{mn} \cdot \cos(2\pi u m \Delta x) \cdot \cos(2\pi v n \Delta y) \Delta x \Delta y$$

where $F(u, v)$ is the amplitude response of the derived coefficient set C_{mn} . This relation is easily programed on a digital computer, and affords a good approximation of the two-dimensional amplitude response of any symmetrical coefficient set.

Practical Refinements in Operator Design

In preparing a coefficient set for practical application, certain refinements must be included in the basic design methods already outlined. When the inverse transform is employed in the derivation of high-gain operators, the input frequency response will require some form of attenuation. To minimize distortion of the derived operator response the coefficient set must be multiplied by a smoothing function and then normalized. These three refinements: a) spectrum attenuation, b) coefficient smoothing, and c) normalization will be considered in turn.

a) In dealing with high-gain operators such as downward continuation and the second vertical derivative, close approximation to the theoretical response is undesirable at the higher frequencies. The coefficient response, unlike the ever-increasing theoretical response takes a plunge at its folding or Nyquist frequency. If this cut-off is too severe the mid-band response of the coefficient set may suffer serious distortion. This effect can be reduced by using an attenuated version of the theoretical response in the vicinity of the folding frequency. The severity of the folding point cut-off can be softened further if the limit of integration for the inverse Hankel transform, in equation 2-23, page 70, is set somewhat above the Nyquist

frequency. Since the coefficient determined by the inverse Hankel transform approximates a continuous operator at the particular radial distance ρ , integration past the grid folding point is entirely justified. The radial amplitude response of a discrete second vertical derivative operator is shown in Figure 2-16, page 88, along with the attenuated response used as input in deriving the operator. In addition to reducing spectral distortion, attenuation of the input response serves another purpose. If the response of an applied operator approaches some theoretically high gain near the folding point, the high frequency noise components in the data will be greatly over-amplified at the expense of useful information. Attenuation of the high-gain response helps to minimize this tendency. In contrast, the low and mid-band frequencies are most important in defining the observed potential field. The designed operator response should, therefore, reflect the theoretical response as closely as possible in this range.

b) The theoretical operators dealt with in this chapter are of infinite extent, but in practical situations a coefficient set must be limited to a finite size. The abrupt termination or truncation of the discrete operator at the designated boundary will cause serious periodic mismatch in its amplitude spectrum. This effect can be eliminated quite successfully by multiplying the coefficient set by a smoothing function, such as:

$$S(x,y) = \begin{cases} \frac{1}{2} \left\{ 1 + \cos \left[\pi \left(\frac{x^2 + y^2}{X^2 + Y^2} \right)^{1/2} \right] \right\} \dots \text{FOR } \begin{matrix} x \leq X \\ y \leq Y \end{matrix} \\ 0 \dots \dots \dots \text{FOR } \begin{matrix} x > X \\ y > Y \end{matrix} \end{cases} \quad (2-24)$$

where X and Y are the operator boundaries in the x and y directions. The smoothing process may be viewed as frequency domain convolution. The periodic mismatch is literally filtered out of the coefficient set amplitude response.

c) A third refinement, referred to here as coefficient normalization, is needed to fix the zero frequency point of the amplitude response. For the wavelength filter and continuation operators the zero frequency amplitude response is unity, and according to the discrete Fourier transform:

$$\left[F(u,v) \right]_{u=v=0} = \sum_m \sum_n C_{mn} \Delta x \Delta y = 1 \quad (2-25)$$

The above condition can be fulfilled by dividing each coefficient by the sum of coefficients, that is:

$$CN_{mn} = \frac{C_{mn}}{\sum_m \sum_n C_{mn}}$$

where CN_{mn} represents the normalized coefficients. The second vertical derivative and residual operators show zero amplitude response at the zero frequency point, so that:

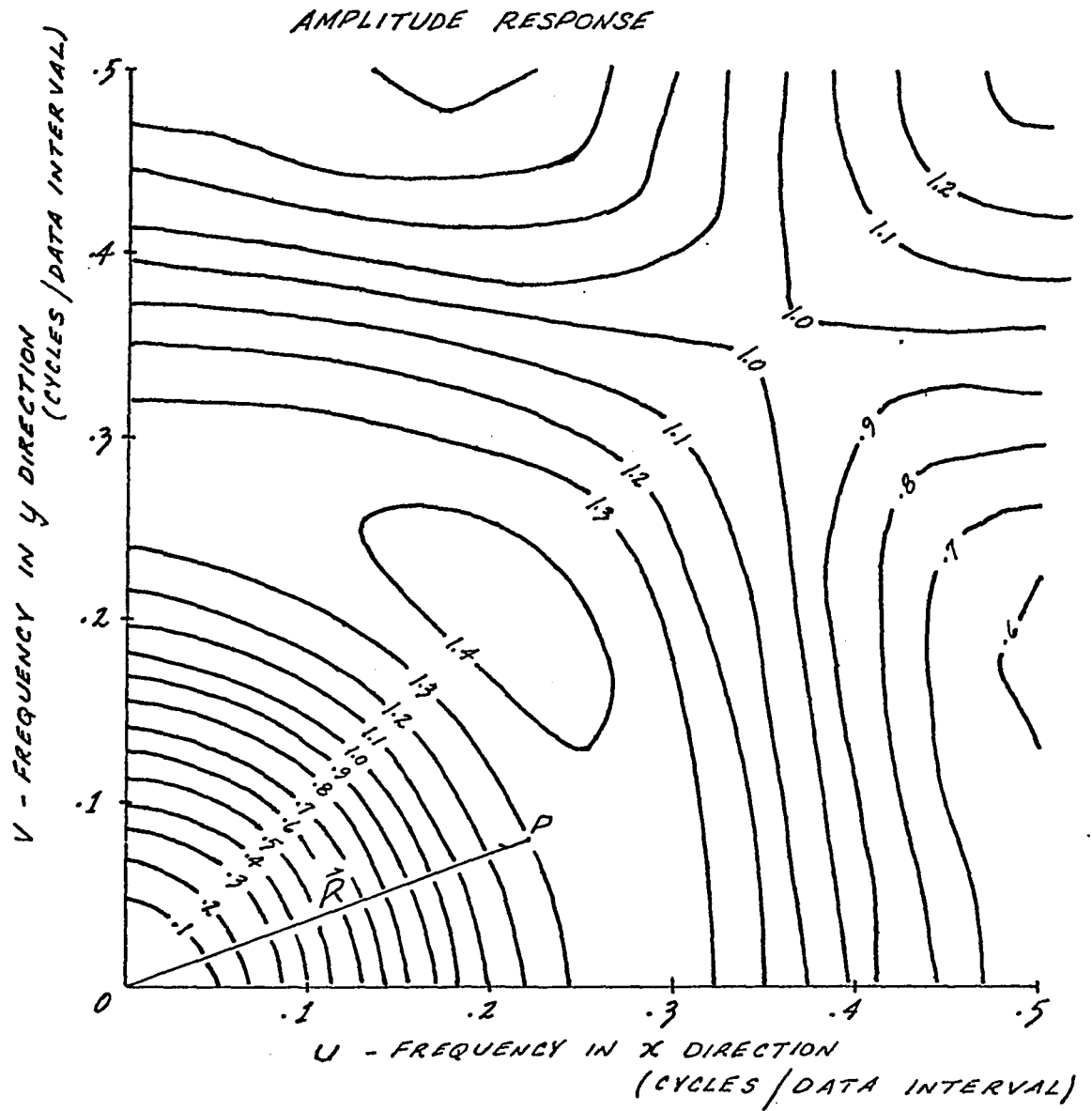
$$\left[F(u,v) \right]_{u=v=0} = \sum_m \sum_n C_{mn} \Delta x \Delta y = 0 \quad (2-26)$$

In this case the coefficient at the operator origin, C_{00} , is adjusted to make the sum of the coefficients equal to zero. It should be pointed out that the grid interval $\Delta x = \Delta y$ is taken as the unit of distance in all discrete operations. Normalization can be thought of as an additional means of compensating for the discrepancy between a continuous infinite operator on the one hand, and its finite approximation by a coefficient set on the other.

2-3 Description and Assessment of Some Proposed Operators

Several discrete operators have been derived to illustrate the basic design concepts involved and to highlight particular design problems which may arise. Various wavelength filters, the second vertical derivative, and continuation operations are represented. For the sake of completeness, several well-known coefficient sets will be examined and compared with the newly derived operators. The two-dimensional Fourier transform will be used as a basis for evaluation and comparison of operators.

The format adopted in describing the various coefficient sets gives a concise, and yet, complete picture of the space and frequency domains. Only the first (i.e. north-east) quadrant of the coefficient set and its amplitude response need be defined, since both the space and frequency expressions exhibit circular symmetry. Consider, for example, the center point, single ring residual operator proposed by Griffin (1949). If we incorporate the grid points at a distance of 2 and $\sqrt{5}$ grid units from the origin in the circle average, the center point assumes a coefficient weight of 1.0 and each of the twelve averaging points a weight of 0.083. The first quadrant format for the discrete operator and its amplitude response is given in Figure 2-7, page 77. The amplitude response has been terminated at the grid folding frequency (0.5 cycles/Data Interval) since it repeats itself past this point. The position vector of any particular point in the u-v plane defines the frequency, direction, and amplitude of a particular harmonic component.



OPERATOR

y (GRID POINTS)	2	1	0
	-0.0833	-0.0833	-0.0833
	1.0000	-0.0833	-0.0833
	0	1	2
	x (GRID POINTS)		

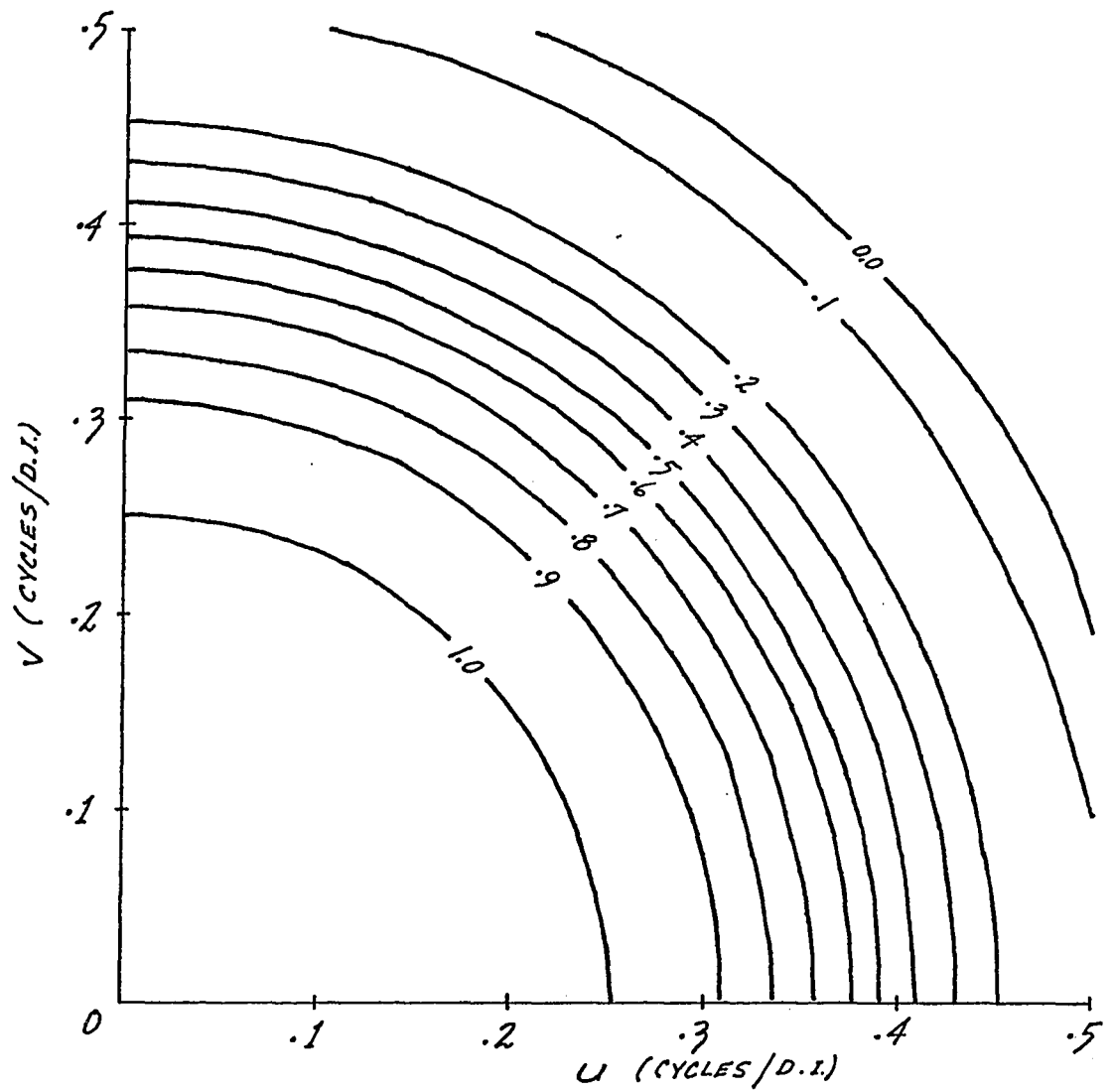
FIG. 2-7: CENTER POINT, SINGLE RING
RESIDUAL OPERATOR.

Point P, shown in Figure 2-7, defines a component of frequency $|\vec{R}|$ cycles/D.I., having an amplitude of 1.3 and whose direction coincides with that of the position vector \vec{R} .

Wavelength Filters

Three low-pass filters with cut-offs of 0.4, 0.2, and 0.075 cycles/D.I. were derived using equation 2-9, page 54. After specifying the size and appropriate cut-off of a proposed operator, the attenuated Bessel function in equation 2-9 was evaluated at each participating grid point. The resulting coefficient sets were multiplied by the smoothing function of equation 2-24, page 74, and then normalized. The operators and their amplitude responses are presented in Figures 2-8 to 2-10, pages 79 to 81. In order to allow a better comparison of gain characteristics, the radial response profiles are given in Figure 2-11, page 82. The 0.4 cycle/D.I. low-pass operator, extending a distance of four grid units from the origin, was designed for the purpose of eliminating high frequency noise components from the potential field data. The cut-off could be made sharper by selecting a larger operator size, but in this case it seems that very little advantage would be gained by such a move. An operator size of eight grid units from the origin was chosen for the 0.2 and 0.075 cycle/D.I. wavelength filters in order to obtain sharper cut-offs. Because the areal extent of the wavelength filter increases as the specified cut-off frequency decreases, greater coefficient coverage will be required for an operator of lower cut-off frequency.

AMPLITUDE RESPONSE

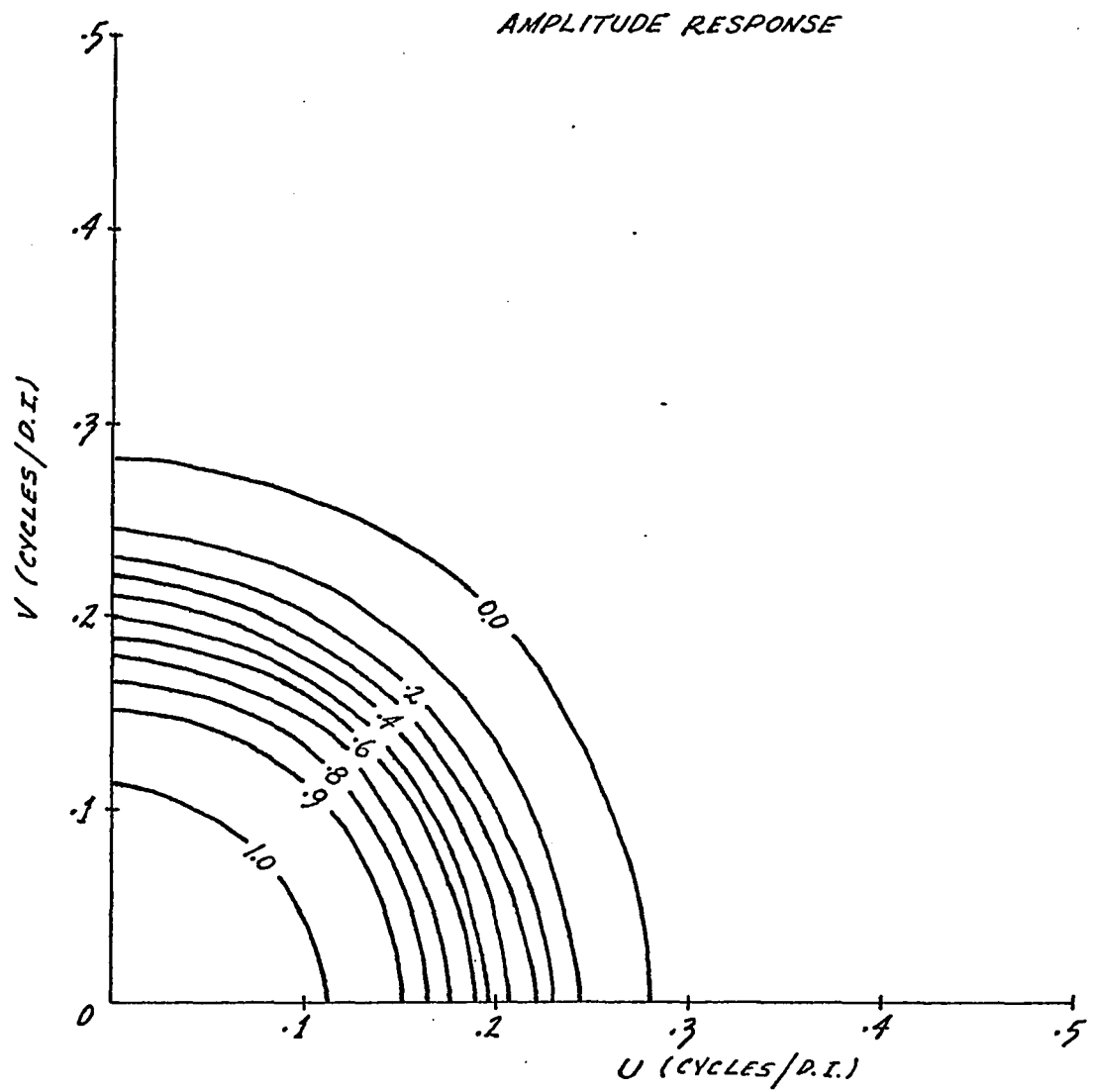


OPERATOR

4	.00059	-.00076	-.00193	-.00040	.00000
3	.00868	.01162	.00761	-.00157	-.00040
2	-.04738	-.03907	.00194	.00761	-.00193
1	.18137	.02747	-.03907	.01162	-.00076
0	.49907	.18137	-.04738	.00868	.00059
	0	1	2	3	4

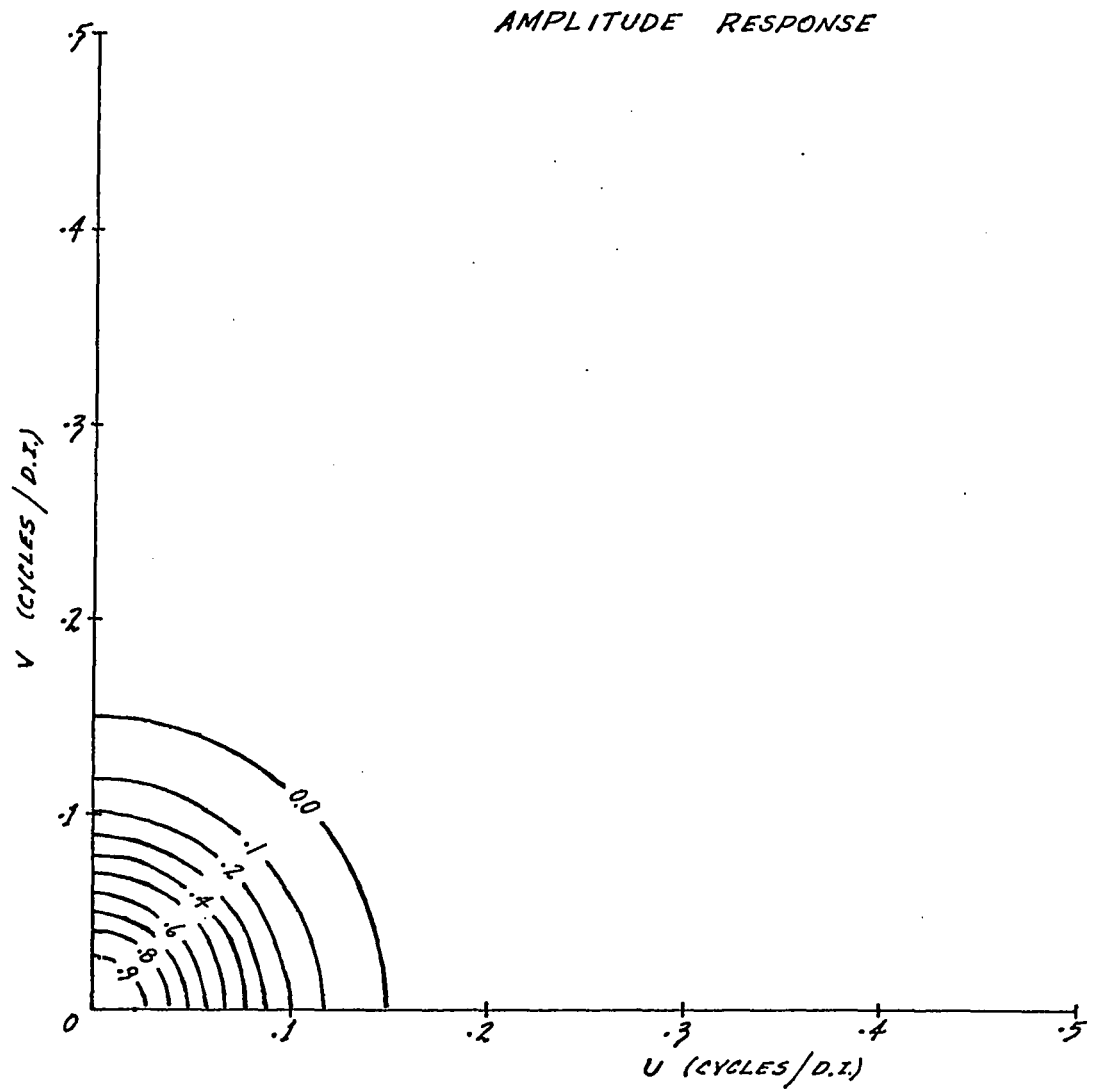
x →

FIG. 2-8: WAVELENGTH FILTER —
0.4 CYCLE/D.I. LOW-PASS



8	.00015	.00005	-.00019	-.00042	-.00048	-.00032	-.00010	.00000	.00000
7	.00236	.00221	.00172	.00091	.00005	-.00044	-.00041	-.00013	.00000
6	.00215	.00241	.00287	.00283	.00188	.00049	-.00039	-.00041	-.00010
5	-.00493	-.00399	-.00147	.00144	.00294	.00221	.00049	-.00044	-.00032
4	-.01172	-.01153	-.00966	-.00493	.00048	.00294	.00188	.00005	-.00048
3	.00137	-.00285	-.01003	-.01108	-.00493	.00144	.00283	.00091	-.00042
2	.04486	.03237	.00679	-.01003	-.00966	-.00147	.00287	.00172	-.00019
1	.09869	.07764	.03237	-.00285	-.01153	-.00399	.00241	.00221	.00005
0	.12343	.09869	.04486	.00137	-.01172	-.00493	.00215	.00236	.00015
	0	1	2	3	4	5	6	7	8

FIG. 2-9: WAVELENGTH FILTER —
0.2 CYCLE/D.I. LOW-PASS



OPERATOR

8	.00005	.00002	-.00004	-.00010	-.00013	-.00012	-.00007	-.00002	.00000
7	.00077	.00070	.00050	.00024	.00002	-.00010	-.00013	-.00008	-.00002
6	.00233	.00216	.00172	.00113	.00056	.00013	-.00009	-.00013	-.00007
5	.00482	.00453	.00375	.00268	.00159	.00070	.00013	-.00010	-.00012
4	.00809	.00765	.00647	.00482	.00308	.00159	.00056	.00002	-.00013
3	.01169	.01111	.00950	.00724	.00482	.00268	.00113	.00024	-.00010
2	.01499	.01428	.01230	.00950	.00647	.00375	.00172	.00050	-.00004
1	.01732	.01651	.01428	.01111	.00765	.00453	.00216	.00070	.00002
0	.01815	.01732	.01499	.01169	.00809	.00482	.00233	.00077	.00005
	0	1	2	3	4	5	6	7	8

FIG. 2-10: WAVELENGTH FILTER —
0.075 CYCLE / D.I. LOW-PASS

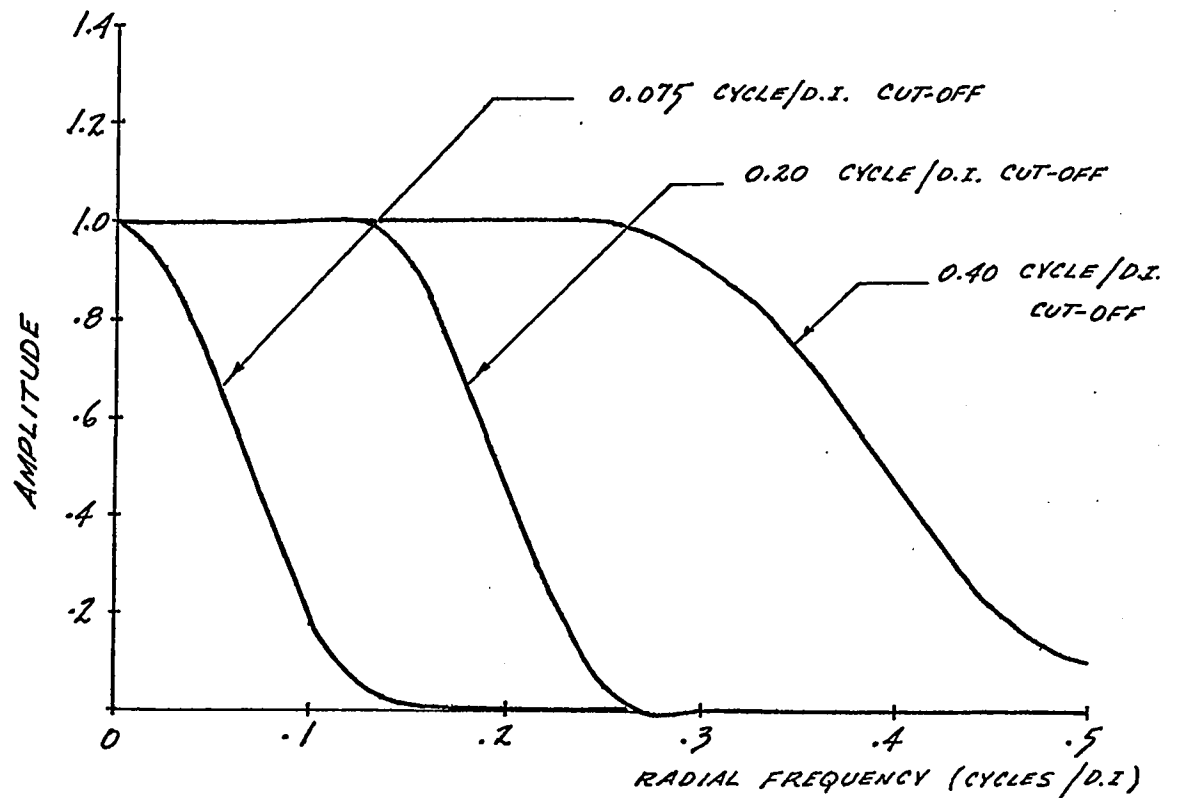


FIG. 2-11 : RADIAL RESPONSE OF WAVELENGTH FILTERS

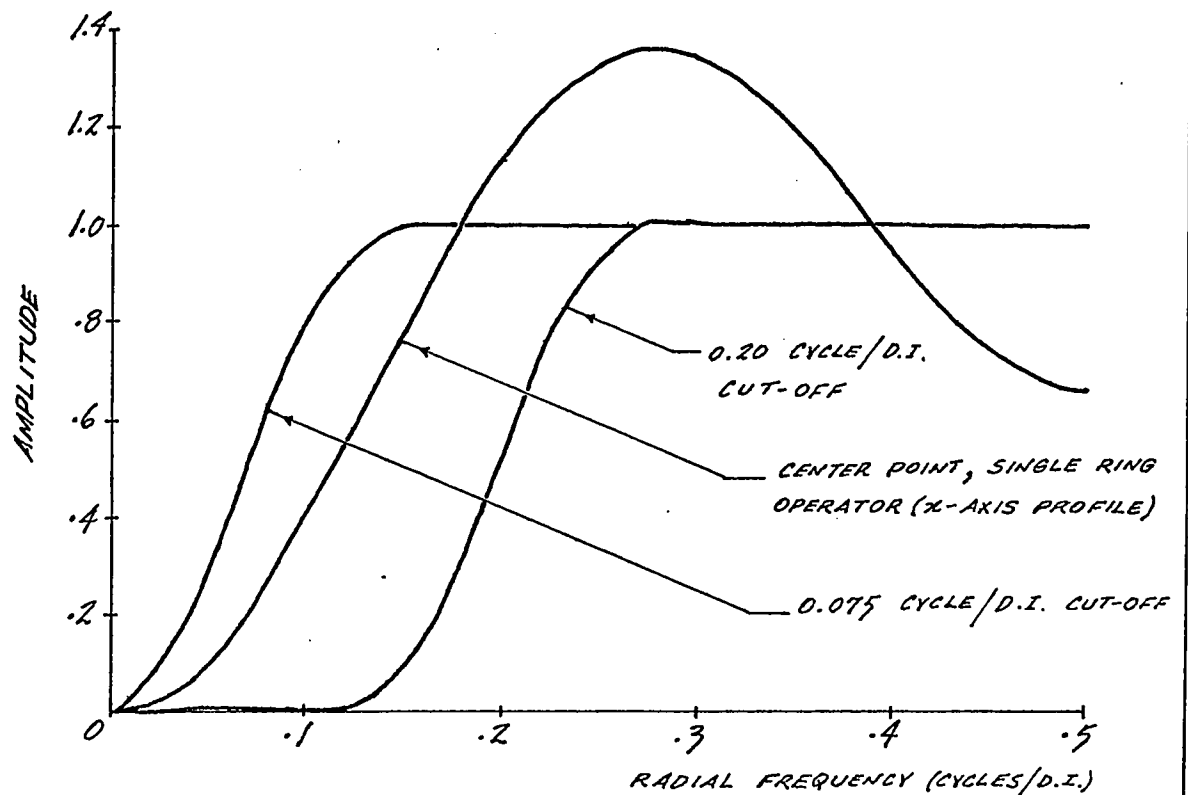
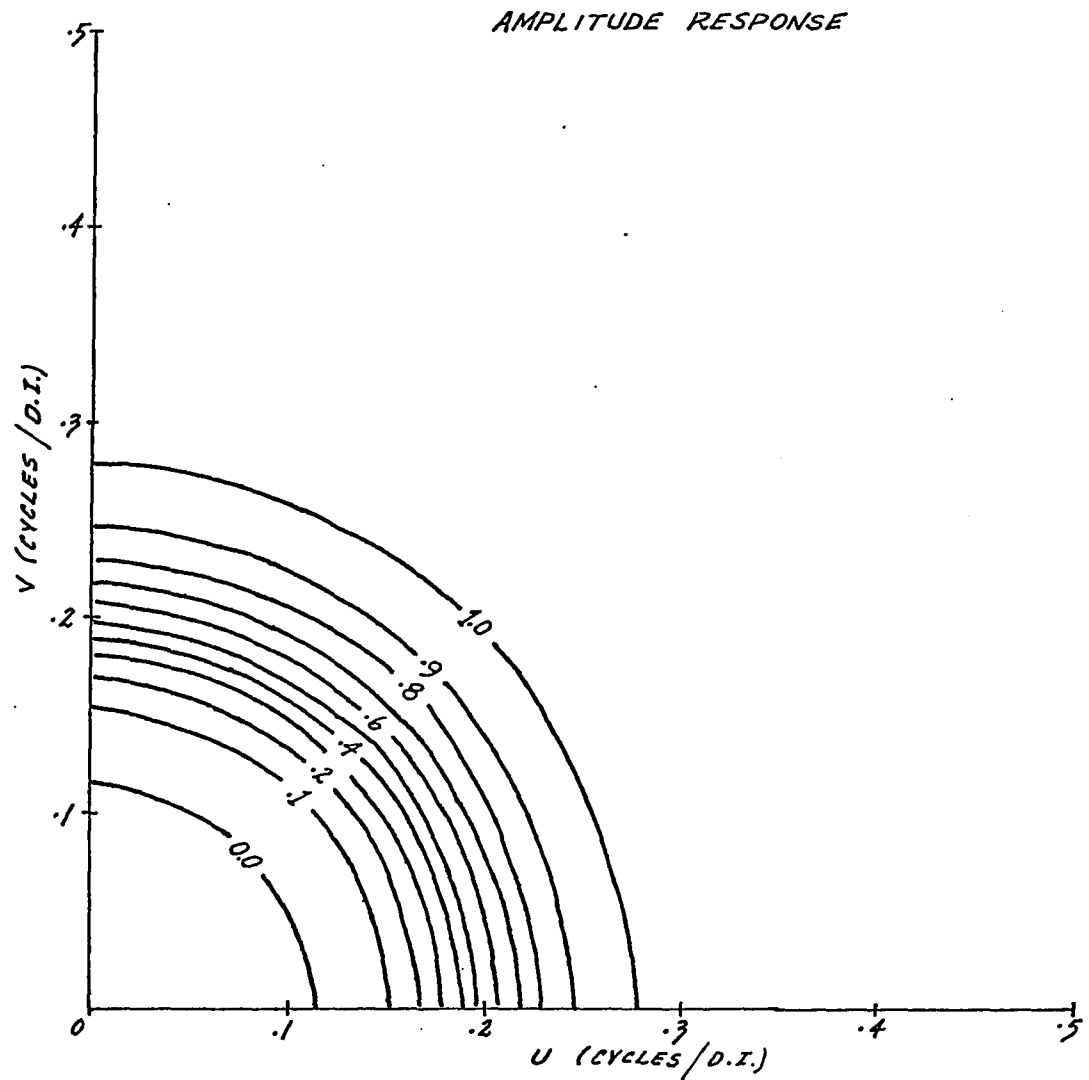


FIG. 2-12 : RADIAL RESPONSE OF INVERSE WAVELENGTH FILTERS AND CENTER POINT, SINGLE RING OPERATOR

The high-pass or residual type operators can be obtained by inverting the standard wavelength filter, as described in section 2-2 and summarized in Figure 2-5, page 56. The 0.2 and 0.075 cycle/D.I. wavelength operators were each subtracted from the discrete unit impulse to yield the corresponding inverse operators shown in Figures 2-13 and 2-14, pages 84 and 85. Inverse wavelength operators derived in this manner can be used to extract residual features of the potential field from the lower frequency regional trends.

Figure 2-12, page 82, compares the radial amplitude responses of the 0.2 and 0.075 cycle/D.I. high-pass operators, with the amplitude response of the center point, single ring operator of Figure 2-7, page 77. The frequency response of a residual filter should have a fairly sharp cut-off before leveling out to a broad-band amplitude of unity, as is the case for the inverse wavelength operators. The response of the single ring operator, however, has a more gradual cut-off and tends to oscillate at higher frequencies. Perhaps the most serious weakness of the single ring operator is its poor coefficient coverage. The effective sampling distance is approximately equal to the radius of the averaging ring, and as a result, the effective Nyquist or folding frequency is substantially lower than the grid folding point. The aliasing effect accompanying this inadequate sampling of data can become quite serious for single ring operators of large radii.

Considering the ease of derivation and the excellent fre-

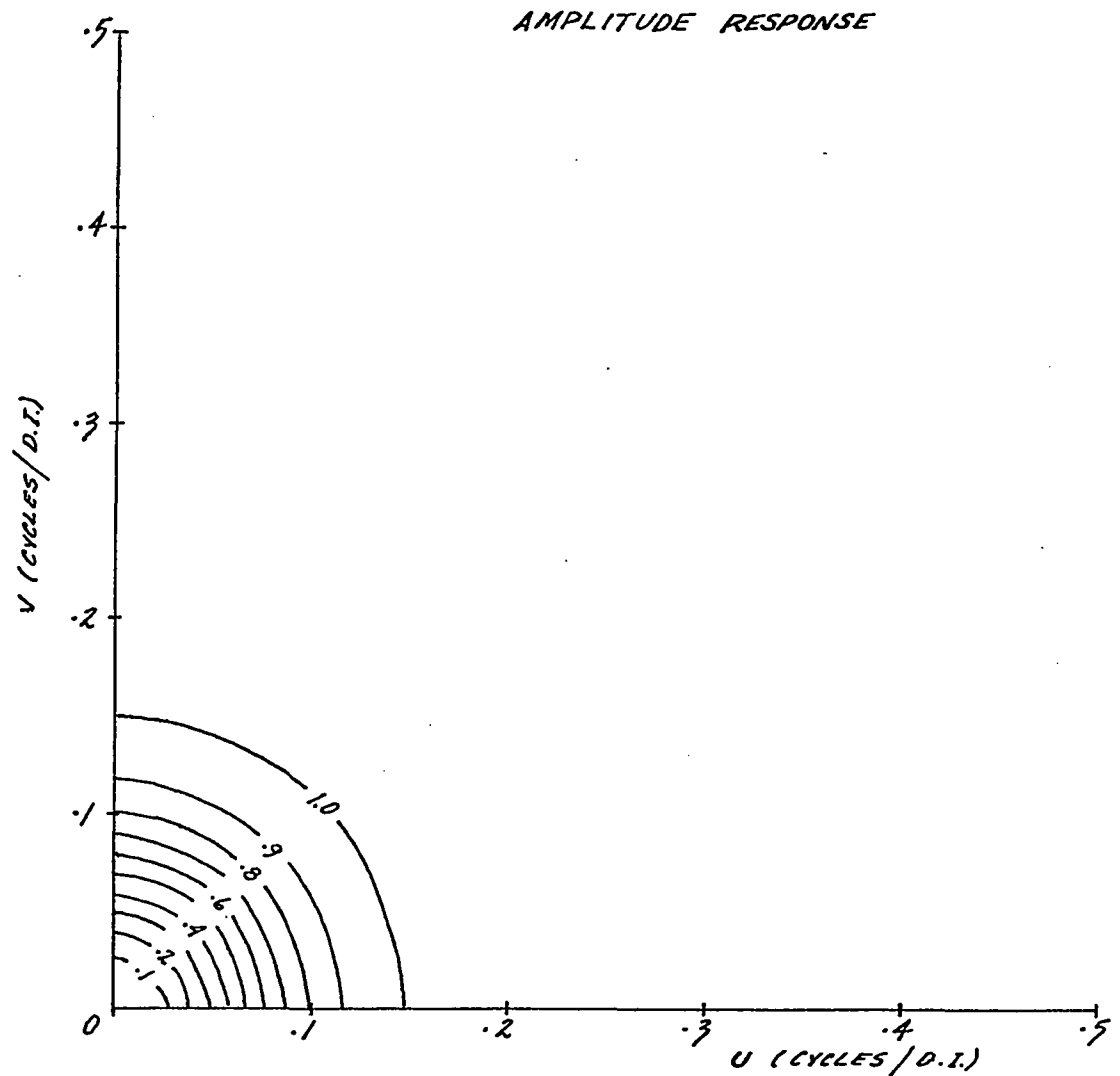


OPERATOR

8	-.00015	-.00005	.00019	.00042	.00048	.00032	.00010	.00000	.00000
7	-.00236	-.00221	-.00172	-.00091	-.00005	.00044	.00041	.00013	.00000
6	-.00215	-.00241	-.00287	-.00283	-.00188	-.00049	.00039	.00041	.00010
5	.00493	.00399	.00147	-.00144	-.00294	-.00221	-.00049	.00044	.00032
4	.01172	.01153	.00966	.00493	-.00048	-.00294	-.00188	-.00005	.00048
3	-.00137	.00285	.01003	.01108	.00493	-.00144	-.00283	-.00091	.00042
2	-.04486	-.03237	-.00679	.01003	.00966	.00147	-.00287	-.00172	.00019
1	-.09869	-.07764	-.03237	.00285	.01153	.00399	-.00241	-.00221	-.00005
0	.87657	-.09869	-.04486	-.00137	.01172	.00493	-.00215	-.00236	-.00015
	0	1	2	3	4	5	6	7	8

$x \rightarrow$

FIG. 2-13: INVERSE WAVELENGTH FILTER —
0.2 CYCLE / D.I. HIGH PASS



OPERATOR

8	-.00005	-.00002	.00004	.00010	.00013	.00012	.00007	.00002	.00000
7	-.00077	-.00070	-.00050	-.00024	-.00002	.00010	.00013	.00008	.00002
6	-.00233	-.00216	-.00172	-.00113	-.00056	-.00013	.00009	.00013	.00007
5	-.00482	-.00453	-.00375	-.00268	-.00159	-.00070	-.00013	.00010	.00012
4	-.00809	-.00765	-.00647	-.00482	-.00308	-.00159	-.00056	-.00002	.00013
3	-.01169	-.01111	-.00950	-.00724	-.00482	-.00268	-.00113	-.00024	.00010
2	-.01499	-.01428	-.01230	-.00950	-.00647	-.00375	-.00172	-.00050	.00004
1	-.01732	-.01651	-.01428	-.01111	-.00765	-.00453	-.00216	-.00070	-.00002
0	.98185	-.01732	-.01499	-.01169	-.00809	-.00482	-.00233	-.00077	-.00005
	0	1	2	3	4	5	6	7	8

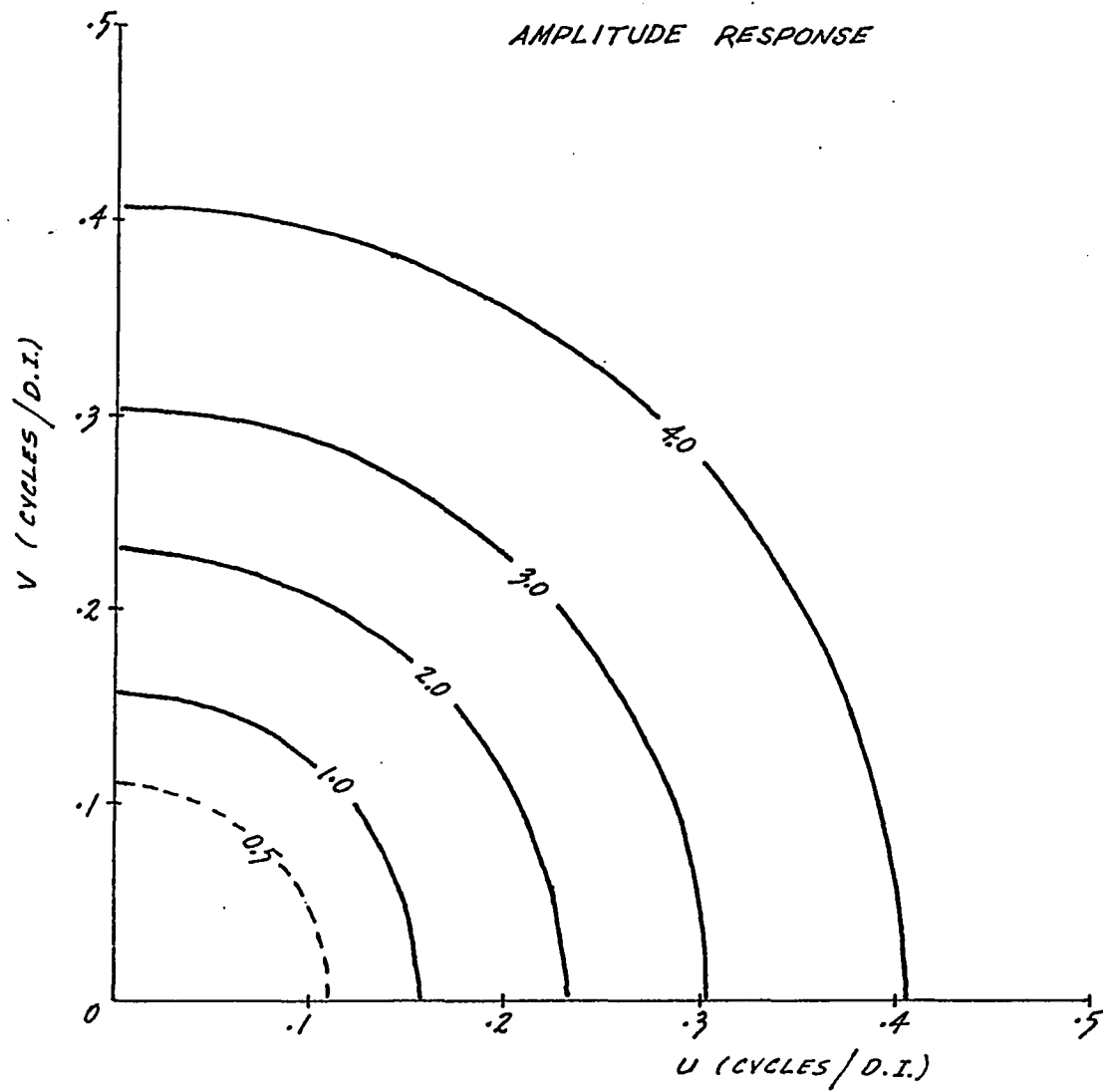
FIG. 2-14: INVERSE WAVELENGTH FILTER —
0.075 CYCLE/D.I. HIGH-PASS

quency characteristics obtained, the wavelength filter provides a highly versatile and convenient approach to the design of regional-residual type potential field operators.

The Second Vertical Derivative

A second vertical derivative operator, developed by the inverse Hankel transform method, is presented in Figure 2-15, page 87. The attenuated version of the theoretical response used as input in the derivation is shown in Figure 2-16, page 88, along with the radial response of the resulting operator. The attenuated spectrum was integrated between the frequencies 0.0 and 1.0 cycle/D.I. in evaluating the inverse transform, and the resulting coefficients were smoothed and normalized. The operator response is a good approximation of the theoretical response at low and intermediate frequencies. The levelling-off of the gain in the vicinity of the folding point should prevent excessive amplification of high frequency noise components present in potential field data. It should be noted, also, that the second vertical derivative operator requires considerably smaller areal coverage than most of the other operators presented here.

The operators of Henderson and Zietz (1949 - a) and Rosenbach (1953), tabulated in Tables A-6 and A-7 on page 127, have been included for comparison. The coefficient set proposed by Henderson and Zietz has strong directional properties dramatically evident in the amplitude response (see Figure 2-17, page 89). In the 45 degree directions, the ampli-



OPERATOR

y ↓	3	.0049	.0036	-.0003	.0000
	2	-.0541	.0059	.0091	-.0003
	1	-.5202	-.2956	.0059	.0036
	0	3.3500	-.5202	-.0541	.0049
		0	1	2	3
		x →			

FIG. 2-15: DERIVED SECOND VERTICAL
DERIVATIVE OPERATOR

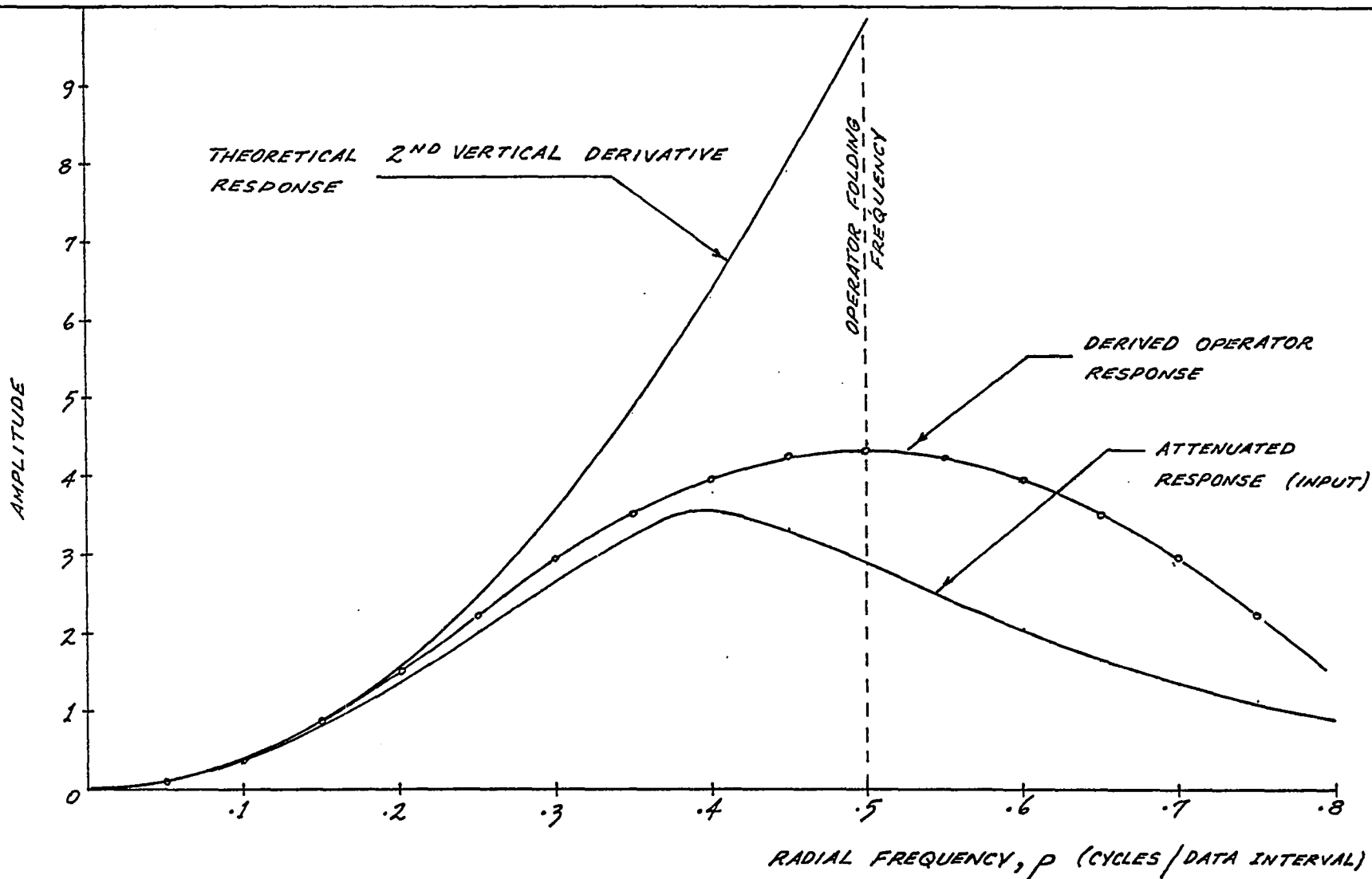
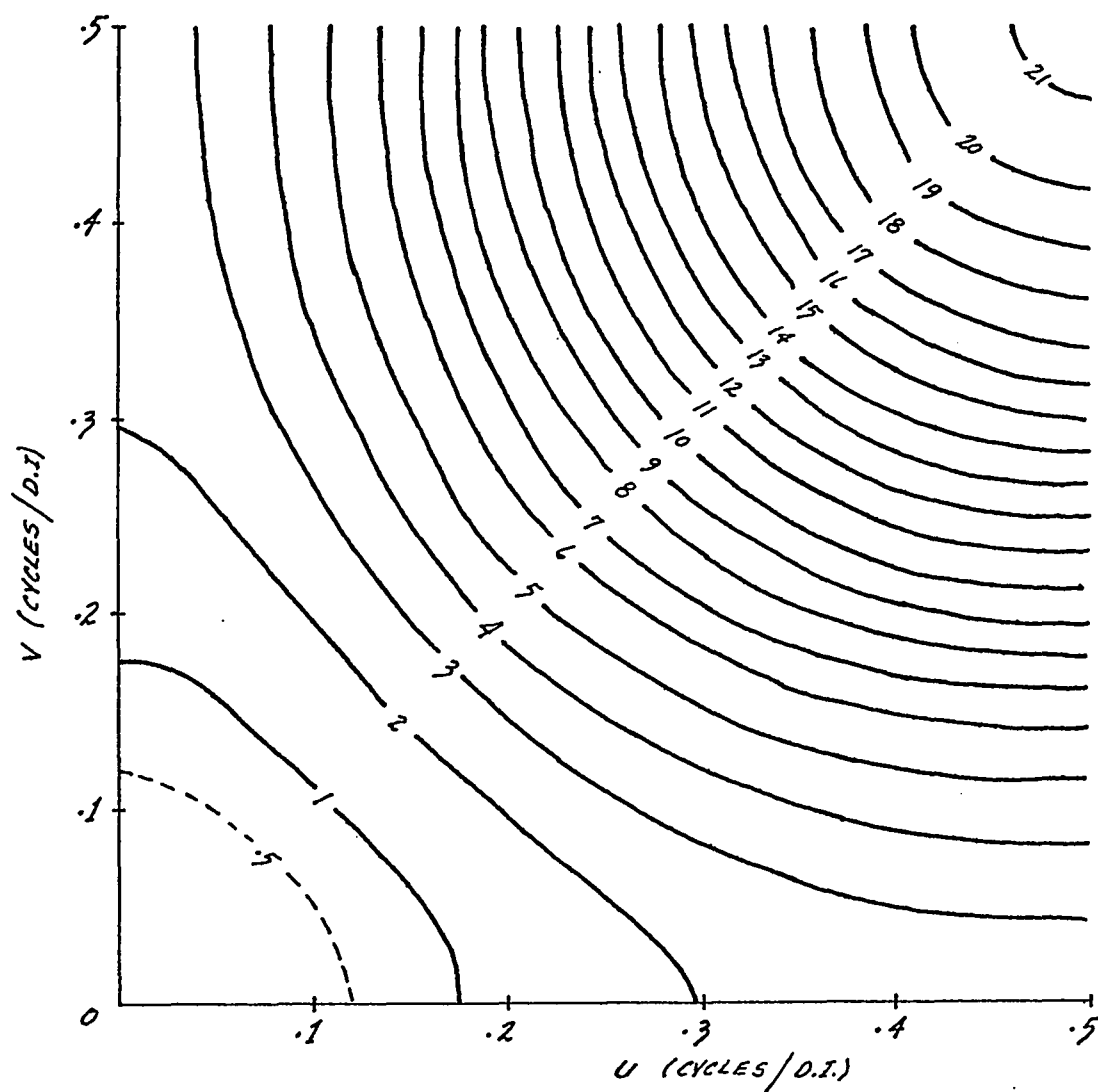


FIG. 2-16: RADIAL RESPONSE OF THE DERIVED SECOND VERTICAL DERIVATIVE OPERATOR



REFER TO THE OPERATOR OF TABLE A-6,
PAGE 127.

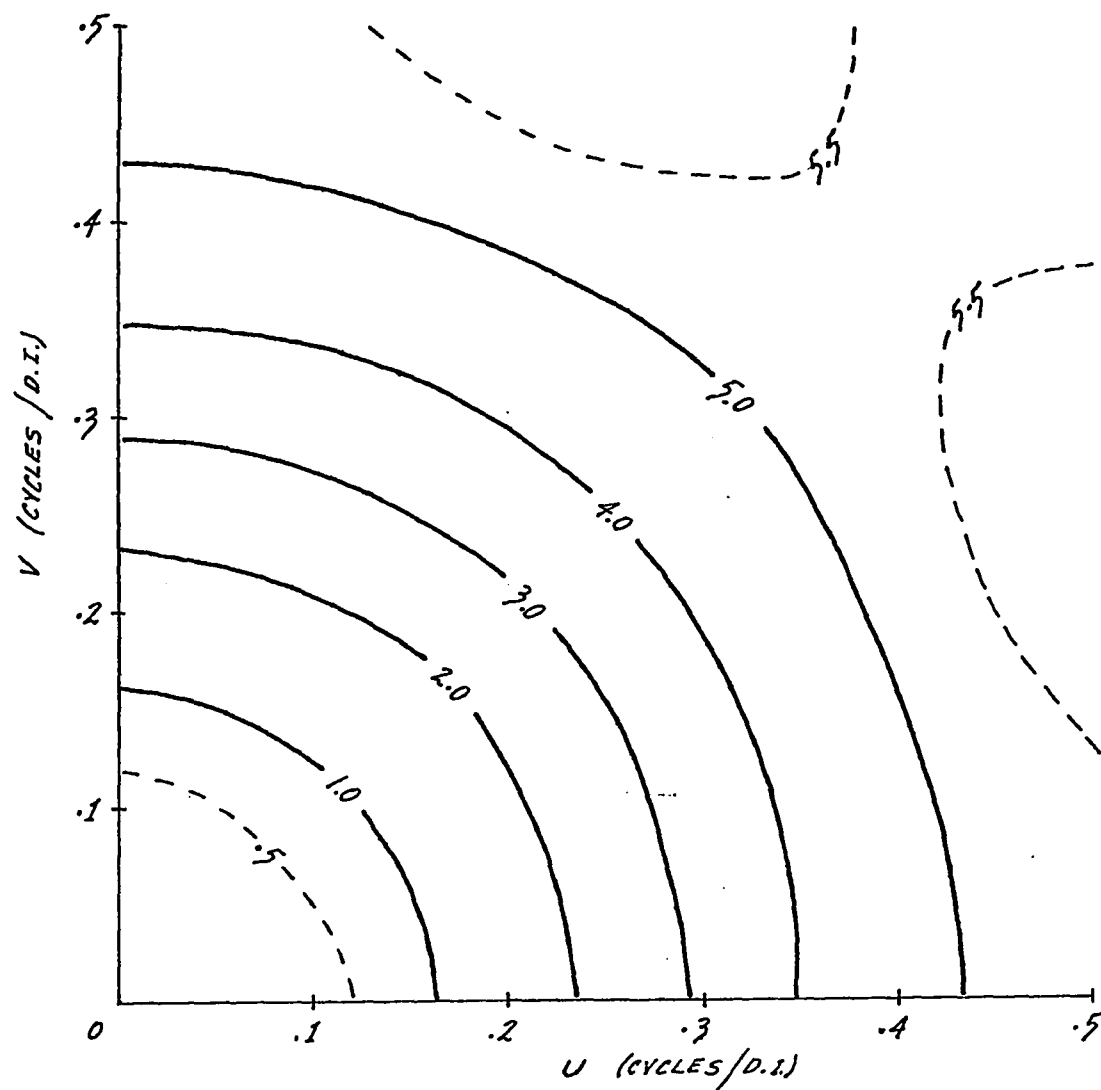
FIG. 2-17: AMPLITUDE RESPONSE OF HENDERSON AND ZIETZ' (1949) SECOND VERTICAL DERIVATIVE OPERATOR

tude response approaches that of the theoretical operator, while along the u and v axes the gain is relatively moderate. These variations in circular symmetry will be transmitted through the convolution process and create artificial trends in the data. The very large gain in the SW-NE and SE-NW directions will inevitably cause over-amplification of any high frequency noise effects present along these directions. The response of Rosenbach's operator, shown in Figure 2-18, page 91, exhibits very good symmetry and gain characteristics.

Both the derived operator of Figure 2-15, page 87, and Rosenbach's operator will provide a suitable approximation to the second vertical derivative operation. In the event that the data contains an excessive proportion of high frequency noise components, some form of noise filtering should be attempted before applying any high-gain operator.

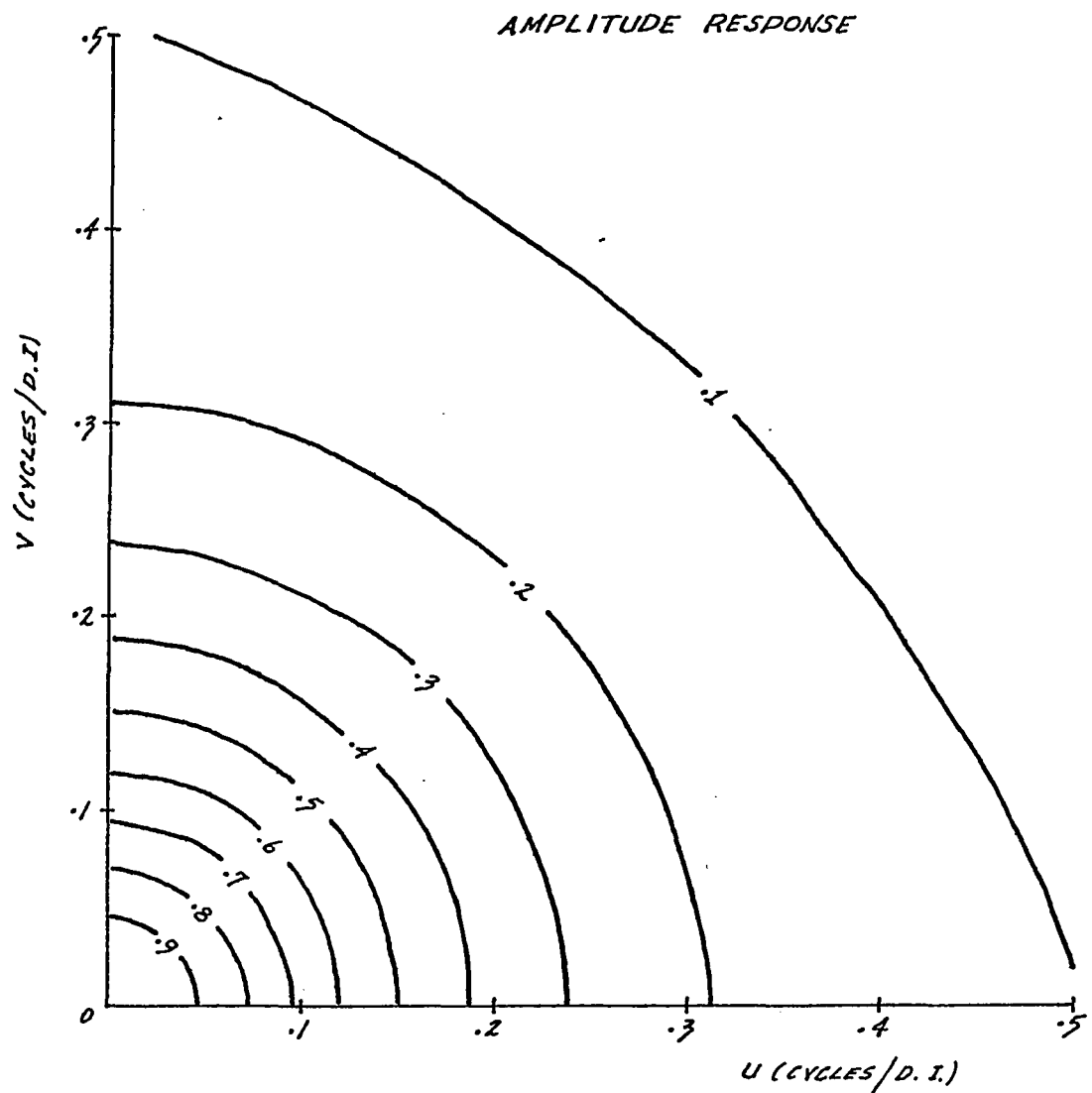
Continuation Operators

The inverse Hankel transform approach was used in the derivation of upward continuation operators for heights of one and two grid intervals above the data plane. Figures 2-19 and 2-20, pages 92 and 93, show the operators and their amplitude responses. The theoretical responses were inserted into the discrete inverse transform without attenuation, and the resulting coefficient sets were smoothed and normalized. Except for a smaller gradient at very low frequencies, the amplitude responses of the derived operators compare quite favorably with their theoretical counterparts. The frequency response of Peters'



REFER TO THE OPERATOR OF TABLE A-7
PAGE 127.

FIG. 2-18: AMPLITUDE RESPONSE OF
ROSENBACH'S (1953) SECOND
VERTICAL DERIVATIVE OPERATOR

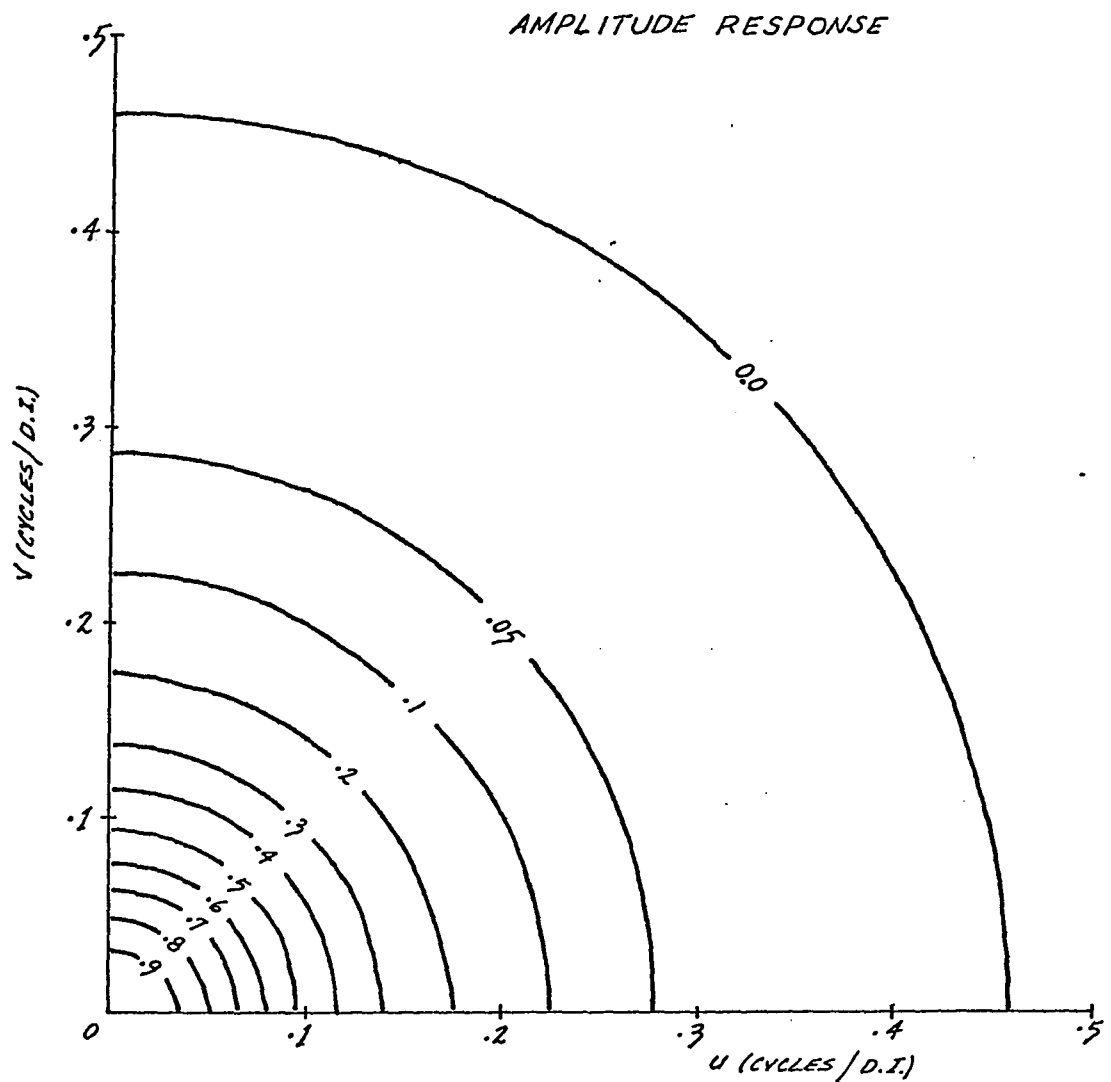


OPERATOR

8	.00010	.00009	.00006	.00003	.00003	.00002	.00000	.00000	.00000
7	.00019	.00017	.00011	.00010	.00009	.00003	.00003	.00001	.00000
6	.00035	.00032	.00029	.00028	.00013	.00011	.00004	.00003	.00000
5	.00081	.00079	.00076	.00046	.00029	.00017	.00011	.00003	.00002
4	.00216	.00205	.00148	.00081	.00060	.00029	.00013	.00009	.00003
3	.00578	.00486	.00275	.00189	.00081	.00046	.00028	.00010	.00003
2	.01734	.01228	.00669	.00275	.00148	.00076	.00029	.00011	.00006
1	.07047	.03733	.01228	.00486	.00205	.00079	.00032	.00017	.00009
0	.19679	.07047	.01734	.00578	.00216	.00081	.00035	.00019	.00010
	0	1	2	3	4	5	6	7	8

x

FIG. 2-19: DERIVED UPWARD CONTINUATION
OPERATOR FOR A HEIGHT OF ONE GRID UNIT



OPERATOR

8	.00018	.00017	.00015	.00011	.00007	.00004	.00002	.00000	.00000
7	.00044	.00041	.00034	.00025	.00017	.00010	.00005	.00002	.00000
6	.00091	.00086	.00073	.00055	.00037	.00021	.00012	.00005	.00002
5	.00200	.00185	.00148	.00104	.00069	.00041	.00021	.00010	.00004
4	.00416	.00379	.00295	.00200	.00119	.00069	.00037	.00017	.00007
3	.00939	.00822	.00568	.00347	.00200	.00104	.00055	.00025	.00011
2	.02115	.01741	.01080	.00568	.00295	.00148	.00073	.00034	.00015
1	.04604	.03422	.01741	.00822	.00379	.00185	.00086	.00041	.00017
0	.06429	.04604	.02115	.00939	.00416	.00200	.00091	.00044	.00018
	0	1	2	3	4	5	6	7	8

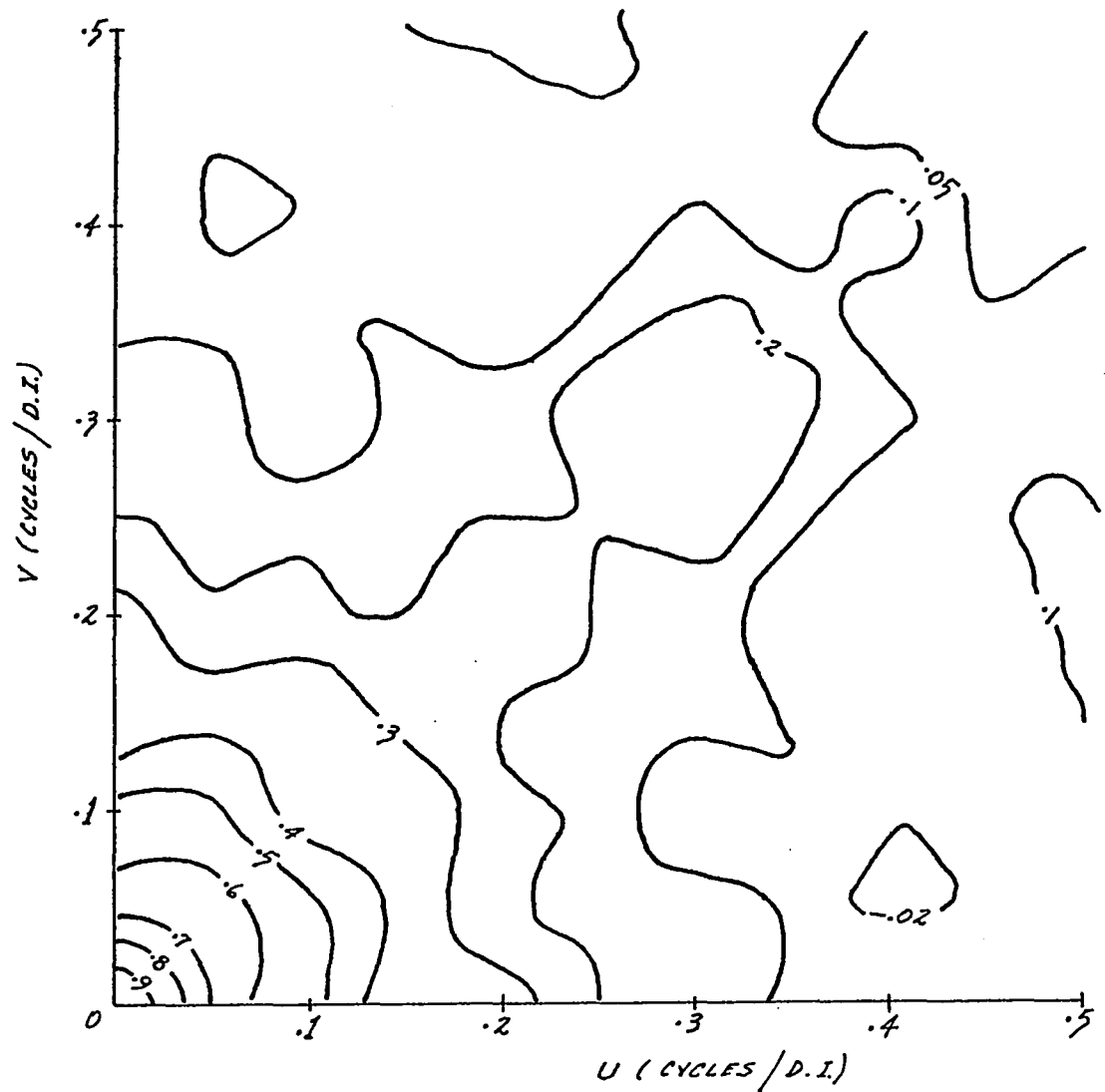
x

FIG. 2-20: DERIVED UPWARD CONTINUATION
OPERATOR, FOR A HEIGHT OF TWO GRID UNITS

upward continuation operator, of Table A-1, page 125, has been included for comparison (see Figure 2-21, page 95). Although a good approximation of the theoretical gain at low frequencies, the response does show undesirable deviations from circular symmetry. This defect could probably be corrected by increasing the coefficient coverage of the operator.

Of the various operations discussed in this thesis, the downward continuation process is the most difficult to approximate. No practical coefficient set can hope to approach the exceedingly high gains realized by the theoretical downward continuation operators. Even if this were possible, the convolution of such a coefficient set with actual potential field data would cause serious over-amplification of high frequency energy.

In designing a workable operator, we want to ensure close agreement between its low frequency response and that of the theoretical operator, since most of the waveform energy of the potential field is generally concentrated in the low frequency end of the spectrum. The high frequency response will be attenuated or levelled-off near the folding point, just as was done for the second vertical derivative operator. The inverse Hankel transform method may be used in the derivation, but the form of response attenuation required for optimum results is not a simple matter to decide. For our purpose, a more convenient approach was found by making use of previously derived operators and Taylor's expansion of the potential field. An approximation to the downward continued field based on Taylor's



REFER TO THE OPERATOR OF TABLE A-1,
PAGE 125.

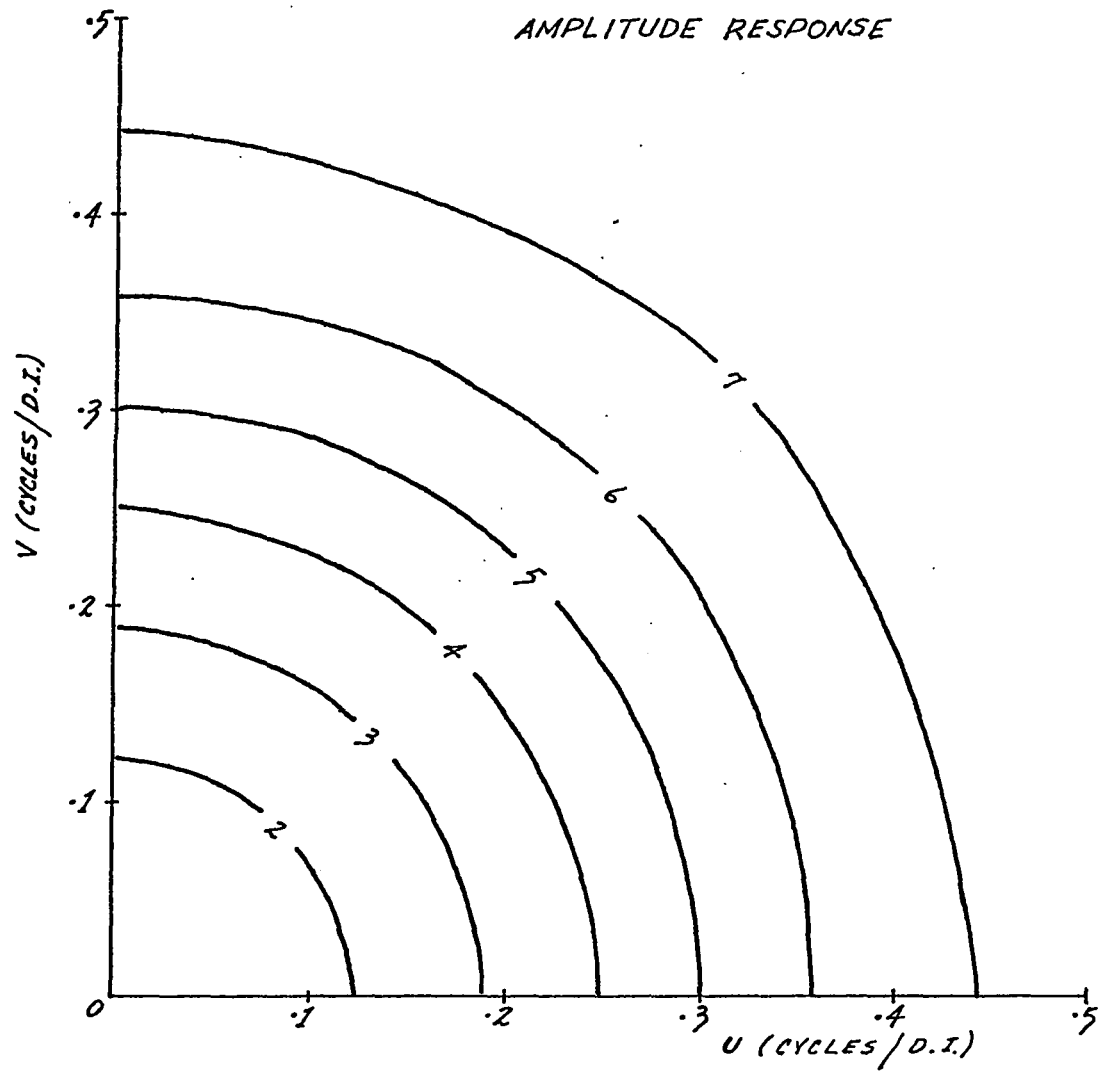
FIG. 2-21: AMPLITUDE RESPONSE OF PETERS' (1949)
UPWARD CONTINUATION OPERATOR FOR A
HEIGHT OF ONE GRID UNIT

expansions above and below the data plane has already been derived in section 2-2 of this chapter:

$$f(0,0,h) \doteq -f(0,0,-h) + 2 \left[f(0,0,0) + \frac{h^2}{2!} f''(0,0,0) \right] \quad (2-16)$$

where $f(0,0,0)$ is the field value at the origin or point of continuation, $f(0,0,-h)$ and $f(0,0,0)$ represent the upward continued field and the second vertical derivative of the field at the origin, respectively. In deriving equation 2-16 all vertical derivatives of order greater than the second have been ignored. If Rosenbach's second vertical derivative operator (Table A-7, page 127) and the derived upward continuation operator of Figure 2-19, page 92, are inserted in the right side of equation 2-16, the downward continuation coefficient set of Figure 2-22, page 97, emerges. The low frequency response of this operator is seen to be a good approximation to that of the theoretical filter, and the high frequency response shows the required attenuation.

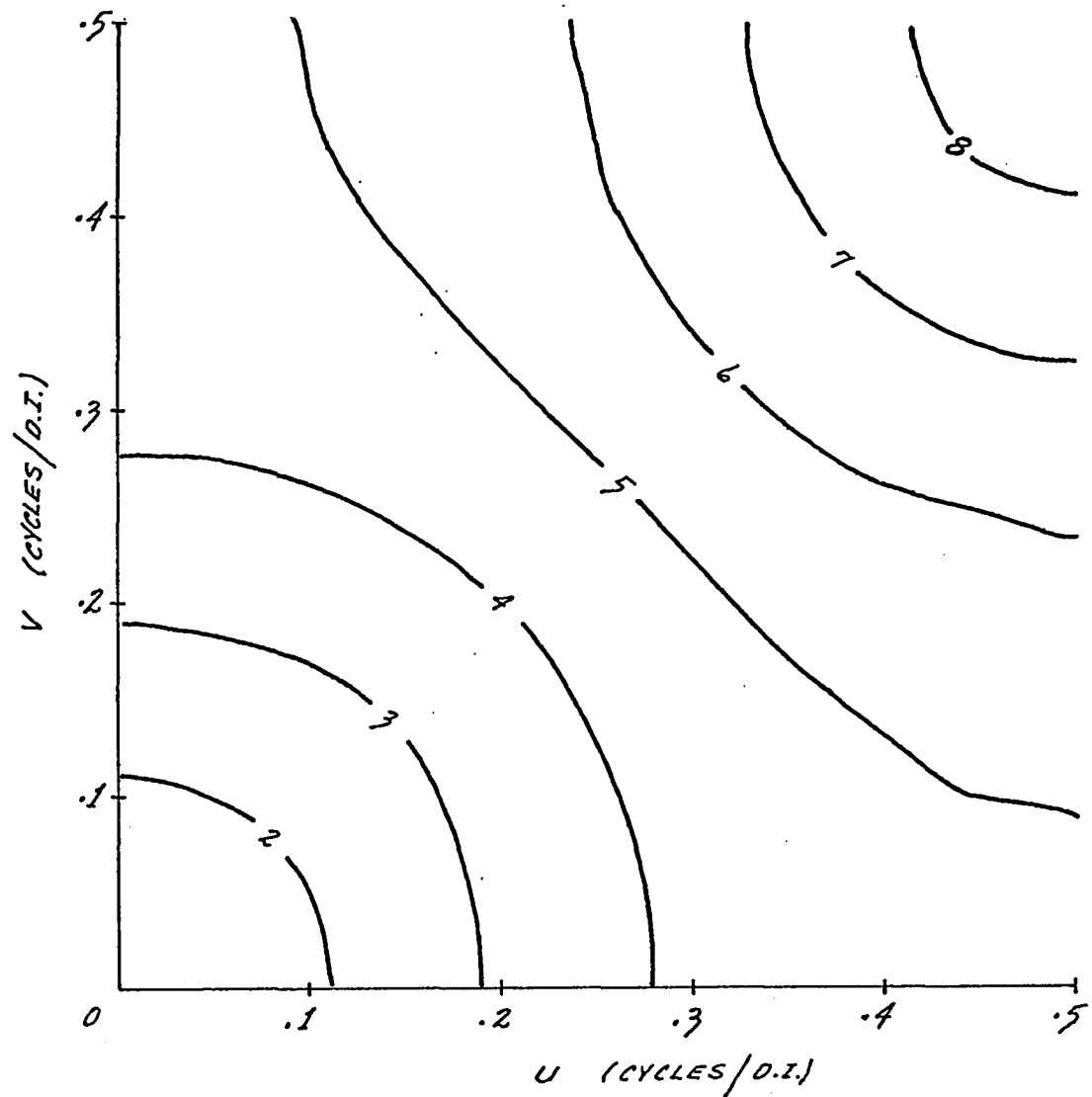
Again, two well-known operators have been included for the sake of comparison. Henderson's downward continuation operator of Table A-4, page 126, is a fairly good approximation of the theoretical operator at low and intermediate frequencies (see Figure 2-23, page 98). The large areal extent of the operator and the poor coefficient coverage, however, limit its usefulness in practical convolution. The downward continuation operator of Table A-5, page 127, derived by Grant and West (1967) shows a severely attenuated response (see Figure 2-24, page 99) and significant directional properties. The exponential atten-



OPERATOR

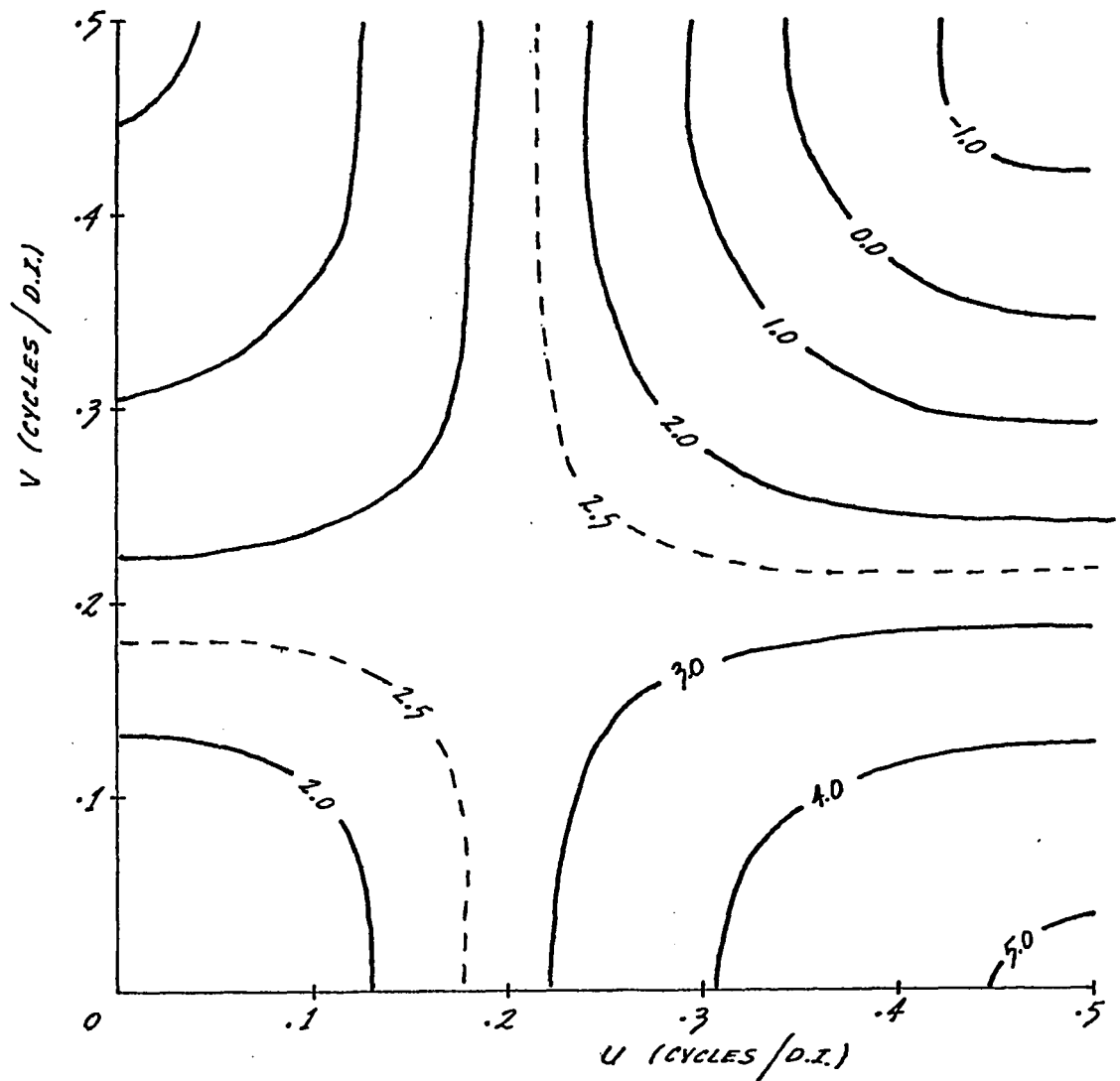
8	-.00010	-.00009	-.00006	-.00003	-.00003	-.00002	.00000	.00000	.00000
7	-.00019	-.00017	-.00011	-.00010	-.00009	-.00003	-.00003	-.00001	.00000
6	-.00035	-.00032	-.00029	-.00028	-.00013	-.00011	-.00004	-.00003	.00000
5	-.00081	-.00079	-.00076	-.00046	-.00029	-.00017	-.00011	-.00003	-.00002
4	-.00216	-.00205	-.00148	-.00081	-.00060	-.00029	-.00013	-.00009	-.00003
3	-.00578	-.00486	-.00275	-.00189	-.00081	-.00046	-.00028	-.00010	-.00003
2	-.01734	.02932	-.00649	-.00275	-.00148	-.00076	-.00029	-.00011	-.00006
1	-.82047	-.37053	.02932	-.00486	-.00205	-.00079	-.00032	-.00017	-.00009
0	5.80321	-.82047	-.01734	-.00578	-.00216	-.00081	-.00035	-.00019	-.00010
	0	1	2	3	4	5	6	7	8

FIG. 2-22: DERIVED DOWNWARD CONTINUATION OPERATOR FOR A DEPTH OF ONE GRID UNIT



REFER TO THE OPERATOR OF TABLE A-4
PAGE 126.

FIG. 2-23: AMPLITUDE RESPONSE OF HENDERSON'S
(1960) DOWNWARD CONTINUATION OPERATOR
FOR A DEPTH OF ONE GRID UNIT



REFER TO THE OPERATOR OF TABLE A-5
PAGE 127.

FIG. 2-24: AMPLITUDE RESPONSE OF GRANT AND WEST'S (1967) DOWNWARD CONTINUATION OPERATOR FOR A DEPTH OF ONE GRID UNIT

uation used in the derivation reduces the high frequency gain but also distorts the mid-band region.

Downward continuation to a depth of two grid units may be attempted, but the problems of operator design and high frequency instability are much more severe. Assuming a reasonable station spacing, continuation downward to a depth of one grid unit should be sufficient for most applications.

Chapter 3:

APPLICATION OF FILTERS TO POTENTIAL FIELD DATA

The purpose of this chapter is to show how discrete filters can be applied to gravity and magnetic data to separate, enhance or subdue various frequency components in the potential field spectrum. The data which will be used in the illustration represents a portion of the gravity and magnetic surveys conducted over the Atlantic Nickel Property near the town of St. Stephen, New Brunswick. A number of filters derived in this thesis will be applied to the data in order to demonstrate the effectiveness of the filtering approach and to illustrate the characteristics of the individual filter outputs. A brief interpretation of the results will be presented and related to the known geology of the area.

3-1 Investigation of the Roger's Farm Sulphide Zone -
St. Stephen, New Brunswick

The Atlantic Nickel Property near St. Stephen, New Brunswick, has been the subject of intensive, albeit sporadic, geological and geophysical investigation since 1942. Although the existence of nickel-copper mineralization in the area was known around 1900, it has only been in the last decade that detailed exploration and pre-development work has been carried out. Over this period no less than twenty-four zones of sulphide mineralization have been located by geophysical and drilling programs,

and of these perhaps three may be considered of marginal or sub-marginal economic importance. The Roger's Farm sulphide zone is one of the more promising deposits with an estimated tonnage of between 0.5 and 0.8 million tons, averaging about 1.0% nickel and 0.5% copper.

In 1968 the Hanna Mining Company picked up the option on the property and conducted extensive geological and geophysical investigations for the purpose of re-evaluating the known sulphide deposits, and to provide information which might be of value in assessing other holdings in the area.

Local Geology

The predominant geological feature in the area consists of a stock-like basic to ultrabasic pluton which has intruded, what appears to have been, an anticlinal structure of metamorphosed sediments. The sediments are of Ordovician age and consist of dark grey argillite, slate, quartzitic mica schist, and gneiss. The main body of sediments underlies the northern and eastern margins of the property, strikes roughly north-east and dips steeply to the north-west. Sediments also occur as inclusions of up to 500 feet by 2000 feet in size within the intrusive rocks of the igneous mass. The intrusion is composed of gabbro-norite, anorthosite, and peridotite and occupies the central and south-western portions of the property. Pyrrhotite occurs quite commonly as veinlets and disseminations within the intrusive rock and is the primary component of the observed zones of sulphide mineralization. The minerals chalcopyrite

and pentlandite occur as blebs and veinlets within the pyrrhotite.

The more important zones of mineralization seem to be located very close to contacts between the intrusives and altered sediments. The zones of weakness created by these contacts may represent potentially favorable sites for sulphide deposition.

Geophysical Surveys

V.L.F. (EM 16) and horizontal loop electromagnetic surveys conducted over the Roger's Farm zone have traced out the extent of the anomalous conductivity associated with the mineralization. The relative position of the sulphide zone and related conductor is shown in Figure 3-1, page 109. The conductor extends along the north-south baseline (105E) for about 400 feet. South of 160N it seems to divide into two zones: one part swinging out to the south-west and the other continuing along the baseline for some distance. Horizontal Loop EM profiles over lines 162N and 160N show an abnormally large electromagnetic coupling effect due to the shallow depth and high conductivity of the mineralized zone. In fact the sulphide zone intersects the surface in the vicinity of lines 160N and 158N and is marked by the presence of a gossan outcrop. The postulated northern contact between gabbro-norite intrusives and the altered sediments is also indicated in Figure 3-1.

A gravity survey was conducted over part of the property in 1955 by Radar Exploration Limited. Readings were taken at

50 foot intervals along lines spaced from 200 to 450 feet apart and running approximately east-west. A portion of the resulting Bouguer gravity contour map in the vicinity of the Roger's Farm zone is shown in Figure 3-2, page 110. The gravity map is characterized by a simple, but predominant, regional trend decreasing in magnitude towards the north. This effect is probably due to the thickening of the sediments in this direction and a corresponding increase in depth of the ultrabasic rocks. The gabbroic rocks of the intrusion would have a significantly greater density than the sediments and would explain the density contrast causing the observed gradient. The regional trend is disturbed by a number of residual effects, one of which, located at approximately 105E and 160N, corresponds to the positive density contrast created by the Roger's Farm sulphide body.

A portion of the magnetic data obtained by the Hanna Mining Company in 1968 is contoured in Figure 3-6, page 114. Readings were taken normally at 50 foot and occasionally at 25 foot intervals along east-west grid lines spaced 200 feet apart. Although the gravity and magnetic maps cover the same surface area, the relationships between their regional and residual features are vastly different. The high amplitude, and at times, erratic residual components of the magnetic field tend to overpower the more subtle regional changes. The reverse is true, of course, for the gravity map which was seen to consist of relatively weak residual anomalies superimposed over a very strong regional trend. The regional features of the

magnetic data show up as depressions and moderate highs of relatively significant areal extent, and may be important in understanding the geological environment of the area. The high frequency, high amplitude fluctuations of the magnetic map arise from two separate sources. The occurrence of massive pyrrhotite as the main constituent of the sulphide zones is partly responsible for associated magnetic anomalies. The other source, in the form of localized, high intensity dipole effects within the ultrabasic rocks, probably represents abnormally high magnetite concentrations.

3-2 Filtering the Roger's Farm Potential Field Data and Discussion of Results

A computer program was written to calculate the discrete form of the two-dimensional convolution integral (equation 2-4, page 52) upon given digitized potential field data and a set of filter coefficients. The gravity and magnetic maps of Figures 3-2 and 3-6 were then digitized using a square grid interval of 100 feet. Considering the erratic nature of the magnetic field, sampling and interpolation of the magnetic data is much more susceptible to aliasing and other sampling effects than is the case for the smoother varying gravity data.

Gravity Maps

In the Bouguer gravity map of Figure 3-2, page 110, the residual features are of primary concern and must be separated

from the well-defined regional trend. The second vertical derivative operator of Figure 2-15, page 87, was convolved with the data in an attempt to emphasize the higher frequency effects and, at the same time, to reject the regional. The resulting output is shown in Figure 3-3, page ///. The second vertical derivative, in effect, represents the curvature of the potential field. Since a positive gravity or magnetic anomaly will generally show positive curvature at its center and negative curvature off its flanks, second vertical derivative highs will usually be associated with adjacent lows; a fact demonstrated in Figure 3-3. The main zone of the Roger's Farm mineralization, located at the center of the map, and its offshoot to the south-west are associated with well-defined second vertical derivative anomalies. The filter has also clearly emphasized two pod-like disturbances north-east of the Roger's Farm zone. These anomalies may be due to the presence of small sulphide showings.

The inverse wavelength filter of cut-off 0.075 cycle/D.I. (shown in Figure 2-14, page 85) was convolved with the Bouguer gravity data in order to obtain the residual map of Figure 3-4, page //2. It can be seen that a well-defined residual anomaly with an approximate magnitude of 0.30 mgals. is associated with the main Roger's Farm sulphide zone. The smaller anomalies to the north-east, noted on the second derivative map, are also brought out by the residual filter. Two relatively broad highs, one going off the map in the north and the other to the south-

east, may result from an upward projection of the gabbroic intrusive.

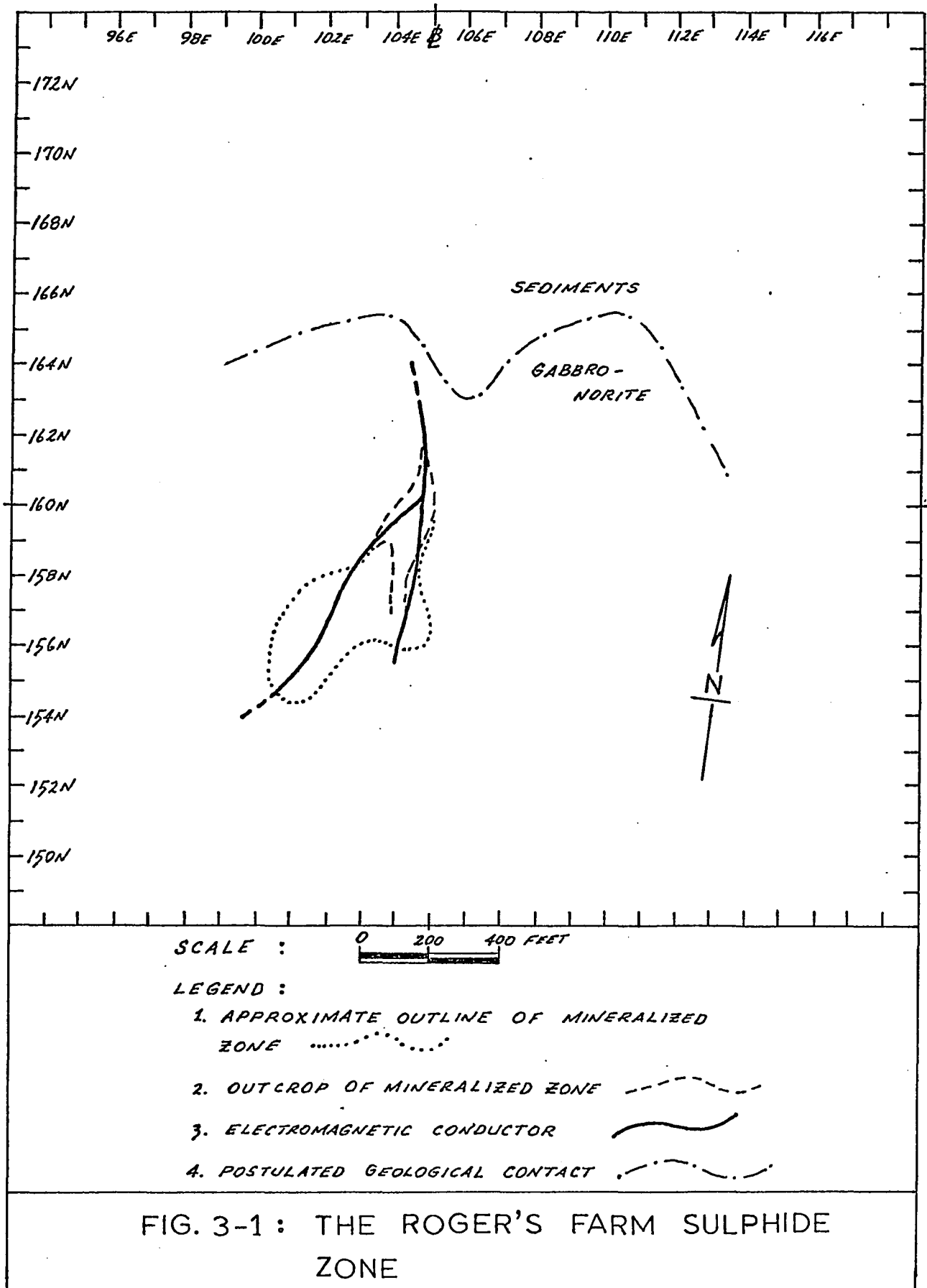
The residual and second vertical derivative filters seem to produce roughly the same results. The low frequency components which make up the regional trend have been rejected and the higher frequency residual retained. The greater gain of the second vertical derivative at higher frequencies tends to produce sharper, more localized peaks than the residual filter. The second derivative also shows considerably less low frequency definition. The residual filter output of Figure 3-4 probably gives a very good approximation to the anomaly pattern produced by near surface density changes, but some low frequency definition has been lost in the process. In detailed interpretations hand profiling methods should be used to separate regional and residual features so that the interpreter can use his own skill and judgement. The value of the second vertical derivative and residual operators lies in their ability to uncover residual anomalies and trends which might be overlooked otherwise. In addition, they provide some idea of anomaly size and character which may assist in the planning of more detailed methods of interpretation.

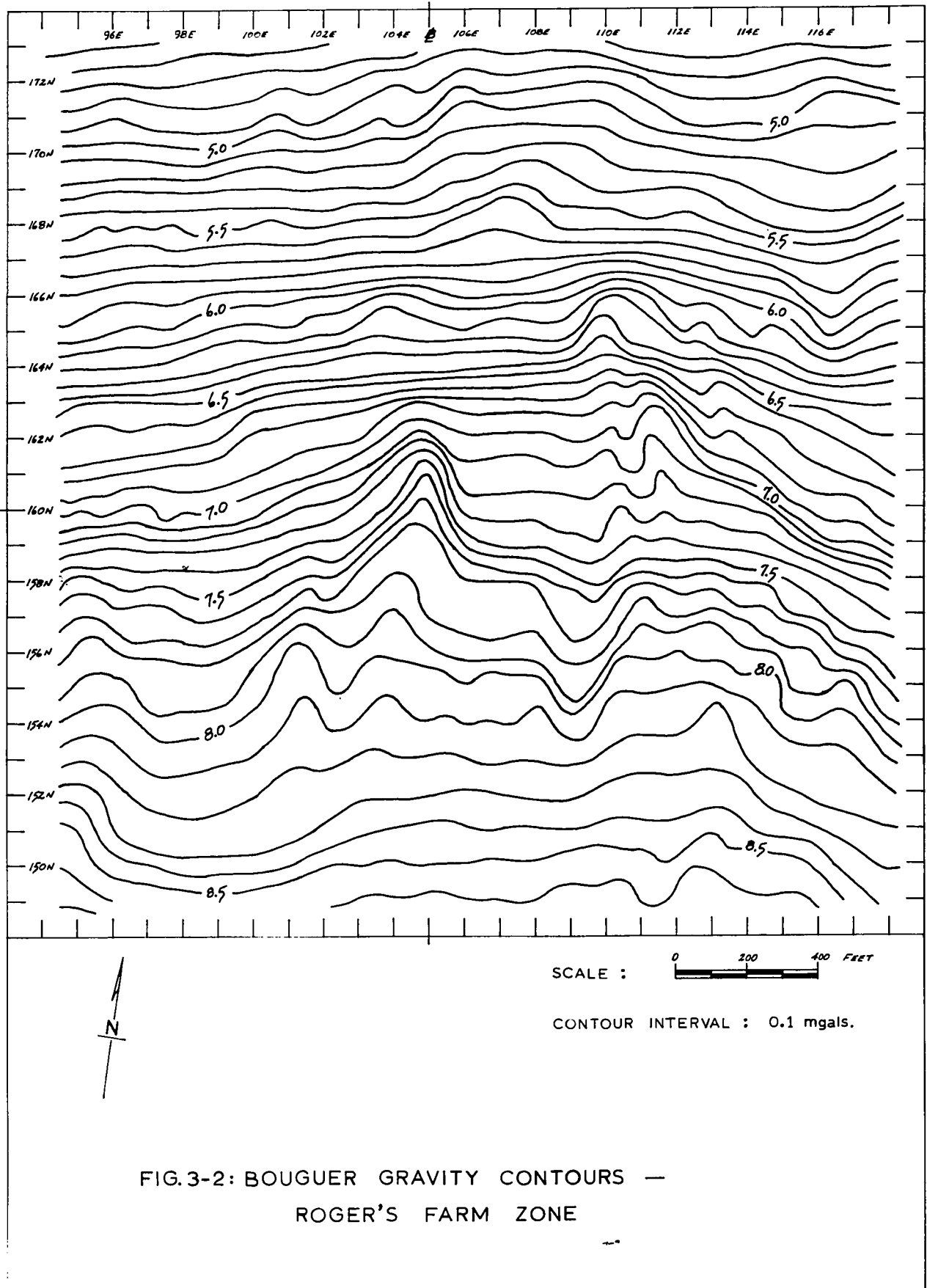
The downward continuation operator presented in Figure 2-22, page 97, was also applied to the Bouguer gravity data. The northern portion of the Roger's Farm sulphide zone outcrops at the surface and raises serious doubts concerning the validity of the downward continuation concept in its vicinity. In deriving

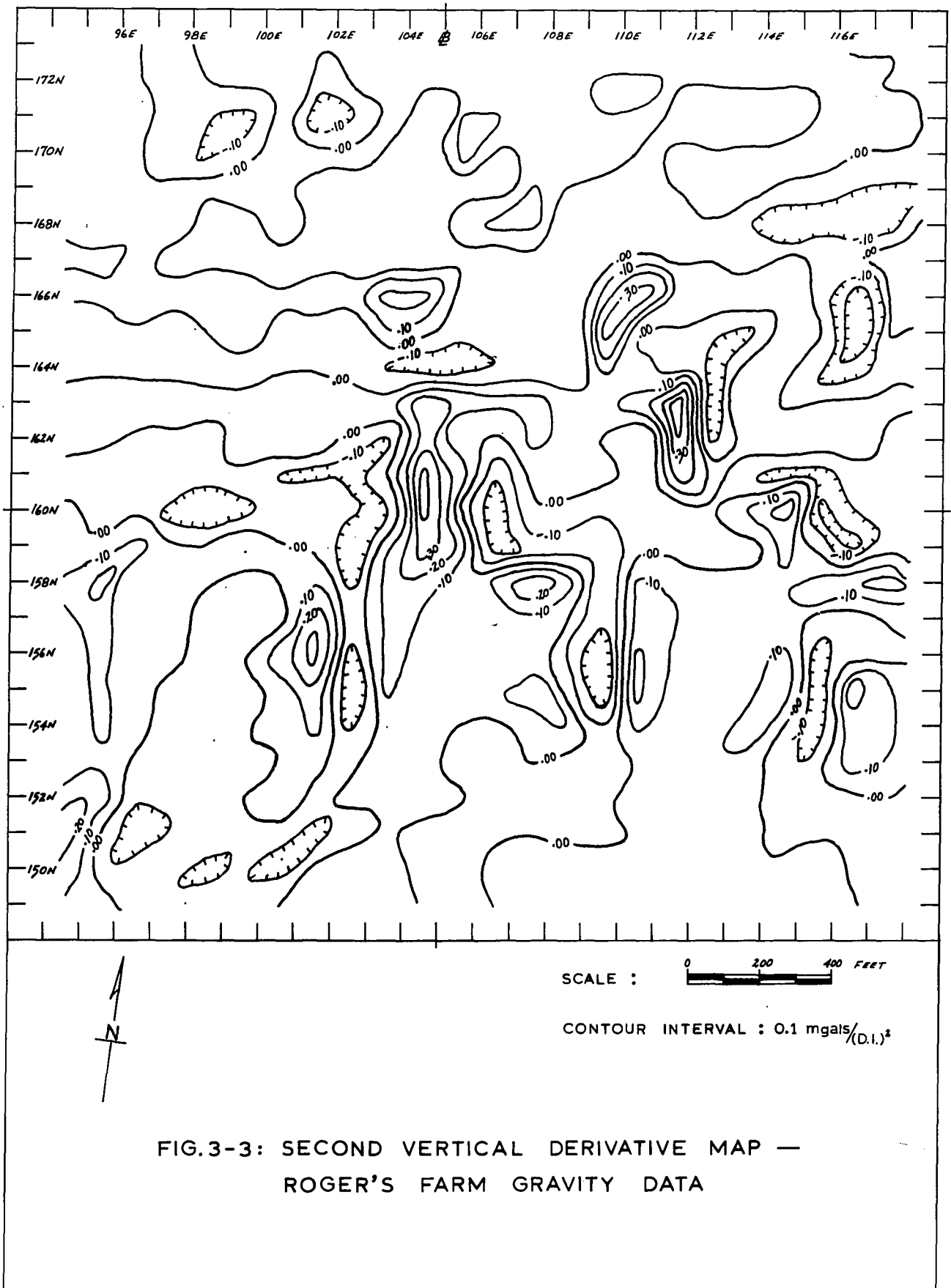
the operator we have assumed that there are no intervening masses between the surface and the level of continuation, a condition almost never realized in practice. By attenuating the high frequency response of the operator, however, we had hoped to reduce the risk of erratic fluctuations caused by near surface sources. Since the gravity data considered here probably violates this harmonic field restriction in certain places, its continuation downward will serve as a test of operator stability. The continuation of the field to a depth of 100 feet (shown in Figure 3-5, page 113) has amplified a good deal of high frequency noise. There are, however, no points of serious distortion and most of the residual features have been brought out. Considering the fact that no smoothing of the field was undertaken prior to convolution, the resulting output is remarkably good. The example does serve to demonstrate the high frequency amplification associated with downward continuation, and also shows that the derived operator can be used without having to resort to severe smoothing. For more complicated potential field maps, exhibiting high amplitude noise components, some form of smoothing would be necessary before any attempt was made to continue the field downward.

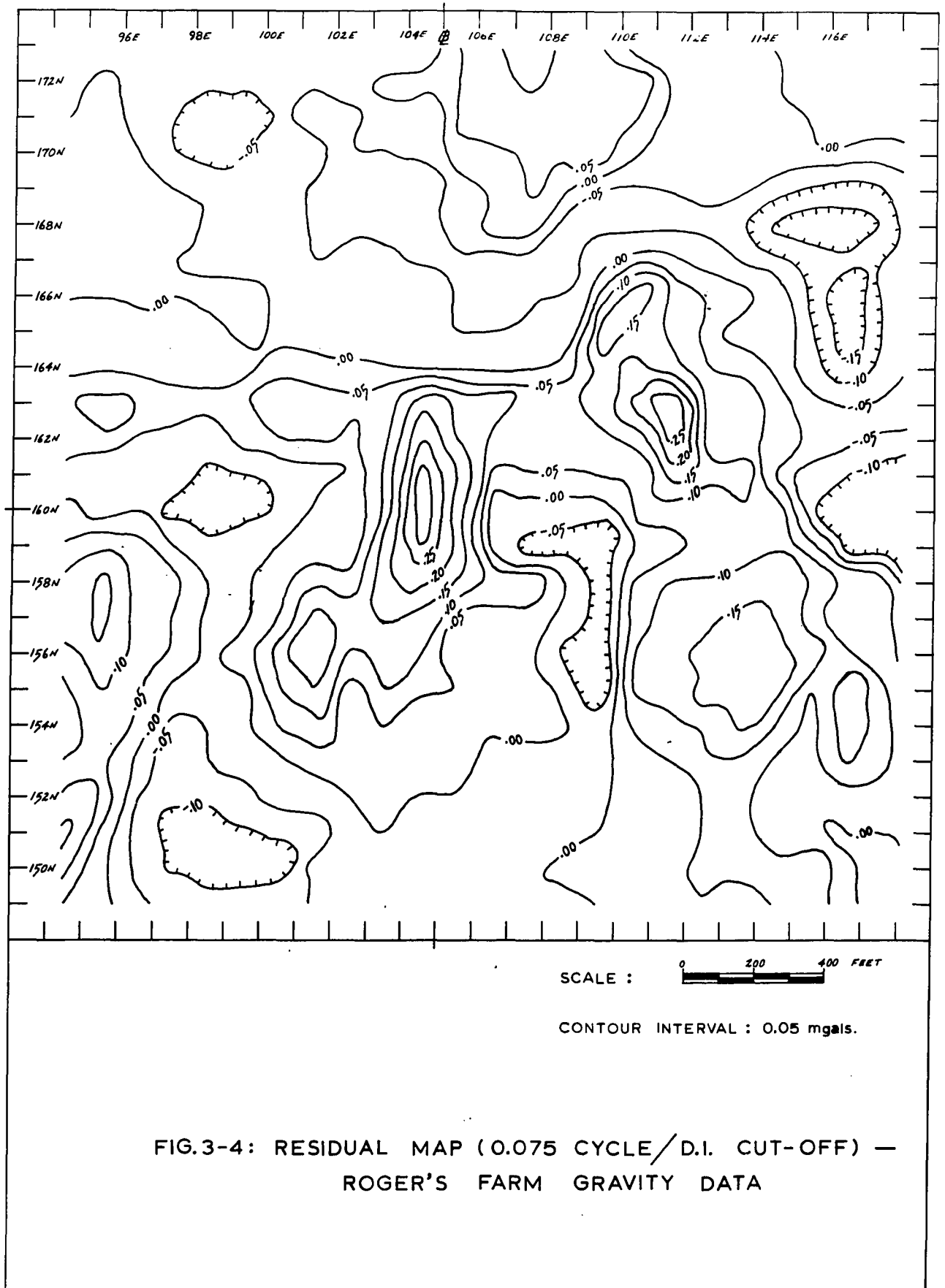
Magnetic Maps

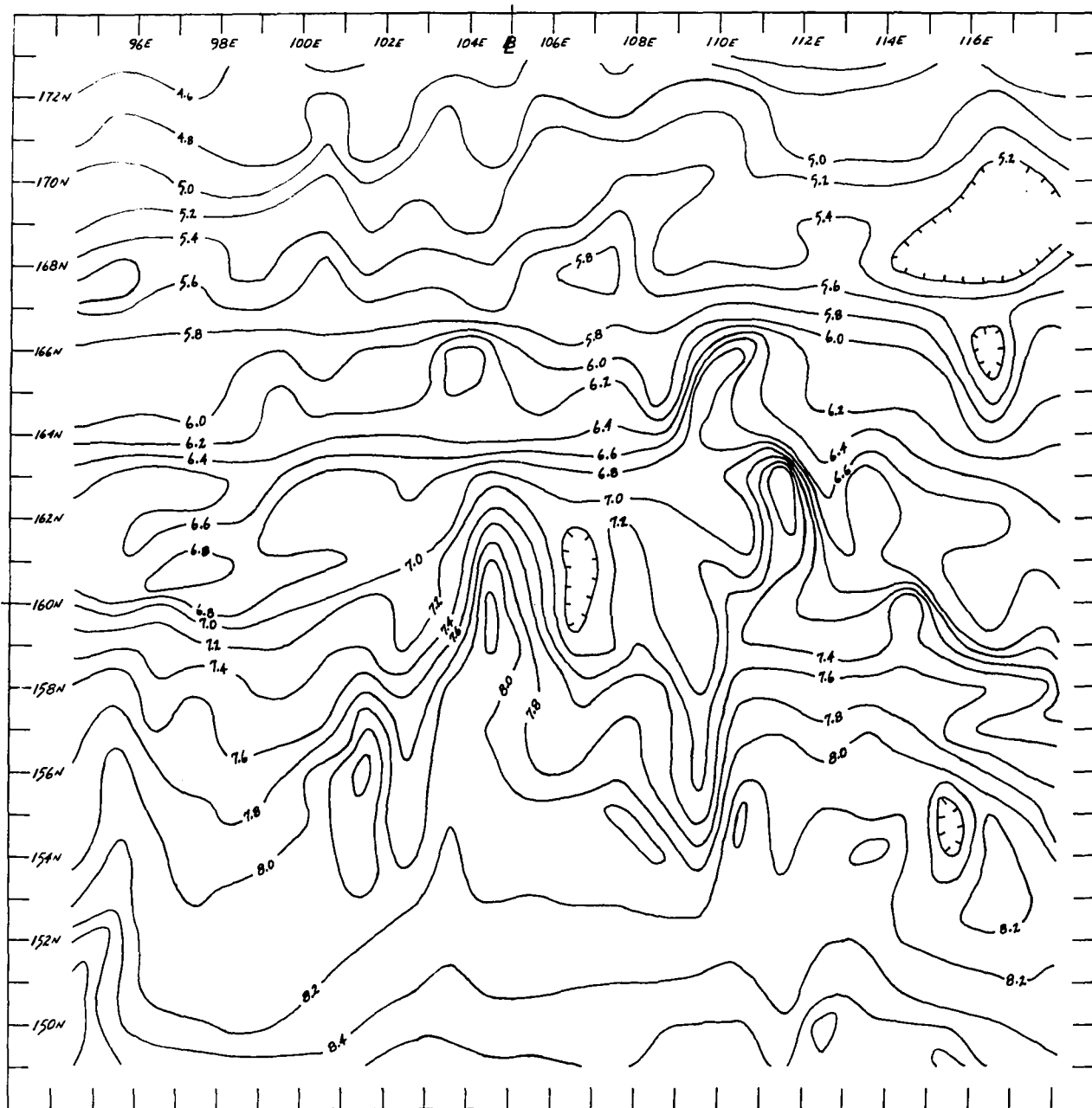
The magnetic map of Figure 3-6, page 114, is characterized by a number of high amplitude, high frequency anomalies, the most distinctive of which seems to be very closely related to the Roger's Farm mineral deposit. The magnetically depressed









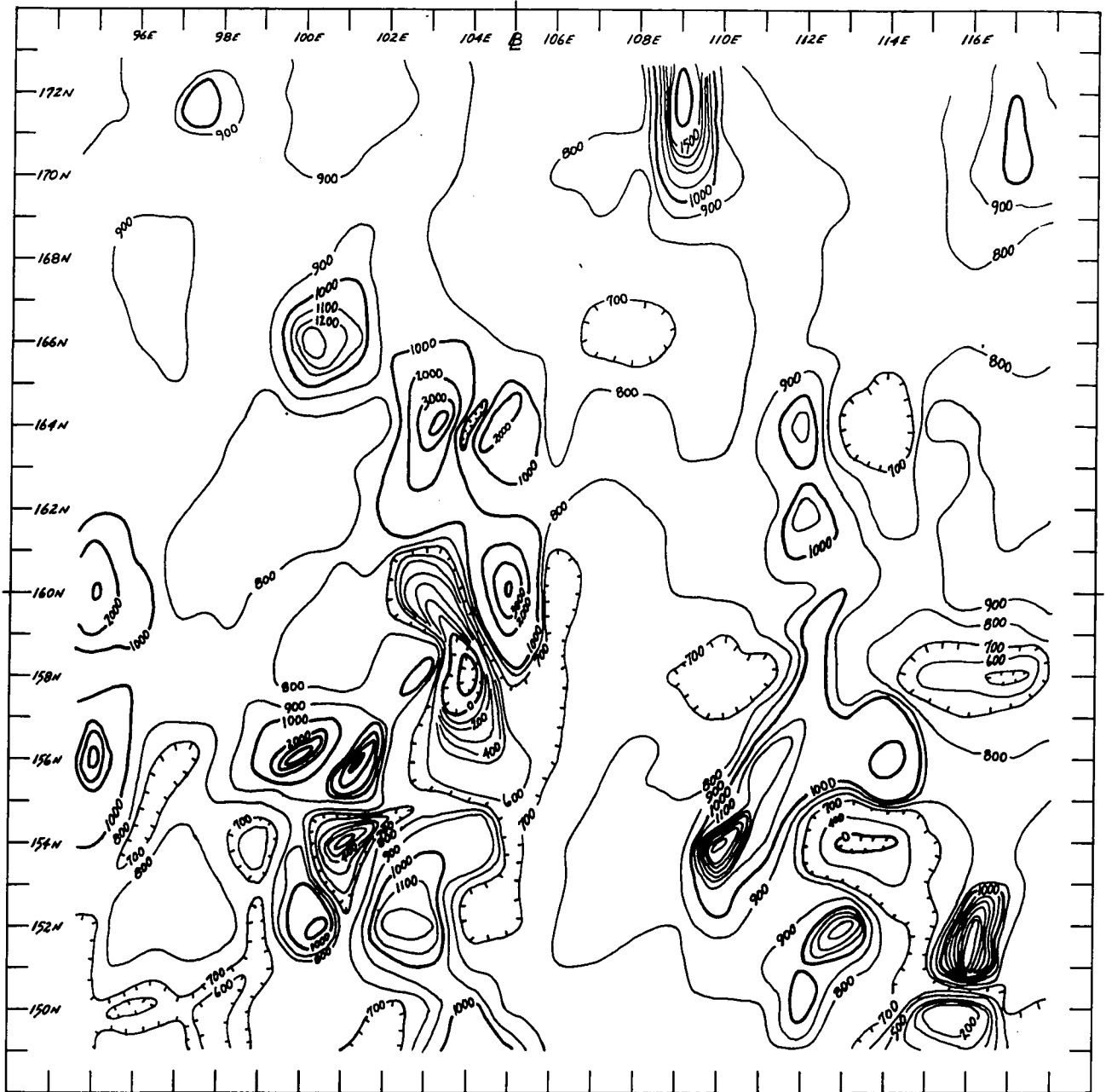


SCALE :



CONTOUR INTERVAL : 0.2 mgal.

FIG.3-5: DOWNWARD CONTINUATION MAP FOR A
DEPTH OF 100 FEET — ROGER'S FARM
GRAVITY DATA



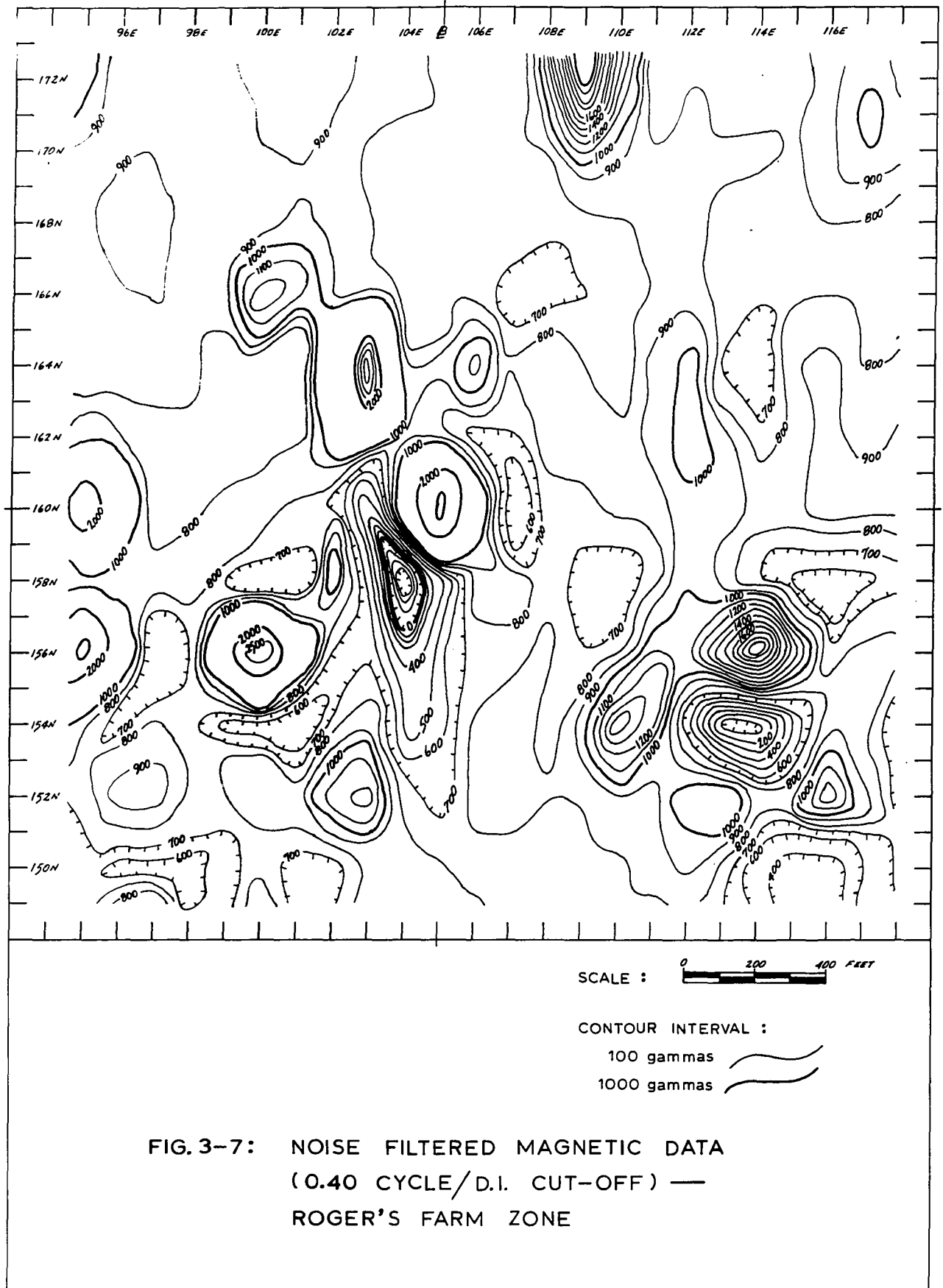
SCALE : 0 200 400 FEET

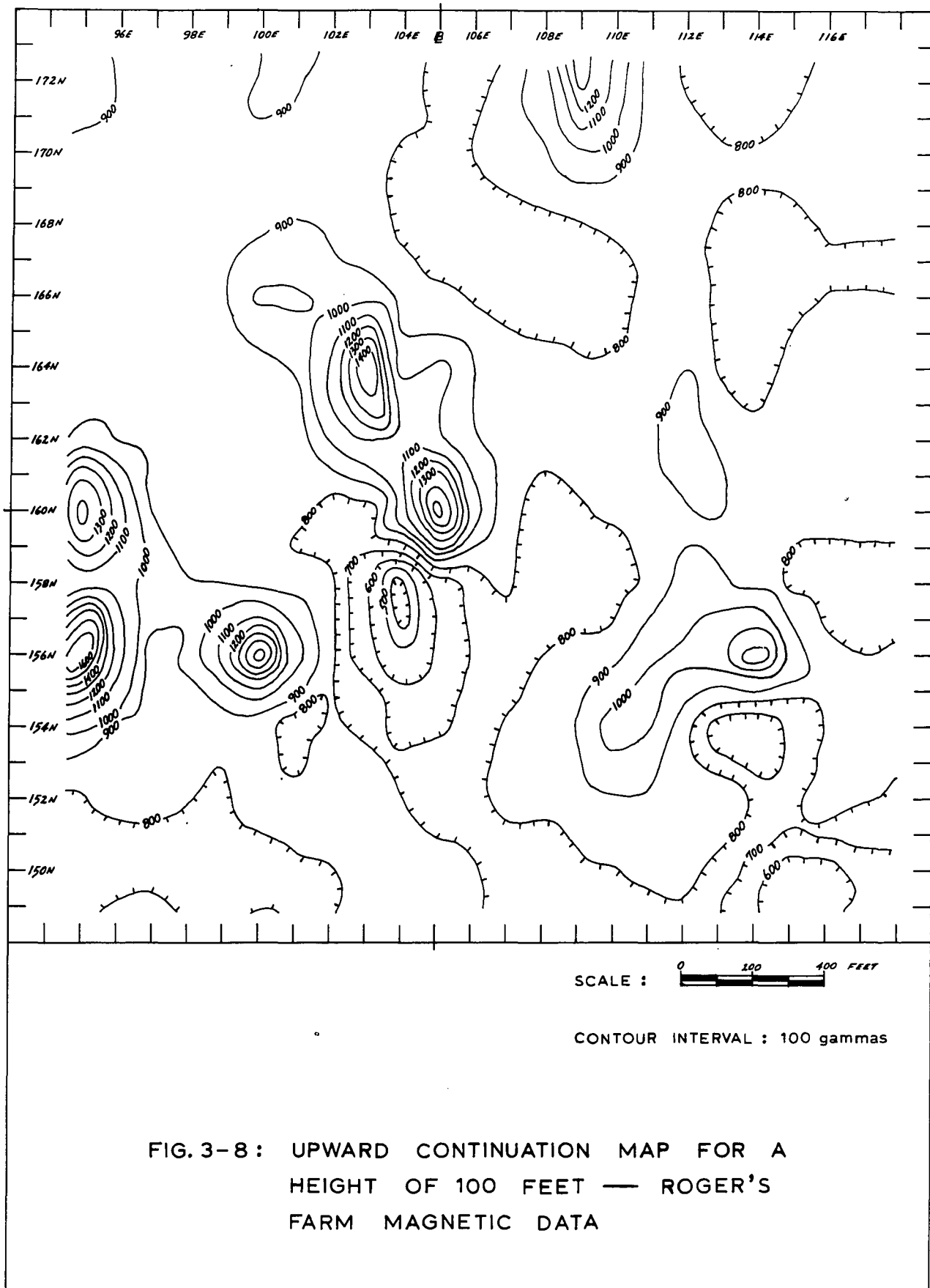
CONTOUR INTERVAL :

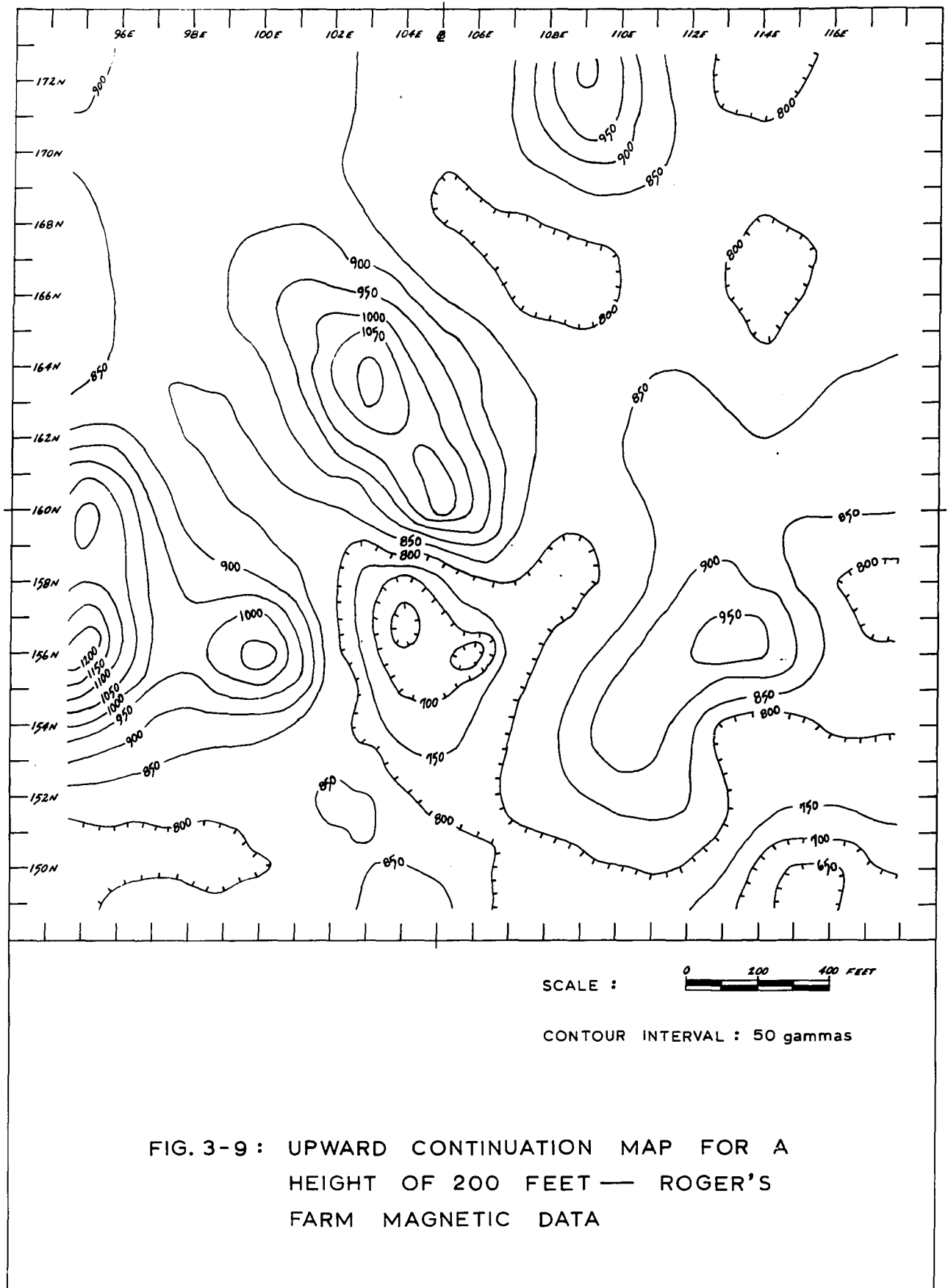
100 gammas

1000 gammas

FIG.3-6: MAGNETIC CONTOURS —
ROGER'S FARM ZONE







areas bounded by the 800 gamma contours and surrounded by moderate magnetic highs are probably of greater interest because of the structural information they provide. These low areas may coincide with islands or inclusions of metamorphosed sediments believed to have been isolated from the main sedimentary mass by the intrusion of basic material. The "high" areas enclosing these depressions may be explained by the greater magnetic susceptibility of the surrounding basic rocks. If these hypotheses are correct, then the boundaries of the magnetically depressed areas would represent the contact between the intrusive and altered sediments and, therefore, potentially favorable zones of mineral deposition. The Roger's Farm sulphide mineralization seems to be located along one of these contact zones. In an attempt to emphasize the boundaries of the magnetically low areas with respect to the dominant residual features, the noise filter of Figure 2-8 page 79, was applied to the magnetic data. Since the higher frequencies have been excluded, the resulting output, shown in Figure 3-7, page 115, is less erratic than the original map, and the delineation of the magnetically depressed areas is somewhat enhanced.

To afford a more drastic attenuation of the high frequency effects, the magnetic map was continued upward to heights of 100 and 200 feet using the operators of Figures 2-19 and 2-20, pages 92 and 93. The continuation upward to 100 feet (shown in Figure 3-8, page 116) reduced the amplitudes of the residual components considerably, but has not greatly affected the lower

frequency components. As a result, the boundaries of the depressed areas stand out clearly and their relationships to the residual features of both the gravity and magnetic fields are easily seen. Figure 3-9, page 117, shows the magnetic field continued upward a height of 200 feet. Very little additional high frequency suppression has been gained at 200 feet and, in fact, the delineation of the boundaries has decreased somewhat.

If the various gravity and magnetic maps are compared and the relative positions of the gravity and magnetic features observed, a number of correlations emerge. The gravity and magnetic residual anomalies associated with the Roger's Farm sulphide zone occur along the boundary of a magnetically depressed area. Residual gravity features to the north-east and south-east of the map center also fall on or very close to similar boundaries. The magnetically depressed areas seem to coincide with lows on the residual gravity map, and magnetic highs of moderate amplitude, surrounding the depressed areas, usually coincide with moderate gravity highs. The hypothesis of sedimentary "islands" surrounded by basic intrusives is compatible with these observations. If similar intrusives occur in the region, the contacts formed with such sediments may be potential sites of mineral deposition.

The foregoing discussion was not intended to be a complete interpretation of the gravity and magnetic data presented, but simply an illustration of a few ways in which potential field filters might help the interpreting geophysicist.

Chapter 4:

DISCUSSION AND CONCLUSIONS

Prior to interpreting potential field surveys, the geophysicist should familiarize himself with the limitations of the data and the conditions under which they were obtained. This should be done for any method in applied geophysics but is of particular concern in gravity and magnetic surveys. Errors introduced by inaccurate observation, sampling effects, and various correction procedures should be known within certain limits and their influences allowed for. In the case of gravity data, the systematic application of detailed corrections is a critical initial stage of the interpretation, and if not executed successfully may render the data unsuitable for subsequent interpretation. The interpreter, in addition to assessing the suitability of the data, should make every effort possible to gather available geological and geophysical information pertaining to the problem at hand. Having completed these initial stages of preparation, the geophysicist will be in a better position to select suitable methods of analysis and interpret the results.

The application of frequency analysis and information theory to the problems of gravity and magnetic interpretation provides more than just a convenient means of operator design and data processing. The insight gained by another point of view helps to clarify the more qualitative aspects of inter-

pretation confronting the geophysicist. Included in this category are the problems of anomaly separation, the elimination of noise effects, the detection and correlation of trends in the data, and the understanding of sampling processes. In these respects, potential field operators are of great assistance to the geophysicist as qualitative indicators or sensors of anomalous conditions in potential field data. Although the use of such operators complements it can never replace the experience and judgement of the interpreter.

The methods of operator design discussed in Chapter 2 have been presented in a relatively elastic format in an attempt to illustrate the convenience and flexibility of the filtering approach. It is hoped that this will encourage improvisation and innovation in the design and application of potential field operators. The author believes that one of the more important benefits to be gained from such a study is an understanding of the concepts of frequency analysis and information theory. Since these topics arise in several other areas of geophysical exploration, particularly in seismic studies, the geophysicist should be aware of some of the more basic concepts and have some degree of facility in applying them.

On the basis of the research undertaken in connection with this thesis a number of conclusions can be drawn:

- 1) Many of the methods used in the past for the development of potential field operators can be substantially improved by the introduction of digital processing techniques.

The main weakness of these operators has been their poor coefficient coverage, a characteristic necessitated by their use in hand calculation schemes.

2) The two-dimensional wavelength filter developed in this thesis appears to be a very useful means of separating the various regional, residual, and noise components of a potential field waveform.

3) The inverse Hankel transform method, proposed in section 2-2, has proven to be a highly versatile means of deriving two-dimensional, circularly symmetric operators of known frequency response.

4) The discrete Fourier transform provides a convenient basis for quality control and comparison of potential field operators.

5) The adaptation of frequency analysis and information theory to the processing and interpretation of gravity and magnetic data adds a new dimension to potential field studies in applied geophysics.

APPENDIX

APPENDIX-A1

DERIVATION OF WAVELENGTH FILTER

RADIAL FREQUENCY RESPONSE:

$$F(p) = \begin{cases} 1, & p < 0.5 \text{ CYCLES/UNIT} \\ 1/2, & p = 0.5 \text{ CYCLES/UNIT} \\ 0, & p > 0.5 \text{ CYCLES/UNIT} \end{cases} \quad (A-1)$$

ACCORDING TO THE INVERSE HANKEL TRANSFORM OF ZERO ORDER:

$$f(r) = 2\pi \int_{p=0}^{\infty} F(p) J_0(2\pi pr) p dp \quad (1-25)$$

WHERE $f(r)$ IS THE DESIRED IMPULSE RESPONSE.

SUBSTITUTING RELATION (A-1) INTO EQUATION (1-25).

$$f(r) = 2\pi \int_{p=0}^{.5} J_0(2\pi pr) p dp,$$

LETTING $Q = 2\pi r$,

$$f(r) = \frac{2\pi}{Q^2} \int_{p=0}^{.5} ap J_0(ap) d(ap) \quad (A-2)$$

NOW SINCE

$$\frac{d[x^v J_v(x)]}{dx} = x^v J_{v-1}(x),$$

AND THUS

$$\int x^v J_{v-1}(x) dx = x^v J_v(x) + C$$

(SEE WYLIE (1966), pg. 365)

THE INTEGRAL OF EQUATION A-2 BECOMES:

$$f(r) = \frac{2\pi}{Q^2} \left[ap J_1(ap) \right]_0^{1/2}, \text{ AND SINCE } Q = 2\pi r$$

$$f(r) = \frac{J_1(\pi r)}{2r}, \text{ THE REQUIRED UNIT}$$

IMPULSE RESPONSE OF THE WAVELENGTH FILTER.

NORMAL EQUATIONS FOR THE HANKEL TRANSFORM DESIGN METHOD

WRITING THE DISCRETE HANKEL TRANSFORM AS :

$$F(\rho) \approx A \sum_{t=0}^M C_t J_0(2\pi\rho t) \cdot t \quad (A-3)$$

WHERE $F(\rho)$ IS THE AMPLITUDE RESPONSE SPECIFIED AT ALL FREQUENCIES " ρ ", C_t REPRESENTS THE UNKNOWN COEFFICIENT SET, AND $A = 2\pi(\Delta t)^2$.

THE LEAST SQUARES ERROR ENERGY FOR EQUATION A-3 IS :

$$I = \sum_p \left[A \sum_t C_t J_0(2\pi\rho t) \cdot t - F(\rho) \right]^2$$

MINIMIZING THE ERROR ENERGY FOR THE j^{th} COEFFICIENT :

$$\frac{\partial I}{\partial C_j} = 2 \sum_p \left\{ \left[A \sum_t C_t J_0(2\pi\rho t) \cdot t - F(\rho) \right] \left[A J_0(2\pi\rho j) \cdot j \right] \right\} = 0$$

$$\text{OR : } \sum_p \left[J_0(2\pi\rho j) \cdot \sum_t C_t J_0(2\pi\rho t) \cdot t \right] = \frac{1}{A} \sum_p F(\rho) J_0(2\pi\rho j)$$

THUS THE j^{th} NORMAL EQUATION IS:

$$C_0 \left(t_0 \sum_p J_0(2\pi\rho j) J_0(2\pi\rho t_0) \right) + C_1 \left(t_1 \sum_p J_0(2\pi\rho j) J_0(2\pi\rho t_1) \right) + \dots \\ + C_M \left(t_M \sum_p J_0(2\pi\rho j) J_0(2\pi\rho t_M) \right) = \frac{1}{A} \sum_p F(\rho) J_0(2\pi\rho j)$$

THE NORMAL EQUATIONS IN MATRIX FORM ARE :

$$\begin{bmatrix} B_{00} & B_{01} & B_{02} & \dots & B_{0M} \\ B_{10} & B_{11} & B_{12} & \dots & B_{1M} \\ B_{20} & B_{21} & B_{22} & \dots & B_{2M} \\ \vdots & \vdots & \vdots & \ddots & \vdots \\ B_{j0} & B_{j1} & B_{j2} & \dots & B_{jM} \\ \vdots & \vdots & \vdots & \ddots & \vdots \\ B_{M0} & B_{M1} & B_{M2} & \dots & B_{MM} \end{bmatrix} \cdot \begin{bmatrix} C_0 \\ C_1 \\ C_2 \\ \vdots \\ C_j \\ \vdots \\ C_M \end{bmatrix} = \begin{bmatrix} D_0 \\ D_1 \\ D_2 \\ \vdots \\ D_j \\ \vdots \\ D_M \end{bmatrix}$$

$$\text{WHERE } B_{ij} = j \sum_p J_0(2\pi\rho j) \cdot J_0(2\pi\rho j) ,$$

$$D_j = \frac{1}{2\pi(\Delta t)^2} \sum_p F(\rho) J_0(2\pi\rho j) .$$

APPENDIX - A3

SOME WELL-KNOWN OPERATORS (DIGITIZED)

TABLE A-1 : PETERS' (1949) UPWARD CONTINUATION
COEFFICIENTS FOR A HEIGHT OF 1 GRID UNIT.

10	.0026					.0119					
9											
8											
7				.0043				.0026			
6	.0066										
5										.0119	
4	.0097				.0066						
3	.0108			.0097				.0043			
2		.0158	.0108								
1	.0528	.0374	.0158								
0	.1464	.0528		.0108	.0097		.0066				.0026
	0	1	2	3	4	5	6	7	8	9	10

X (GRID POINTS)

TABLE A-2 : PETERS' (1949) DOWNWARD CONTINUATION
COEFFICIENTS FOR A DISTANCE OF 1 GRID UNIT.

10	.0156					-.0166					
9											
8											
7				-.0427				.0156			
6	-.0274										
5										-.0166	
4	.0044				-.0274						
3	.0279			.0044				-.0427			
2		.0344	.0279								
1	.0757	.0839	.0344								
0	.3969	.0757		.0279	.0044		-.0274				.0156
	0	1	2	3	4	5	6	7	8	9	10

X (GRID POINTS)

APPENDIX - A3 (cont'd)

TABLE A-3 : TREJO'S (1953) DOWNWARD CONTINUATION
COEFFICIENTS FOR A DISTANCE OF 1 GRID UNIT.

10	.00257					-.01182					
9											
8											
7				-.00431				.00257			
6	-.00659										
5											-.01182
4	-.00971				-.00659						
3	-.01078			-.00971				-.00431			
2		-.01581	-.01078								
1	-1.05283	-.03736	-.01581								
0	5.85355	-1.05283		-.01078	-.00971		-.00659				-.00257
	0	1	2	3	4	5	6	7	8	9	10

X (GRID POINTS)

TABLE A-4 : HENDERSON'S (1960) DOWNWARD CONTINUATION
COEFFICIENTS FOR A DISTANCE OF 1 GRID UNIT.

GRID POINT (x,y)	OPERATOR WEIGHT	GRID POINT (x,y)	OPERATOR WEIGHT
(0,0)	4.8948	(3,4)	-.0050
(1,0)	-.7528	(0,5)	-.0050
(5,0)	-.0050	(5,5)	-.0044
(25,0)	-.0015	(10,6)	-.0048
(0,1)	-.7528	(1,7)	-.0044
(1,1)	.0022	(15,7)	-.0028
(2,1)	-.0701	(24,7)	-.0015
(7,1)	-.0044	(6,10)	-.0048
(1,2)	-.0701	(7,15)	-.0028
(2,2)	-.0094	(20,15)	-.0015
(3,2)	-.0086	(15,20)	-.0015
(2,3)	-.0086	(7,24)	-.0015
(4,3)	-.0050	(0,25)	-.0015

APPENDIX - A3 (cont'd)

TABLE A-5: GRANT AND WEST'S (1967) DOWNWARD CONTINUATION COEFFICIENTS FOR A DISTANCE OF 1 GRID UNIT - ATTENUATION FACTOR (γ) = 1/6.

6			-.0001				
5	-.0022			-.0030	-.0001		
4		-.0041	-.0018	-.0022		-.0001	
3		-.0043	-.0041		-.0022	-.0030	
2		-.0191	-.0114	-.0041	-.0018		-.0001
1	.3653	-.6505	-.0191	-.0043	-.0041		
0	2.5038	.3653				-.0022	
	0	1	2	3	4	5	6

X (GRID POINTS)

TABLE A-6: HENDERSON AND ZIETZ' (1949) SECOND VERTICAL DERIVATIVE COEFFICIENTS - BASED ON THE EQUATION:

$$\frac{\partial^2 f(x,y)}{\partial z^2} = \frac{1}{35^2} \left[21\bar{f}(0) - 8\bar{f}(5) + 3\bar{f}(\sqrt{2}5) - \frac{1}{4}\bar{f}(25) \right]$$

2	-0.0838		
1	-2.6667	1.0000	
0	7.0000	-2.6667	-0.0838
	0	1	2

TABLE A-7: ROSENBACH'S (1953) SECOND VERTICAL DERIVATIVE COEFFICIENTS - BASED ON THE EQUATION:

$$\frac{\partial^2 f(x,y)}{\partial z^2} = \frac{1}{245^2} \left[96\bar{f}(0) - 18\bar{f}(5) - 8\bar{f}(\sqrt{2}5) + \bar{f}(1\sqrt{5}5) \right]$$

2		0.0416	
1	-0.7500	-0.3333	0.0416
0	4.0000	-0.7500	
	0	1	2

BIBLIOGRAPHY

- Avison, A. T. (1969) - Report on the Atlantic Nickel Mines Property, St. Stephen, New Brunswick - 1968 Exploration Program by the Hanna Mining Company, unpublished.
- Bhattacharyya, B. K. (1965) - Two-dimensional Harmonic Analysis as a Tool for Magnetic Interpretation - Geophysics, Vol. 30, pp. 829.
- Bracewell, R. (1965) - The Fourier Transform and its Applications - McGraw-Hill.
- Bullard, E. C. and Cooper, R. I. B. (1948) - The Determination of the Masses Necessary to Produce a Given Gravitational Field - Proceedings of the Royal Society of London, Vol. 194, pp. 332-347.
- Byerly, P. E. (1965) - Convolution Filtering of Gravity and Magnetic Maps - Geophysics, Vol. 30, pp. 281-283.
- Darby, E. K. and Davies, E. B. (1967) - The Analysis and Design of Two-dimensional Filters for Two-dimensional Data - Geophysical Prospecting, Vol. 15, no. 3, pp. 383-405.
- Dean, W. C. (1958) - Frequency Analysis for Gravity and Magnetic Interpretation - Geophysics, Vol. 23, no. 1, pp. 97-127.
- Elkins, T. A. (1951) - The Second Derivative Method of Gravity Interpretation - Geophysics, Vol. 16, pp. 29-50.
- Fuller, B. D. (1967) - Two-dimensional Frequency Analysis and Design of Grid Operators - Mining Geophysics, Vol. II, Society of Exploration Geophysicists.
- Grant, F. S. and West, G. F. (1965) - Interpretation Theory in Applied Geophysics - McGraw-Hill, Toronto.
- Gray, A. and Mathews, G. B. (1931) - A Treatise on Bessel Functions and Their Application to Physics - MacMillan and Company Limited, London.
- Griffin, W. R. (1949) - Residual Gravity in Theory and Practice - Geophysics Vol. 14. pp. 39-56.
- Henderson, R. G. (1960) - A Comprehensive System of Automatic computation in Magnetic and Gravity Interpretation - Geophysics, Vol. 25, no. 3, pp. 569-585.

BIBLIOGRAPHY (cont'd)

- Henderson, R. G. and Zietz, I. a) (1949) - The Computation of Second Vertical Derivatives of Geomagnetic Fields - Geophysics, Vol. 14, pp. 508-516.
- b) (1949) - The Upward Continuation of Anomalies in Total Magnetic Intensity Fields - Geophysics, Vol. 14, pp. 517.
- Kellogg, O. D. (1929) - Foundations of Potential Theory - Ungar, New York.
- Macmillan, W. D. (1958) - The Theory of the Potential - Dover, New York.
- Mesko, A. (1965) - Some Notes Concerning the Frequency Analysis for Gravity Interpretation - Geophysical Prospecting, Vol. 13, no. 3, pp. 475-488.
- (1966) - Two-dimensional Filtering and the Second Derivative Method - Geophysics, Vol. 31, pp. 606-617.
- Nettleton, L. L. (1954) - Regionals, Residuals, and Structures - Geophysics, Vol. 19, pp. 10-22.
- Papoulis, A. (1962) - The Fourier Integral and its Applications - McGraw-Hill.
- Peters, L. J. (1949) - The Direct Approach to Magnetic Interpretation and Its Practical Application - Geophysics, Vol. 14, no. 3, pp. 290-319.
- Robinson, E. A. and Treitel, S. (1967) - Principles of Digital Wiener Filtering - Geophysical Prospecting, Vol. 15, no. 3, pp. 311-333.
- Rosenbach, O. (1953) - A Contribution to the Computation of the "Second Derivative" From Gravity Data - Geophysics, Vol. 18, pp. 894-912.
- Trejo, C. A. (1954) - A Note on Downward Continuation of Gravity - Geophysics Vol. 19, no. 1, pp. 71-75.
- Wadsworth, G.P. ; Robinson, E. A. ; Bryan, J. G. ; and Hurley, P.M. (1953) - Detection of Reflections on Seismic Records by Linear Operators - Geophysics, Vol. 18, no. 3, pp. 539-585.

BIBLIOGRAPHY (cont'd)

Wiley, C. R. (1966) - Advanced Engineering Mathematics -
McGraw-Hill, New York.

Zerflueh, E. G. (1967) - Applications of Two-dimensional
Linear Wavelength Filtering - Geophysics, Vol. 32, no. 6,
pp. 1015-1035.